

名古屋工業大学博士論文

甲第335号(課程修了による)

平成13年3月23日授与

TURBULENT CHARACTERISTICS AND  
TRANSITION BEHAVIOR OF  
COMBINED-CONVECTION BOUNDARY LAYER  
ALONG A VERTICAL HEATED PLATE

YASUO HATTORI

JANUARY 2001

**TURBULENT CHARACTERISTICS AND  
TRANSITION BEHAVIOR OF  
COMBINED-CONVECTION BOUNDARY LAYER  
ALONG A VERTICAL HEATED PLATE**

by

**Yasuo Hattori**

**B.S., Nagoya Institute of Technology, 1991**

**M.S., Nagoya Institute of Technology, 1993**

**Doctoral Dissertation**

**Submitted to  
Nagoya Institute of Technology  
in partial fulfillment of  
the requirements for the degree of  
Doctor of Engineering**

**January 2001**

*To my parents, my wife, and my son*



# ABSTRACT

Fluid flow and heat transfer characteristics in a turbulent combined-convection boundary layer along an isothermally-heated flat plate in air aided by a weak freestream are investigated experimentally and theoretically.

The heat transfer rates and turbulent statistics measured with hot and cold wires show that the turbulent transition moves downstream with a slight increase in freestream velocity. Simultaneously, the heat transfer rate rapidly decreases to about 40 % of that obtained in a turbulent natural-convection boundary layer, and velocity and temperature fluctuations become smaller in amplitude and change from random to harmonic at a specific frequency. Thus, the characteristics of the turbulent combined-convection boundary layer differ in several respects from those observed in both natural and forced convection.

The turbulent statistics of the combined-convection boundary layer for different Grashof numbers are examined. With an increase in the freestream velocity, a similar change in the turbulent quantities appears independently of local Grashof number. Then, based on the experimental results, the regimes of boundary layer flows are classified as a function of local Reynolds and Grashof numbers, and it is indicated that the reduction in heat transfer rates and the decays in velocity and temperature fluctuations, showing the transition from turbulent to laminar, arise at  $Gr_x / Re_x \simeq 3 \times 10^6$ .

The spatio-temporal structure of the turbulent combined-convection boundary layer is investigated with particle image velocimetry (PIV). For instantaneous velocity vectors obtained with PIV, large-scale fluid motions, which play a predominant role in the generation of turbulence, are frequently observed in the outer layer, while quasi-coherent structures do not exist in the near-wall region. Thus, it is revealed that increasing freestream restricts large-scale fluid motions in the outer layer, and consequently the generation of turbulence is suppressed and the boundary layer becomes laminar.

The stabilizing effects of a freestream are also investigated theoretically and

experimentally. It is confirmed that a linear stability analysis in a wide range of freestream velocities can well express the stabilizing behavior of the boundary layer, i.e., the calculated critical Grashof number increases exponentially with freestream velocity. In addition, turbulence measurements with hot wires indicate that, as freestream velocity increases, the maximum intensity of the temperature fluctuation decays exponentially, which implies the presence of linear fluid motions. Then, a peculiar profile of the cross-correlation coefficient between velocity and temperature fluctuations appears independently of  $Gr_x$ , indicating that velocity and temperature disturbances have the same frequency with different phases.

# TABLE OF CONTENTS

<b>ABSTRACT</b>	<b>iii</b>
<b>TABLE OF CONTENTS</b>	<b>v</b>
<b>NOMENCLATURE</b>	<b>ix</b>
<b>ACKNOWLEDGMENTS</b>	<b>xiii</b>
<b>LIST OF FIGURES</b>	<b>xv</b>
<b>1 INTRODUCTION</b>	<b>1</b>
1.1 Background .....	1
1.2 Objectives .....	5
1.3 Organization of Dissertation .....	6

<b>2</b>	<b>EXPERIMENTAL APPARATUS AND PROCEDURE</b>	<b>11</b>
2.1	Outline of Experimental Apparatus .....	11
2.2	Vertical Wind Tunnel .....	12
2.3	Heated Plate .....	14
2.4	Hot Wire Measurement .....	15
2.5	PIV Measurement .....	18
2.6	Qualification .....	18
2.7	Experimental Conditions .....	20
<b>3</b>	<b>BASIC TURBULENT STATISTICS</b>	<b>41</b>
3.1	Local Heat Transfer Rate .....	41
3.2	Mean Velocity and Mean Temperature Profiles .....	42
3.3	Intensities of Velocity and Temperature Fluctuations and Turbulent Heat Flux .....	43
3.4	Waveforms and Spectra of Velocity and Temperature Fluctuations	46
<b>4</b>	<b>REGIMES OF BOUNDARY LAYER FLOWS</b>	<b>59</b>
4.1	Criterion for Reduction in Heat Transfer Rate .....	59
4.2	Grx-dependency of Turbulent Statistics .....	61
4.3	Regimes of Boundary Layer Flows .....	63
<b>5</b>	<b>STRUCTURAL CHARACTERISTICS</b>	<b>75</b>
5.1	Skewness and Flatness Factors .....	75
5.2	Fluid Motion in Outer Region .....	76
5.3	Structure of Velocity Field in Near-Wall Region .....	77

<b>6</b>	<b>LINEAR STABILITY ANALYSIS</b>	<b>91</b>
	6.1 Stability Equations .....	91
	6.2 Numerical Solution of Eigenvalue Problem .....	93
	6.3 Results and Discussions .....	94
<b>7</b>	<b>CONCLUSIONS</b>	<b>101</b>
	<b>BIBLIOGRAPHY</b>	<b>105</b>
	<b>APPENDICES</b>	<b>113</b>
	APPENDIX A TABULATED EXPERIMENTAL DATA .....	113
	APPENDIX B HOT WIRE DATA PROCESSING PROGRAM .....	121
	APPENDIX C PROGRAM FOR LINEAR STABILITY ANALYSIS ·	127



# NOMENCLATURE

$c$	specific heat
$d$	diameter
$e$	voltage
$E_u, E_t$	power spectra of velocity fluctuations $u$ and $t$
$f$	frequency
$F(u), F(t)$	flatness factors of $u$ and $t$
$Gr_x$	local Grashof number, $= g \beta \Delta T_w x^3 / \nu^2$
$g$	gravitational acceleration
$h$	heat transfer coefficient
$i$	electric heating current
$Nu_x$	local Nusselt number, $= hx / \lambda$
$(Nu_x)_f$	local Nusselt number of pure forced-convection boundary layer
$(Nu_x)_n$	local Nusselt number of pure natural-convection boundary layer
$Pr$	Prandtl number, $= \nu / \alpha$
$R$	electric resistance
$Re_x$	local Reynolds number, $= U_\infty x / \nu$
$Ri_x$	local Richardson number, $= Gr_x / Re_x^2$
$R_{ut}$	cross-correlation coefficient between $u$ and $t$ , $= \overline{ut} / (\sqrt{u^2} \sqrt{t^2})$

$S(u), S(t)$	skewness factors of $u$ and $t$
$T$	mean temperature
$T$	mean fluid temperature
$t$	temperature fluctuation
$T_n$	Chebyshev polynomials
$U$	mean streamwise velocity
$U_m$	maximum velocity along flat plate
$u$	streamwise velocity fluctuation
$u_*$	friction velocity, $= (\tau_w / \rho)^{1/2}$
$V$	mean transverse velocity (perpendicular to flat plate)
$v$	transverse velocity fluctuation (perpendicular to flat plate)
$w$	spanwise velocity fluctuation (parallel to flat plate)
$x$	distance from leading edge of flat plate
$x^+$	dimensionless distance from leading edge of flat plate, $= u_* x / \nu$
$y$	distance perpendicular to flat plate
$z$	spanwise distance from center line of flat plate
$z^+$	dimensionless spanwise distance from center line of flat plate, $= u_* z / \nu$

### Greek

$\alpha$	thermal diffusivity
$\beta$	coefficient of volume expansion
$\phi$	disturbance amplitude function for velocity
$\gamma$	wave number
$\gamma^*$	non-dimensional wave number, $= \gamma x / (Grx / 4)^{1/4}$
$\lambda$	thermal conductivity



$\eta$	similarity variable for laminar boundary layer
$\varphi$	disturbance stream function
$\nu$	kinematic viscosity
$\rho$	density
$\theta$	disturbance amplitude function for temperature
$\tau$	time
$\tau_w$	wall shear stress
$\omega$	frequency (real part) and disturbance amplification rate (imaginary part).

### *Superscript and Subscripts*

$(\bar{\phantom{x}})$	time-averaged quantities
$m$	maximum value
$w$	wall condition
$\infty$	ambient condition
$'$	differentiation with $y$
$*$	non-dimensional value.



## ACKNOWLEDGMENTS

First of all, the author would like to express his gratitude to the Examining Committee members, Professor T. Tsuji, Professor Y. Nagano and Professor O. Kitoh, for carefully reviewing the manuscript and making appropriate suggestions.

The author would like to express his sincere gratitude to his supervisor, Professor T. Tsuji, for his encouragement, careful guidance, and many helpful suggestions in the progress of this investigation.

During the author's Ph.D. program at the Nagoya Institute of Technology (NIT), he received much help from the members of the Heat Transfer Laboratory in the Department of Mechanical Engineering. Special thanks are due to Professor Y. Nagano, Dr. O. Iida and Dr. T. Houra, for their valuable discussions and helpful comments. Several helpful discussions with Mr. H. Hattori, Mr. S. Tsujimura and Ms. T. Irikado are gratefully acknowledged.

The author also would like to express his appreciation to Dr. Y. Esashi, Dr. M. Kato, and Dr. N. Tanaka of the Central Research Institute of Electric Power Industry (CRIEPI), for providing him with valuable experience, supporting his studies at NIT. The author is also grateful to Dr. S. Shiomi, Dr. T. Saegusa, Dr. S. Ozaki and Mr. M. Wataru of CRIEPI for drawing his attention to this problem. The author wishes to express his appreciation to Mr. E. Kashiwagi and Mr. K. Sakamoto of Sumitomo Metal Mining co., LTD. for their helpful comments on the study of spent fuel storage.

The author is deeply indebted to Mr. T. Mizuno of Central Research Service co., LTD. for his devoted help in conducting these experiments.

Finally, the author is most indebted to his family for continuous encouragement and support. The author would like to express his gratitude and appreciation to his parents for their love, for their consistent encouragement throughout my education. Much credit for the completion of this program must be given to his wife who carried out these experiments through the night with him. She has shared with him the disappointment at failure in the

experiments as well as the delight of a successful measurement.

# LIST OF FIGURES

- 1.1 Reduction in heat transfer rate of turbulent combined-convection boundary layer due to increase in aiding flow: (a) due to increase in buoyant force; (b) due to increase in freestream velocity
- 1.2 Geometry and coordinate system
- 2.1 Schematics of laboratory
- 2.2 Photograph of laboratory
- 2.3 Schematics of experimental apparatus
- 2.4 Photograph of experimental apparatus
- 2.5 Schematics of wind tunnel
- 2.6 Photographs of wind tunnel: (a) diffuser; (b) settling chamber; (c) contraction cone
- 2.7 Photograph of blower
- 2.8 Schematics of traverse mechanism
- 2.9 Photographs of traverse mechanism
- 2.10 Schematics of heated plate
- 2.11 Photograph of back of heated plate (rear cover close)
- 2.12 Photographs of temperature controller system: (a) outside; (b) inside
- 2.13 Locations of thermocouples for measuring surface temperature of heated plate
- 2.14 Details near leading edge of plate

- 2.15 Schematics of hot and cold wire probe
- 2.16 Hot wire measurement system
- 2.17 Example of calibration curve
- 2.18 Schematics of PIV measurement system
- 2.19 Photographs of PIV system: (a) YAG-LASER; (b) timing controller; (c) CCD camera; (d) particle feeder
- 2.20 Examples of visualized images and calculated velocity vectors
- 2.21 Freestream velocity profiles in test section
- 2.22 Mean velocity and temperature profiles near wall measured with hot and cold wires
  
- 3.1 Local heat transfer rates of turbulent combined-convection boundary layer
- 3.2 Change in mean velocity profile with increase in aiding freestream velocity: (a) semi-logarithmic scale; (b) linear scale
- 3.3 Change in mean temperature profile with increase in aiding freestream velocity: (a) semi-logarithmic scale; (b) linear scale
- 3.4 Change in intensity of streamwise velocity fluctuation with increase in aiding freestream velocity: (a) semi-logarithmic scale; (b) linear scale
- 3.5 Change in intensity of temperature fluctuation with increase in aiding freestream velocity: (a) semi-logarithmic scale; (b) linear scale
- 3.6 Change in turbulent heat flux with increase in aiding freestream velocity: (a) semi-logarithmic scale; (b) linear scale
- 3.7 Waveforms of velocity and temperature fluctuations: (a) near-wall location; (b) maximum mean velocity location; (c) location in outer region
- 3.8 Power spectra of velocity and temperature fluctuations: (a)  $Gr_x / Re_x^3 = \infty$ ; (b)  $Gr_x / Re_x^3 = 4.68 \times 10^{-4}$ ; (c)  $Gr_x / Re_x^3 = 1.65 \times 10^{-4}$ ; (d)  $Gr_x / Re_x^3 = 1.05 \times 10^{-4}$

- 4.1 Heat transfer rates and wall shear stresses with  $R_{ix}$
- 4.2 Heat transfer rates and wall shear stresses with  $G_{rx} / R_{ex}$
- 4.3 Maximum values of temperature fluctuations with  $G_{rx} / R_{ex}$
- 4.4 Intensities of streamwise velocity fluctuation for different Grashof numbers
- 4.5 Intensities of temperature fluctuation for different Grashof numbers
- 4.6 Cross-correlation coefficients between velocity and temperature fluctuations for different Grashof numbers
- 4.7 Power spectra of velocity and temperature fluctuations: (a)  $G_{rx} / R_{ex} = 3.08 \times 10^6$ ; (b)  $G_{rx} / R_{ex} = 2.40 \times 10^6$
- 4.8 Regimes of boundary layer flows
- 4.9 Regimes of boundary layer flows at high  $G_{rx}$  numbers
- 4.10 Comparison of convective heat transfer regimes
  
- 5.1 Change in skewness and flatness factors of velocity and temperature fluctuations
- 5.2 Example of instantaneous velocity vectors
- 5.3 Signal traces of velocity fluctuations  $u$  and  $v$ , and Reynolds stresses  $uv$  in combined-convection boundary layer
- 5.4 Velocity fluctuation vectors in  $(x - y)$  plane: (a)  $uv > 0$ ; (b)  $uv \sim 0$ ; (c)  $uv < 0$
- 5.5 Temporal variation of instantaneous streamwise velocity profiles in  $(x - y)$  plane
- 5.6 Distributions of turbulent quantities near wall
- 5.7 Signal traces of velocity fluctuations  $u$  and  $v$
- 5.8 Example of velocity fluctuation vectors in  $(x - y)$  plane
- 5.9 Velocity fluctuation vectors near wall in  $(x - z)$  plane

- 5.10 Temporal variation of velocity fluctuation vectors near wall in ( $x - z$ ) plane: (a)  $\Delta \tau = 0 / 30$  s ; (b)  $\Delta \tau = 1 / 30$  s ; (c)  $\Delta \tau = 2 / 30$  s ; (d)  $\Delta \tau = 3 / 30$  s ; (e)  $\Delta \tau = 4 / 30$  s
- 5.11 Two-point correlations in near wall velocity field
- 6.1 Neutral curves for natural convection and combined convection
- 6.2 Comparison of mean velocity profiles for natural convection and combined convection
- 6.3 Critical Grashof number
- 6.4 Cross-correlation coefficients between velocity and temperature fluctuations measured with hot and cold wires



# Chapter 1

## INTRODUCTION

### 1.1 Background

Combined convection is defined as heat transfer situations where both natural convection and forced convection heat transfer mechanisms interact. Owing to this interaction, the heat transfer and fluid flow characteristics of the boundary layer drastically change with physical and geometric parameters. In particular, in cases when turbulent flow is under the control of the non-linear effects of velocity and temperature fields, the structural characteristics of the boundary layer become enormously complicated. The characteristics of turbulent heat transfer in such a boundary layer strongly depend on the following parameters:

- 1) Directions of freestream and buoyancy: either an aiding flow (e.g. a vertical upward flow along a heated plate) or an opposite flow (e.g. a vertical downward flow along a heated plate).
- 2) Reynolds number  $Re$ , Grashof number  $Gr$ , and the ratio between these parameters (e.g. Richardson number  $Ri = Gr / Re^2$ ).
- 3) Internal flows (e.g. pipe flows, channel flows) or external flows (e.g. boundary layer flows).

Of the above parameters, it has been determined that the freestream direction has a noticeable effect on the turbulence characteristics, i.e., the heat transfer of the combined-convection boundary layer with an aiding flow is qualitatively different from that with an opposite flow. With an opposite flow, the turbulent heat transfer of combined convection becomes more active than that of natural and forced convection. On the contrary, an aiding flow gives rise to the suppression of turbulence generation and a reduction in the heat transfer rate. This indicates that the turbulent heat transfer takes a minimum value in the combined-convection boundary layer with an aiding flow.

Explorations of the reductions in turbulent heat transfer of a combined-convection boundary layer with an aiding flow are eagerly awaited, because such combined-convection boundary layer flows are frequently encountered in engineering applications, for example the designs of the cooling systems for turbine blades, nuclear power plants and electronic circuitry; the performance evaluation of large-scale solar central power systems; and positioning of heating elements in furnaces (Easby, 1978; Quintiere, Rinkinen and Jones, 1981; Chao, Chen and Yao, 1983; Kraus and Bar-Cohen, 1983; Siebers, 1983; Jaluria, 1984; Incropera, 1986). In particular, the accurate estimation of reductions in the heat transfer rate is essential for safe and rational designs for electric power constructions, such as spent fuel storage facilities, in which the decay heat of spent fuel is principally removed by combined-convection flow (Hattori et al., 1995; Sakamoto et al., 1998; Hattori et al., 1999a; Sakamoto et al., 2000).

Since essential differences exist in the turbulent structures between natural and forced convection (Cheesewright and Doan, 1978; Kitamura et al., 1985; Tsuji and Nagano, 1988a), these phenomena of reductions in heat transfer rate are divided into two broad categories according to the main driving force of the boundary layer. One of these is observed in turbulent forced convection aided by a buoyant force, and the other is observed in the boundary layer created by imposing a weak aiding freestream on turbulent natural convection (c.f. Fig. 1.1).

For the former flow, the heat transfer characteristics of pipe flows were investigated experimentally and with numerical analysis. Easby (1978) investigated the buoyancy effects on isothermal pipe flows, and suggested that the changes in the heat transfer and the friction factor with the influence of buoyancy could be attributed to the distortion of the shear stress profile. Abdelmeguid and Spalding (1979) predicted the turbulent flow and the heat transfer in horizontal, inclined and vertical pipes when influenced by buoyancy with a  $k-\epsilon$  turbulence model, and they confirmed the good agreement between experiments and predictions. Cotton and Jackson (1990) calculated the vertical tube airflows in a turbulent combined-convection regime with a low-Reynolds-number  $k-\epsilon$  model, and they found that a serious impairment of heat transfer could occur due to buoyancy. In addition, the close agreement with a range of experimental heat transfer and flow profile results was shown for a developing flow in a tube. Celata et al. (1998) dealt with the heat transfer of combined-convection in a water-cooled vertical pipe. Their experiments suggested a reduction in the heat transfer rate for combined-convection in an upward heat flow due to a laminarization effect in the near-wall region. In addition, a new method for the calculation of the heat transfer rate in combined convection flow was proposed. The turbulent flow between vertical parallel plates at different wall temperatures, which is referred to as a channel flow, was also examined. An experimental and theoretical study of Nakajima et al. (1980) indicated the substantial effects of the buoyancy. Recently, direct numerical simulations (DNS) of channel flows were conducted by Kasagi and Nishimura (1997), and these simulations revealed that if the buoyant force is rather small compared with the forced pressure gradient in the driving force of the combined-convection boundary layer, the buoyancy affects the mean flow field only, and some modification of stress balance leads to a change in the Reynolds stress distribution and a reduction in heat transfer rate.

For the latter flow, many studies on suppression in turbulent heat transfer of the combined-convection boundary layer with a weak aiding flow have been reported. However, most of them are concerned only with the change in the heat transfer rate due to an

increase in freestream velocity, and there are few investigations on the turbulent structure in a combined-convection boundary layer. Thus, the mechanism for the reduction in the heat transfer rate is not fully understood. Hall and Price (1970) conducted experiments with air and isothermally heated vertical plates, and they found that the wall surface temperature initially increases and then decreases. This implies that the heat transfer rate of the combined-convection boundary layer becomes smaller than those of a natural- and forced-convection boundary layer under certain conditions. Kitamura and Inagaki (1987) and Inagaki and Kitamura (1987; 1988) also performed experiments with water and air as the working fluids and obtained a quantitative correlation between the heat transfer rate and flow conditions. In their experiment with water (Kitamura and Inagaki, 1987), the changes in the velocity and temperature fields were also investigated by using a hot-film probe and a flow visualization technique. However, they reported no experimental data on the near-wall turbulent quantities directly controlling the heat transfer characteristics, because reliable measurements of turbulent quantities are very difficult for low-speed flows with relatively large fluctuations in velocity and temperature. Thus, the origin of the reduction in heat transfer rate was not clearly identified in their study.

Moreover, there is poor agreement among previous reports on the value of the reduced heat transfer rate and the thermal and flow conditions leading to a drop in heat transfer rate (Inagaki, 1996). Since the development of boundary layers strongly depends on the disturbance of the freestream, it is important to give due consideration to the control of the freestream. Nevertheless, previous experiments have not always taken sufficient care to eliminate fluctuations in the freestream. Indeed, in previous studies, relatively large disturbances were involved in the freestream, which yielded a substantially small transition Reynolds number value for pure forced convection. Thus, the quantitative disagreements, even as to the heat transfer rate, may be attributed to the disturbance in the freestream.

Numerical analyses were also performed by Chen, Armaly and Ali (1987), Inagaki (1996), and Patel, Armaly and Chen (1998). In these studies, the heat transfer characteristics from

turbulent natural convection to turbulent forced convection along a vertical plate were investigated using a low Reynolds-number turbulence model. They predicted a reduction in heat transfer rate in the combined-convection region. In addition, a map of the various convection flow regimes classified based on a criterion for the variation in heat transfer rate was proposed (Patel, Armaly and Chen, 1998). However, the usefulness of the turbulence model was not verified because of the lack of conclusive experimental data for turbulent quantities in combined convection.

On the other hand, for the transition of the combined-convection boundary layer from laminar to turbulent, Krishnamurthy and Gebhart (1989) measured the combined-convection boundary layer flow of compressed air. Through these measurements, they indicated that the turbulent transition of the boundary layer was delayed with an increase in the aiding freestream velocity. However their study focused on the transition from laminar to turbulent in combined convection, so they considered only a limited region of Grashof and Reynolds numbers, and no data for heat transfer rate were reported. Theoretical studies (Merkin, 1969; Mucoglu and Chen, 1978; Carey and Gebhart, 1983) with a linear stability analysis have also been conducted. Recently, Moresco and Healey (2000) analyzed the stability properties of the flow over an isothermal, semi-infinite vertical plate, placed at zero incidence to an otherwise uniform stream at a different temperature. To calculate the base flows, they proposed a coordinate transformation that describes in a smooth way the evolution between these two limiting similarity states. The stability of this flow was then investigated, and the change in the spatio-temporal stability modes was shown, but their results do not provide basic information about the turbulent heat transfer of combined convection.

## 1.2 Objectives

In the present study, which aims to determine the essential characteristics of a turbulent combined-convection boundary layer generated by a large heated plate and by a slight

assisting freestream, we considered a two-dimensional turbulent combined-convection boundary layer along an isothermally-heated plate in air aided by a weak freestream, which is a simple and typical flow. The geometry of this is shown schematically in Fig. 1.2.

The specific objectives of the present study are:

- 1) To accumulate credible experimental data for turbulent combined convection, with special attention to the turbulent quantities including the wall region.
- 2) To examine the variations in mean and turbulent quantities of the velocity and thermal fields in a turbulent natural-convection boundary layer that are due to the introduction of freestream velocity.
- 3) To investigate how the fluid flow and heat transfer characteristics in a turbulent combined-convection boundary layer change with an increasing freestream velocity.
- 4) To clarify why the heat transfer rate in the turbulent combined-convection boundary layer decreases with an increasing freestream velocity.
- 5) To firmly grasp the thermal and flow conditions leading to reductions in the heat transfer rate of the turbulent combined-convection boundary layer.
- 6) To identify the regimes of various boundary layer flows.
- 7) To show the spatio-temporal structures of the turbulent combined-convection boundary layer.
- 8) To explain the stabilizing process of the combined-convection boundary layer due to freestream effects.

## **1.3 Organization of Dissertation**

This thesis consists of seven Chapters. Each chapter is summarized in the following.

In Chapter 1, the background and the object of the present study are explained.

Chapter 2 deals with the experimental apparatus and procedure. The experimental

apparatus consists of a vertical wind tunnel, heaters and measurement instruments. A heated plate generating a buoyant flow (4 m high and 0.8 m wide) is placed vertically in the test section of the vertical wind tunnel with solid boundaries. To reduce the disturbance of freestream in the test section, four-fine mesh damping screens and a honeycomb are installed in the settling chamber, which is placed upstream of the contraction cone. Two kinds of measurement are carried out: one is the measurement of instantaneous velocity and temperature with a probe consisting of normal hot and cold wires, and the other is a particle image velocimetry (PIV) measurement to observe instantaneous two-dimensional velocity fields.

Chapter 3 describes the experimental results on the variations in mean and turbulent quantities in the velocity and thermal fields with increasing freestream velocity, with special attention to the effect of a slight freestream on turbulent natural convection. The measured heat transfer rate and turbulent quantities shows that with an increase in freestream velocity, the local heat transfer rate rapidly decreases to about 40 % of that obtained in the turbulent natural-convection boundary layer, and velocity and temperature fluctuations become smaller in amplitude and change from random to harmonic at a specific frequency. Then, through these measurements, it is revealed that the turbulent transition moves downstream with a slight increase in freestream velocity.

Chapter 4 discusses the turbulent statistics of the combined-convection boundary layer for different Grashof numbers. It is found that a similar change in the turbulent quantities appears independently of local Grashof number, and the regimes of various boundary layer flows are then identified based on the turbulence characteristics. The experimental results clearly demonstrate the thermal and flow conditions leading to the laminarization.

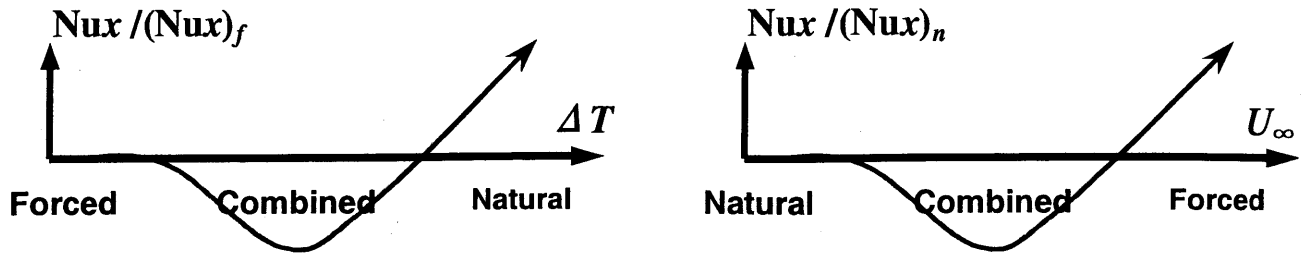
Chapter 5 shows the spatio-temporal structures of the turbulent combined-convection boundary layer. For instantaneous velocity vectors obtained with particle image velocimetry, large-scale fluid motions, which play a predominant role in the generation of turbulence, are frequently observed in the outer layer, while quasi-coherent structures do not exist in the near-

wall region. The increasing freestream then restricts large-scale fluid motions in the outer layer, and consequently the generation of turbulence is suppressed and the boundary layer becomes laminar.

Chapter 6 provides the experimental and theoretical results to explain the stabilizing process of the combined-convection boundary layer due to freestream effects. With a linear stability analysis, neutral stability curves corresponding to experimental conditions are obtained, and the stabilizing effect of the freestream is discussed in detail.

The important conclusions of this study are summarized in Chapter 7.





(a) due to increase in buoyant force

(b) due to increase in freestream velocity

Figure 1.1 Reduction in heat transfer rate of turbulent combined-convection boundary layer due to increase in aiding flow

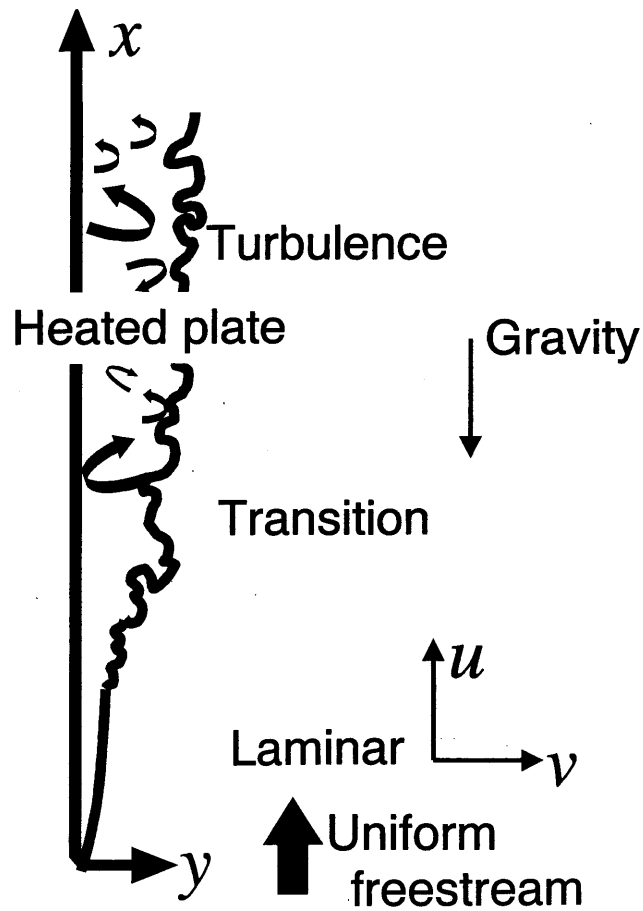


Figure 1.2 Geometry and coordinate system



# **Chapter 2**

## **EXPERIMENTAL APPARATUS AND PROCEDURE**

### **2.1 Outline of Experimental Apparatus**

As shown in Figs. 2.1 and 2.2, the experimental apparatus was placed in the pit of the laboratory at the Central Research Institute of Electric Power Industry to avoid the direct effects of external winds and solar radiation. A schematic of the experimental apparatus is shown in Fig. 2.3 and a photograph in Fig 2.4. The apparatus comprises a vertical wind tunnel, a heated smooth flat plate and measurement instruments. A heated plate generating a buoyant flow was installed in the test section of the vertical wind tunnel with solid boundaries, and the detailed measurement of the turbulent quantities in the boundary layer that developed along a heated plate was carried out with normal hot and cold wires and with particle image velocimetry. The key features of the apparatus are summarized as follows:

- 1) The turbulent boundary layer in both natural and forced convection along a vertical heated plate can be developed.
- 2) The surface temperature of a heated plate can be kept uniform.
- 3) The velocity fluctuation in the freestream is reduced to the lowest possible level.
- 4) The turbulent quantities in the boundary layer including the wall region can be

measured with normal hot and cold wires.

- 5) The fluid motion in the whole boundary layer region can be observed with particle image velocimetry.

## 2.2 Vertical Wind Tunnel

The low-speed wind tunnel was designed in accordance with previous reports (Fukatsu, 1934; Lumley, 1964; Bradshaw, 1965; Pankhurst and Holder, 1965; Loehrke and Nagib, 1976; Morel, 1977; Rae and Pope, 1984; Shehata, 1984; Visualization Soc. of Japan, 1994) to produce an ideal flow field. A schematic of the vertical wind tunnel is shown in Fig. 2.5 and photographs are shown in Fig. 2.6. The wind tunnel was rigidly fixed on the support frame, which is made of steel weldment. The wind tunnel, which consists of a blower, diffuser, settling chamber, construction cone and test section with a heated plate, is an open circuit tunnel with solid boundaries.

A photograph of the blower, which is an electrical drive system, is shown in Fig. 2.7. The direct current blower (Hitachi; ODS-RHF #5) was driven by a synchronous motor. The maximum power of the motor-driven blower was 11 kW, and a freestream velocity  $U_\infty$  up to about 10 m/s was obtained in the test section. With a DC machine drive system (Yasukawa: VS-505), freestream velocity was manually controlled. This blower was mounted on the floor of the laboratory with rubber vibration isolations.

The diffuser, which was placed downstream of the blower, is sensitive to design errors due to the occurrences of flow separation and oscillations in test section velocities. Diffusers are mainly described by cone angle. The cone angle of the present wind tunnel was  $21^\circ$  in the  $x$ - $y$  direction, and  $27^\circ$  in the  $x$ - $z$  direction, respectively. This cone angle is quite large compared with that recommended to avoid the danger of separation. Thus, to smooth out the velocity variations and maintain satisfactory flow, three safety screens were placed in the diffuser.

The disturbance in the freestream was reduced by the installation of four fine mesh damping screens and a honeycomb in the settling chamber, which was  $2000 \times 2000 \text{ mm}^2$  in area and 1028 mm long. The porosity of a damping screen (Nippon Filcon:  $16 \times 16$  size) made of SUS316 wires (0.51 mm diameter) was 46.2 %, and the dimensions of an aluminum honeycomb (Yokohama Rubber: high vex core A 3/16) were 3/16" in width and 50 mm in thickness.

Many contraction curves have been proposed, and in the present study, the curve described by Eq. (2.1) was applied.

$$\left(\frac{r_{in}}{r}\right)^4 - 1 = \frac{1}{2\pi} \left\{ \left(\frac{r_{in}}{r}\right)^4 - 1 \right\} \left( \frac{2\pi x}{l} - \sin \frac{2\pi x}{l} \right) \quad (2.1)$$

where  $r_{out}$  (= 1000 mm),

$r_{in}$  (= 2000 mm),

$l$  (= 1400 mm)

The test section ( $1 \times 1 \text{ m}^2$  in area and 6.2 m high) was made of wood and steel. The heated plate was fixed on the back wall of the test section. To minimize heat loss by conduction, the whole test section was coated with a thick layer (100 mm thickness) of heat insulating material (Nichias: fine flex blanket T/# 5120 #130). Heat resisting glazed windows for visualized experiments and measuring holes for a hot-wire measurement were positioned in the front and side walls. The air temperature profile in the test section was measured with thermocouples to estimate the effects of thermal stratification. There was no divergence of the test section in the downstream direction because pressure axial pressure gradients due to boundary layer growth on the wall are quite small.

The schematics of the traverse mechanism for measurement instruments are shown Fig. 2.8, and the photographs are shown in Fig. 2.9. The traversing system consists of a main

carriage, which moves parallel to the plate, and a cross slide, which moves perpendicular to the plate. No lateral movement was possible. In the horizontal direction, a micrometer permitted a resolution of 1/100 mm.

## 2.3 Heated Plate

The heated plate was mounted vertically on the back wall of the wind tunnel. Figure 2.10 shows the schematics of a front and a cross-section of the heated plate and Fig. 2.11 shows a photograph of the backside of the heated plate. The heated plate is composed of a heated surface, heat insulating materials, electric heaters, and a control system.

The heated surface was an aluminum plate, which was 4 m high and 0.8 m wide, to generate a two-dimensional turbulent flow, and 0.02 m thick to prevent the deformation due to the thermal stress. To minimize the heat loss by radiation, the surface was finished to a smooth mirror.

The electric heater was made of four sheath Nichrom wires, and twenty electric heaters were attached to the backside of the plate with cement (Thermon Manufacturing: Thermon T-63) and binding metals. The maximum output of each heater was 4 kW, and the surface temperature of the plate could be increased up to about 500 °C.

The surface temperature was kept uniform by controlling the heating current of each heater. The photographs of temperature controller system are shown in Fig. 2.12. Since the thermal conductivity of this aluminum is quite large, a uniform surface temperature of the heated plate could be easily obtained. The surface temperature of the heated plate was measured with K-type sheath thermocouples, whose locations are shown in Fig. 2.13. Twenty-eight thermocouples were used for controlling heater current and twelve thermocouples were used for monitoring surface temperature. Based on the output from each thermocouple, the electric supply for each heater was controlled with the digital indicating controllers (Chino: DB500) and thyristor regulators (Chino: JA2020N).

A detail of a cross-section of the leading edge of the heated surface is shown in Fig. 2.14. The heated surface protruded 10 mm from the back wall of the wind tunnel to determine the leading edge of itself.

## 2.4 Hot Wire Measurement

Instantaneous velocity and temperature in the boundary layer including the near-wall region were measured with normal hot and cold wires made of 3.1  $\mu\text{m}$  diameter tungsten. Figure 2.15 shows the hot and cold wire probes. The shape and dimensions of the probes were set so as to minimize measurement errors (Paranthoen, Petit and Lecordier, 1982; Tsuji and Nagano, 1988b; Tsuji, Nagano and Tagawa, 1992b). The sensitive length of the hot and cold wires was 2 mm and 4 mm ( $\simeq 16 \nu / u_*$ ), respectively, and the cold wire was located 2.5 mm upstream of the hot wire.

The hot wire was built into a Wheatstone bridge, as shown schematically in Fig. 2.16. A constant overheat ratio was maintained with a bridge circuit (Kanomax 1016), and a uniform surface temperature of the hot wire  $T_{\text{wire}} = 236^\circ\text{C}$  was obtained.

The outputs of these wires were amplified, and then after analog to digital conversion with an A/D board, the instantaneous velocity and temperature were calculated with digital processing at workstations. The sampling frequency and sampling time were 500 Hz or 2000 Hz, and 270 s or 60 s, respectively. The temperature compensation of the hot wire and the improvement for frequency response of the cold wire was performed in accordance with the thermal-equilibrium equations for two fine wires proposed by Hishida and Nagano (1978). In the following, the detail of this compensation of the hot wire is described.

The thermal equilibrium of the hot wire diameter  $d$ , length  $l$ , and electric resistance  $R$  gives the following equation (Hoshin and Sawada, 1972):

$$i^2 R = \{h(T_{\text{wire}} - T_{\text{air}}) + q_{\text{cond}} + q_{\text{rad}}\} \pi d l \quad (2.2)$$

where  $i$  denotes the electric heating current,

$h$  denotes the heat transfer rate, and

$q_{cond}$  and  $q_{rad}$  denote the heat loss by conduction and radiation, respectively.

Applying Eq. (2.2) for the static condition:

$$i_o^2 R = \{h_{nc}(T_{wire} - T_{air}) + q_{cond} + q_{rad}\} \pi dl \quad (2.3)$$

where  $i_o$  denotes the electric heating current under the static condition, and

$h$  denotes the heat transfer rate of a natural convection.

From Eqs (2.2) and (2.3), the following equation is obtained

$$(i^2 - i_o^2) R = \{h(T_{wire} - T_{air})\} \pi dl \quad (2.4)$$

In the present measurement, an empirical relation proposed by Kramers is used for estimating Nusselt number  $Nu$  around the wire:

$$Nu = A + B Re_d^n \quad (n = 0.5) \quad (2.5)$$

$$h = A' + B' \sqrt{u} \quad (2.5)'$$

where

$$A' = 0.42 Pr_f^{0.2} \lambda_f / d,$$

$$B' = 0.57 Pr_f^{0.33} \lambda_f / \sqrt{d \nu_f}$$

Substituting Eq. (2.5)' into Eq. (2.4) yields the following equation:

$$u = \left\{ \frac{(e^2 - e_o^2)}{B' \pi dl R (T_{wire} - T_{air})} \right\} \quad (2.6)$$



Thus, if the value of  $e_o$  in the left-hand side of this equation is found, the flow velocity  $u$  can be calculated easily using Eq. (2.6). From Eq. (2.5)', the following equation is derived:

$$\frac{e_o^2}{T_{wire} - T_{air}} = \pi dl R A' + \pi dl R \frac{q_{cond} + q_{rad}}{T_{wire} - T_{air}} \quad (2.7)$$

Since the first term on the right-hand side of this equation can be expressed by a linear function of  $T_{air}$ , Eq. (2.7) can be rearranged as follows (Makita, Mori and Sawada, 1992a):

$$\frac{e_o^2}{T_{wire} - T_{air}} = C + D T_{air} \quad (2.8)$$

The values of  $C$  and  $D$  are determined by calibration under the static condition. With a decrease in the flow velocity, the effects of heat loss due to conduction from the wire to the relatively cold supports grow (Hinze, 1975). Thus, the calibration curve is applied in calculating the flow velocity. An example of the calibration curve that accounted for the buoyancy effects is shown in Fig. 2.17.

An improvement in frequency response of the cold wire was also made with the following equation.

$$T_{air} = T_{wire} + \frac{\rho_{wire} c_{wire} d}{4h} \frac{dT}{d\tau} \quad (2.9)$$

In addition, the measurement error caused by the streamwise displacement between the wires was eliminated by delaying the temperature signals of the cold wire according to Taylor's hypothesis (Fabris, 1978; Tsuji and Nagano, 1988a; Makita, Sawada and Mori, 1992b).

## 2.5 PIV Measurement

The PIV was measured in order to observe instantaneous two-dimensional velocity fields. Figure 2.18 shows the system of PIV, and Fig. 2.19 shows the photographs of PIV instruments. Plastic microspheres of about  $30\text{ }\mu\text{m}$  in diameter (Japan Fillite: EXPANCEL461DE) were added to the boundary layer flow as tracer particles. Laser light sheets were formed with a double pulse YAG laser (New Wave Research: DPIV-N90-30) and sheet-forming optic illuminated particles, and two-dimensional velocity fields in the streamwise-transverse ( $x$ - $y$ ) or streamwise-spanwise ( $x$ - $z$ ) planes were visualized. Figure 2.20 is an example of the visualized images. Particle-containing flow images of about  $0.2 \times 0.2\text{ m}^2$  in area were captured by a CCD camera (Sony: XC-003) with a wide-angle lens ( $f\text{ }20 / F\text{ }2.8$ ), which was fixed at  $x = 2.965\text{ m}$ . The NTSC image-outputs were recorded on a laser disc (Sony: CRV-3000AN) at 30 frames per second. Through a frame grabber, the NTSC composite signals were converted to digitized images of  $512 \times 480$  pixels in size and 8 bit gray level, and transferred to the host memory of a NEC 266 MHz PC. Each digital TV frame was separated into two digital TV fields.

Then, velocity vectors were obtained with a pattern cross-correlation method. To improve the spatial resolution, a hierarchical recursive scheme (Hu et al., 2000) was applied: after a rough estimation for large interrogation windows of  $70 \times 70$  pixels, the velocity vectors were determined from small interrogation windows with a size of  $20 \times 20$  pixels. In addition, a sub-pixel algorithm was used with the assumption of a Gaussian profile for the spatial correlation.

## 2.6 Qualification

The thermal and flow conditions in the test section were verified in the preliminary experiments. The uniformity of the surface temperature was within  $0.5\text{ }^{\circ}\text{C}$ , and the spatial

non-uniformity ratio of the freestream velocity was below 1.6 %, as shown in Fig 2.21. The measured relative fluctuation ratio of the freestream was below 0.3 %, and it was confirmed that measurements for the pure forced-convection boundary layer on a flat plate gave a critical Reynolds number of  $Re_x \simeq 3.5 \times 10^5$ . This value corresponds to flows with an extremely small intensity of turbulence in the freestream (Schlichting, 1979). Therefore, the effect of the relative ratio of fluctuation to freestream velocity was insignificant, and an ideal uniform freestream could be obtained.

Since, in the present study, particular attention was given to the reduction in the heat transfer rate of the turbulent boundary layer due to the addition of a weak freestream, the accuracies of the hot-wire and PIV measurements were also demonstrated in preliminary experiments conducted for a natural-convection boundary layer along a vertical heated plate. The agreement between our hot and cold wire measurements and the data obtained by Tsuji and Nagano (1988a; 1988b) was excellent for turbulent quantities even in the near wall region, as seen in Chaps. 3, 4, and 5. The example of profiles of measured mean velocity and temperature in the near-wall region are shown in Fig. 2.22. In addition, the mean velocity profile closely correlates to a cube curve and the mean temperature profile can be approximated to a straight line, assuring that the present measurements were highly accurate (Tsuji and Nagano, 1988b).

On the other hand, the turbulent quantities measured with PIV tended to be slightly larger than those measured with the hot wire, although there was general agreement between both profiles in the boundary layer. In particular, some discrepancies existed in the near-wall and outer regions of the boundary layer, where the visualized images with tracing particles could not be captured continuously, and considerable error-vectors for instantaneous velocities were calculated. Moreover, from the frequency spectra of measured velocity fluctuations, only low frequency fluctuations below 7 Hz were judged to be reliable for PIV. Thus, the discrepancies might have been due to peak-locking vectors (Raffel, Willert and Kompenhans, 1998) and error vectors, and PIV was adequate only for the observation of large-scale fluid

motions.

## 2.7 Experimental Conditions

Experiments were carried out under the conditions of a uniform surface temperature  $T_w$  in the range of  $44\sim 104$  °C. The ambient fluid temperature  $T_\infty$  was somewhat different for each experiment, within  $13\sim 29$  °C. The vertical distance  $x$  from the leading edge of the flat plate to the measuring locations changed from 0.265 to 3.765 m. The ranges of local Reynolds number  $Re_x$  and local Grashof number  $Gr_x$  were  $0\sim 1.9\times 10^6$  and  $1.3\times 10^8\sim 3.5\times 10^{11}$ , respectively. Physical properties were evaluated at the film temperature  $T_f = (T_w + T_\infty) / 2$  except for  $\beta$ .

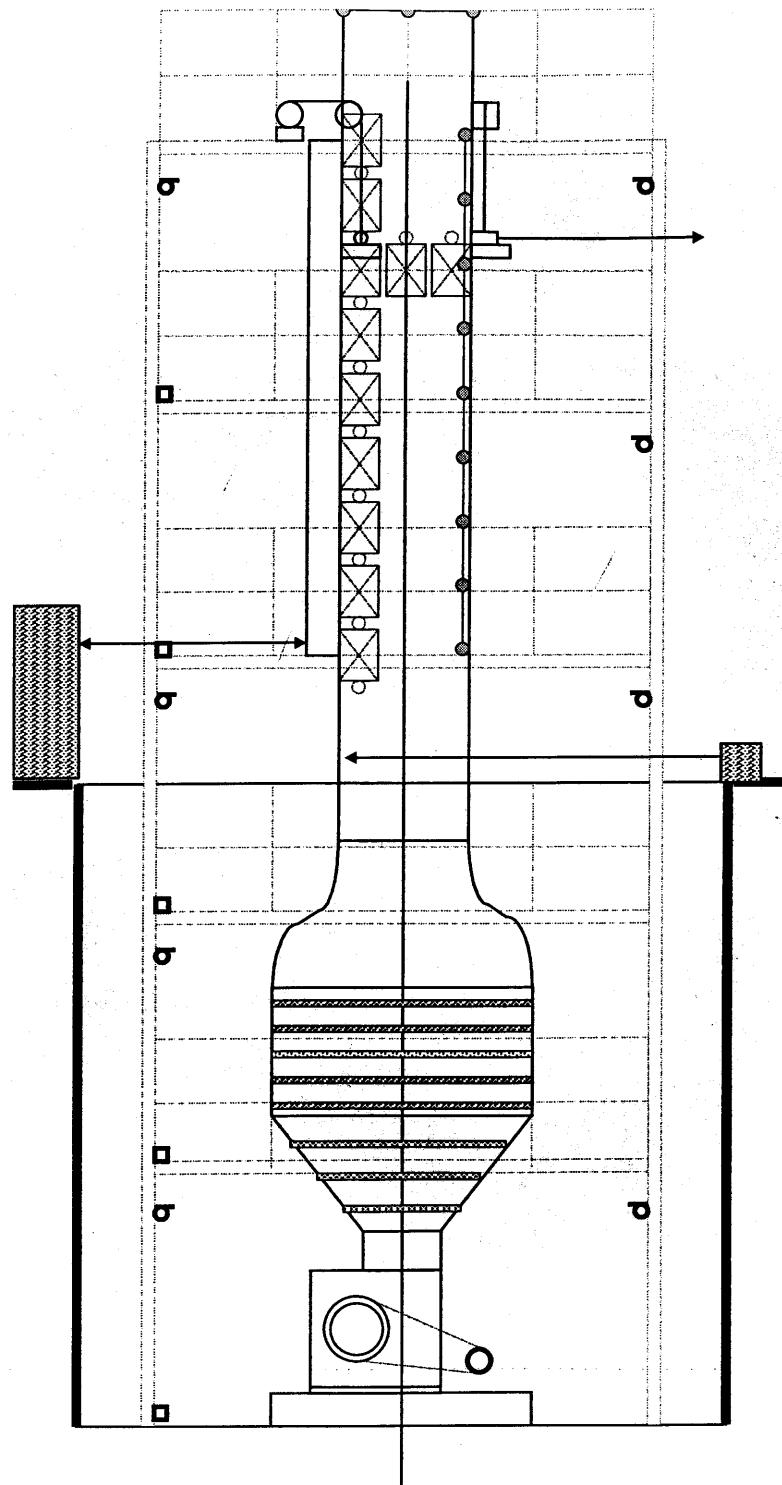


Figure 2.1 Schematics of laboratory

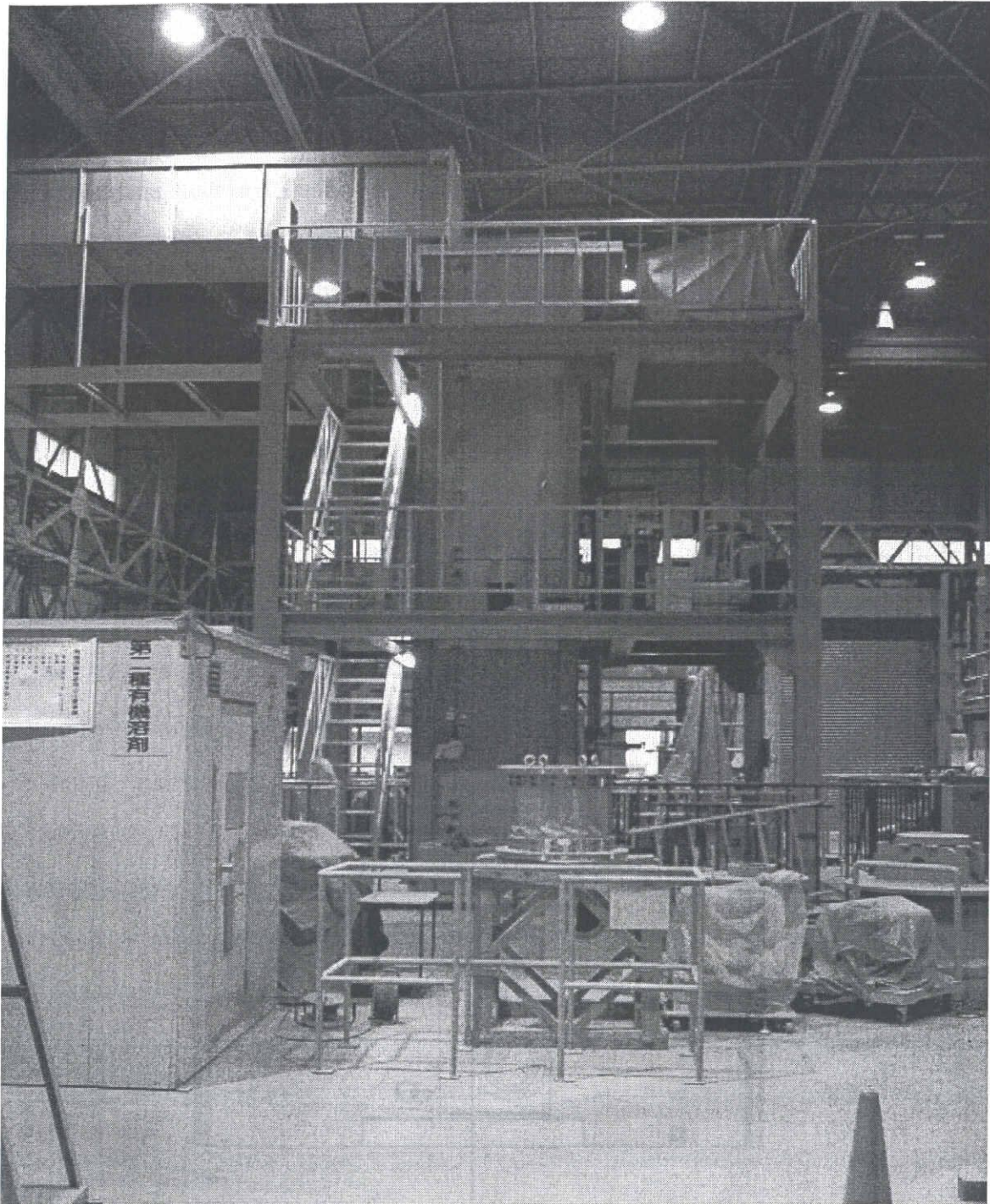


Figure 2.2 Photograph of laboratory

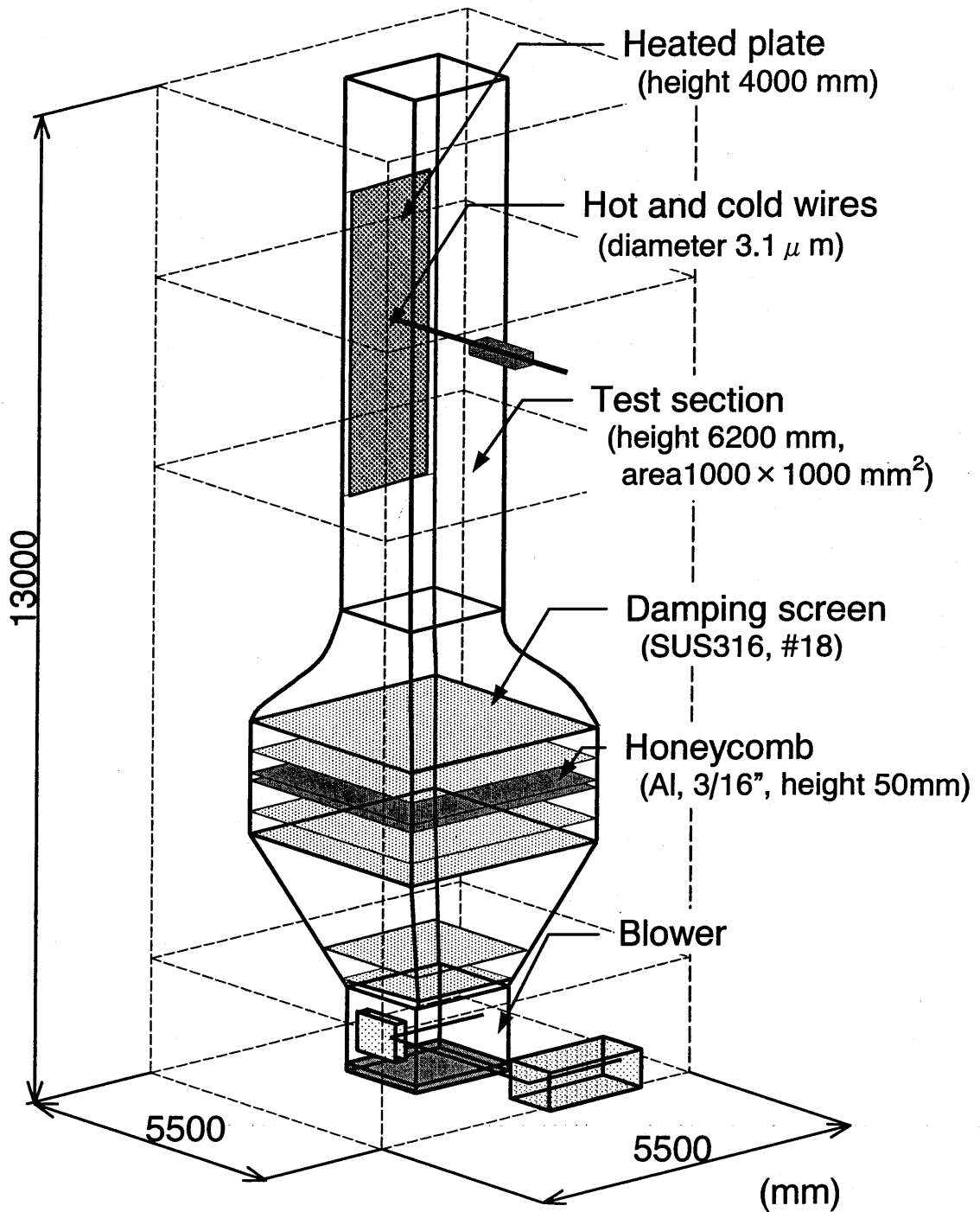


Figure 2.3 Schematics of experimental apparatus





Figure 2.4 Photograph of experimental apparatus



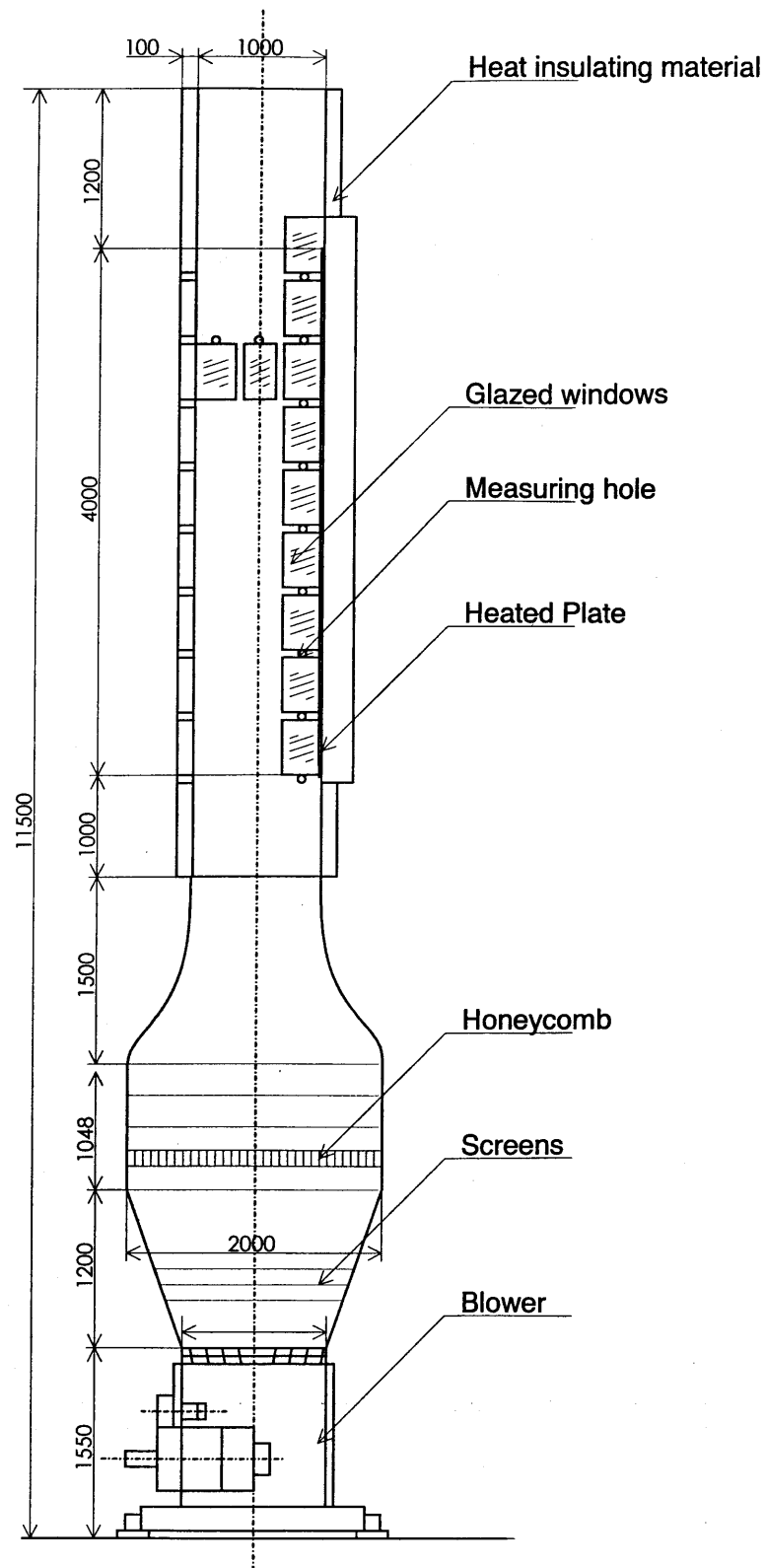
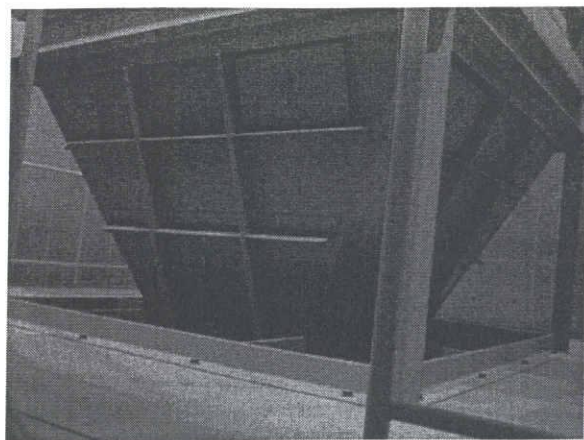
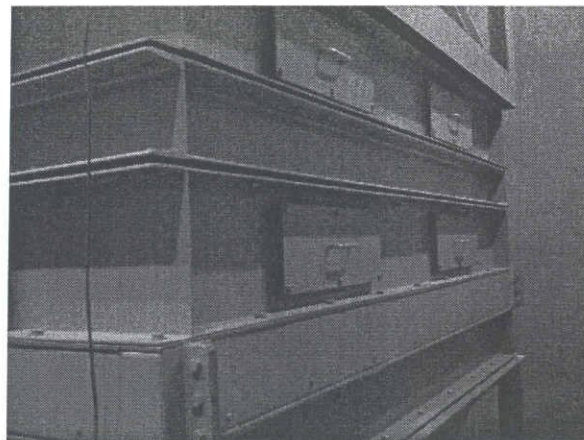


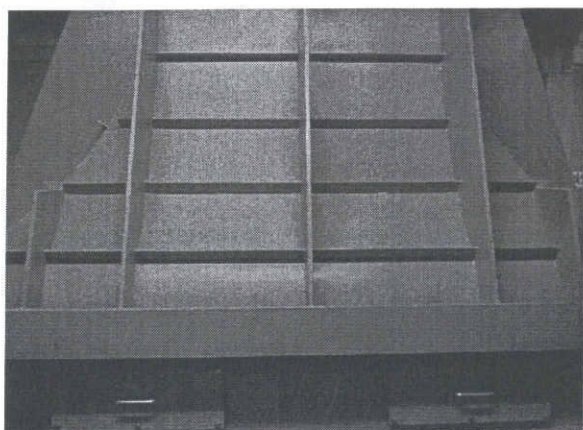
Figure 2.5 Schematics of wind tunnel



(a) diffuser



(b) settling chamber



(c) contraction cone

Figure 2.6 Photographs of wind tunnel

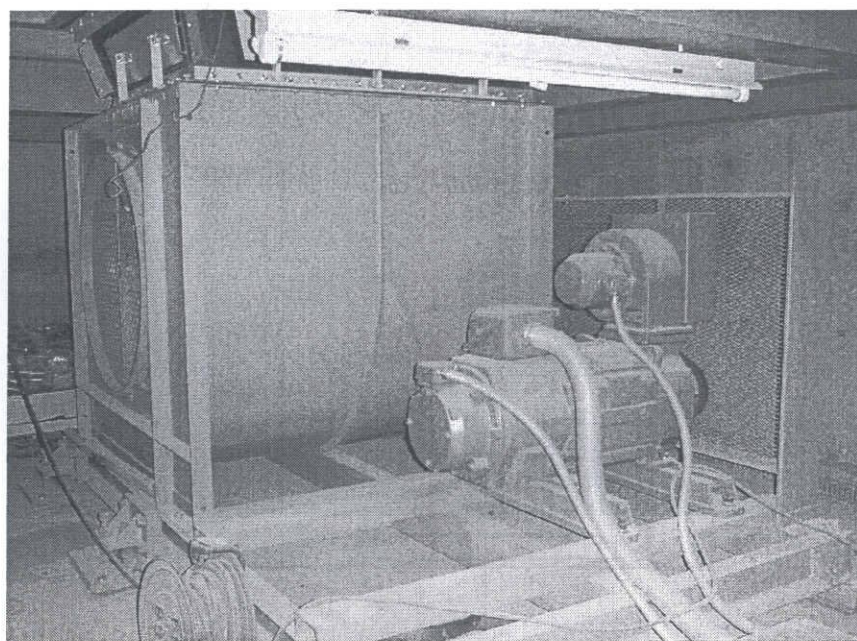


Figure 2.7 Photograph of blower

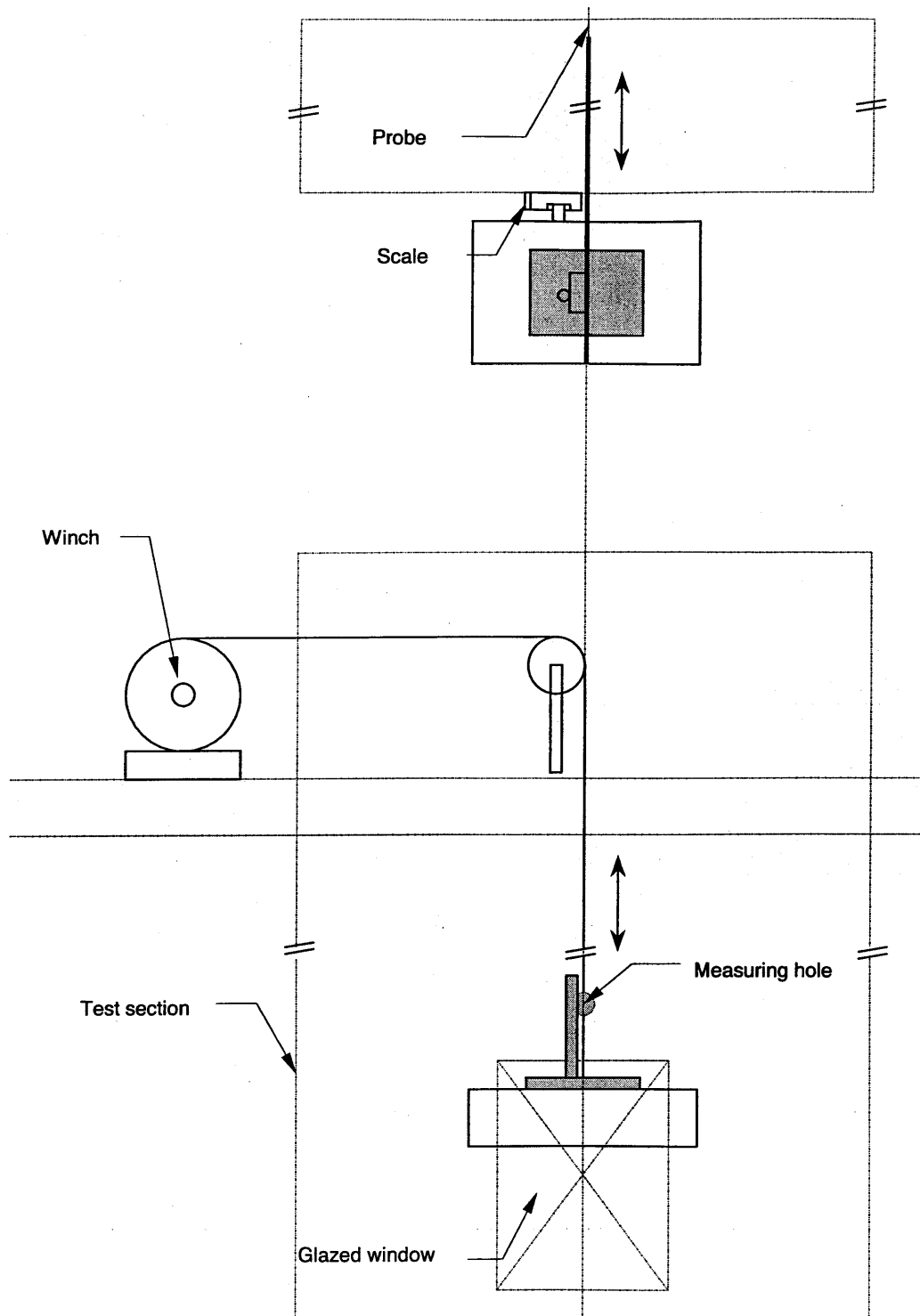


Figure 2.8 Schematics of traverse mechanism

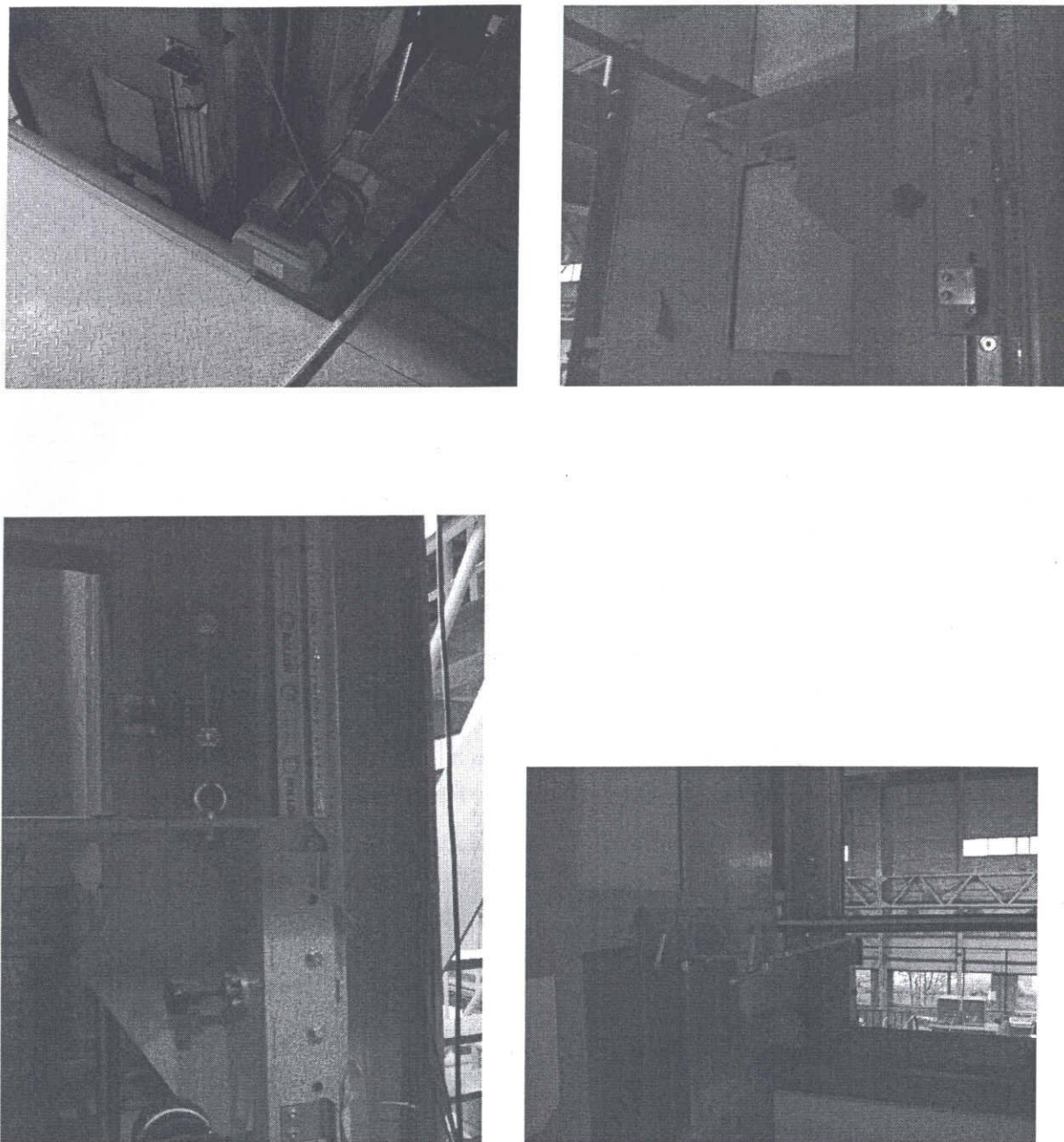


Figure 2.9 Photographs of traverse mechanism

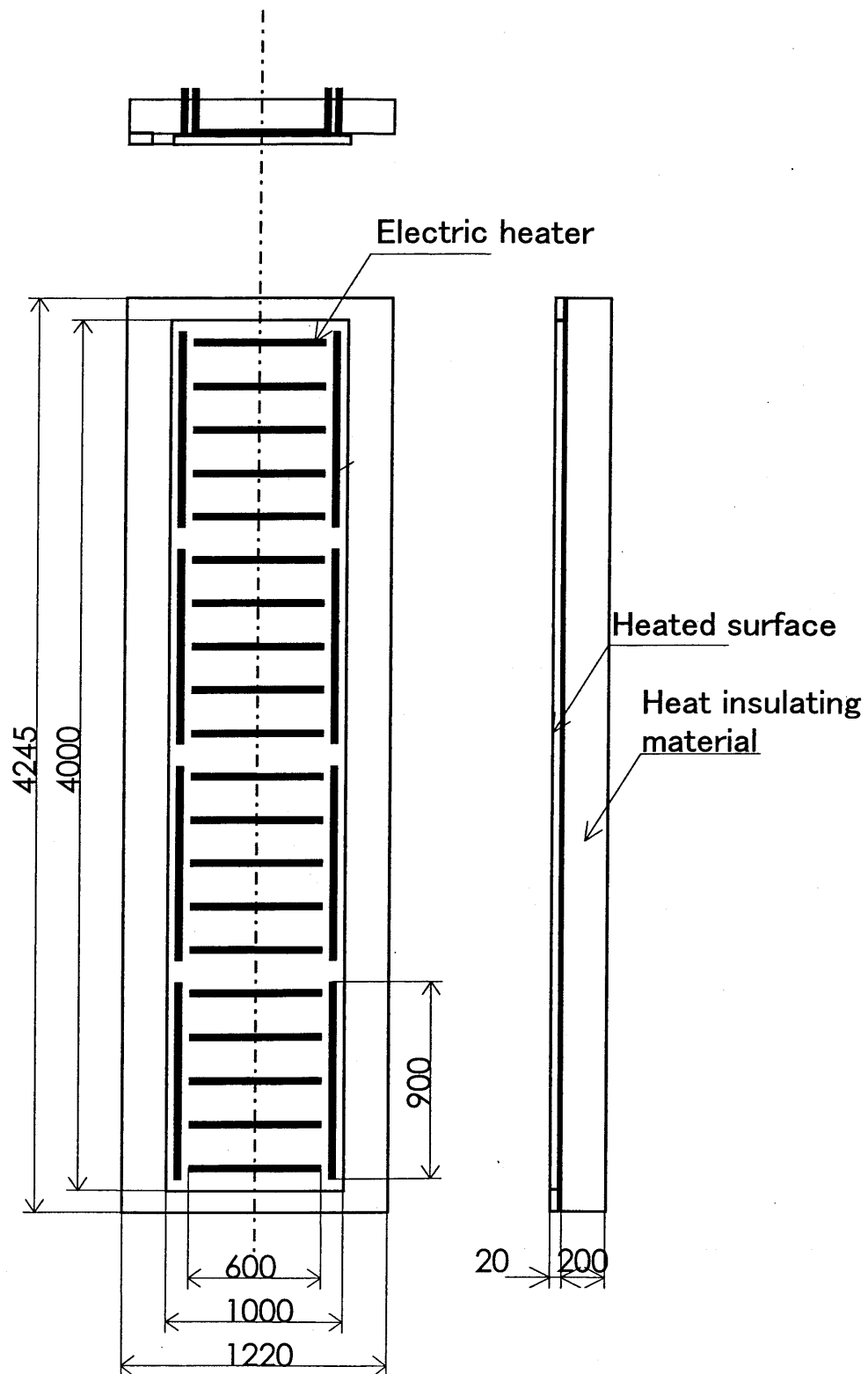


Figure 2.10 Schematics of heated plate



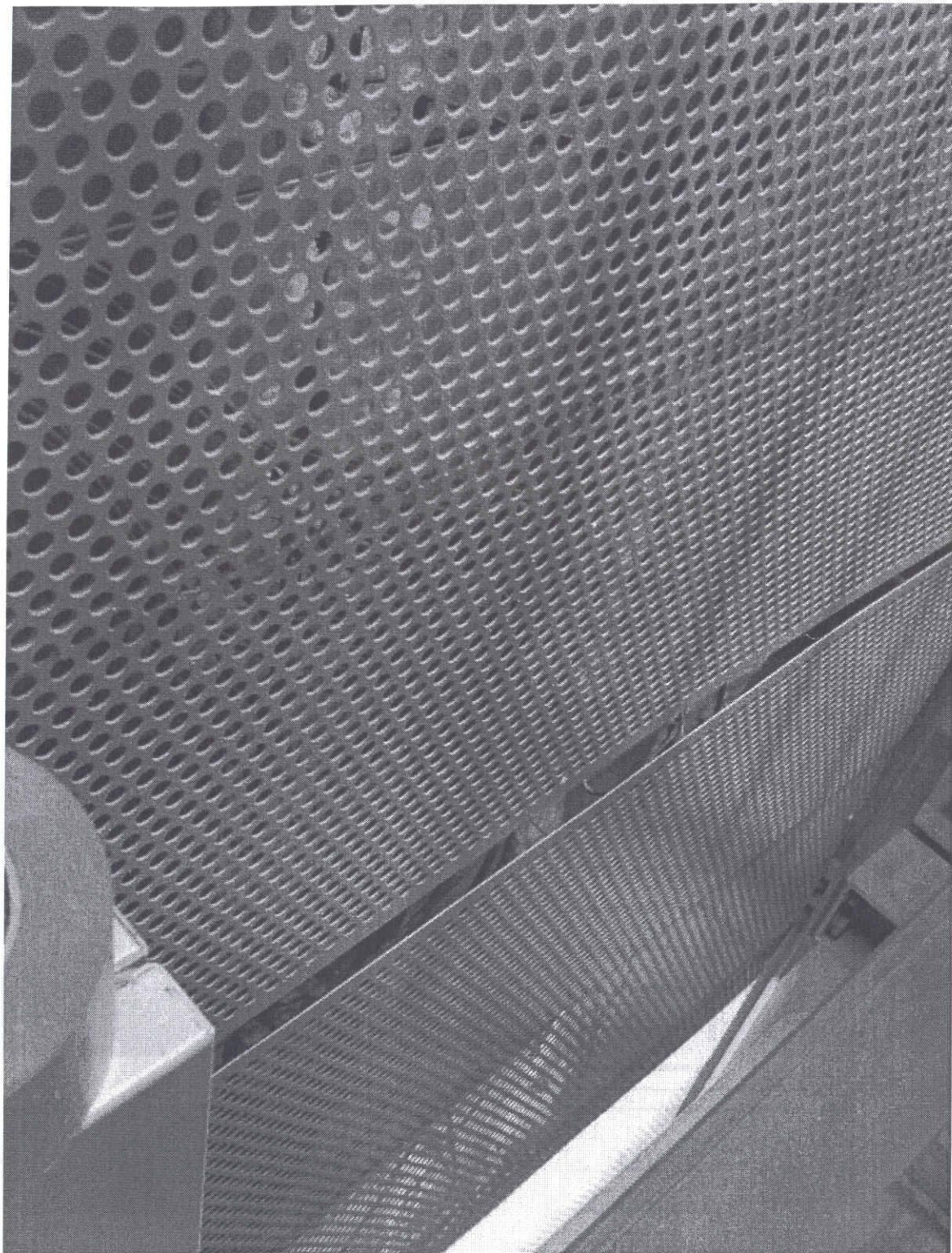
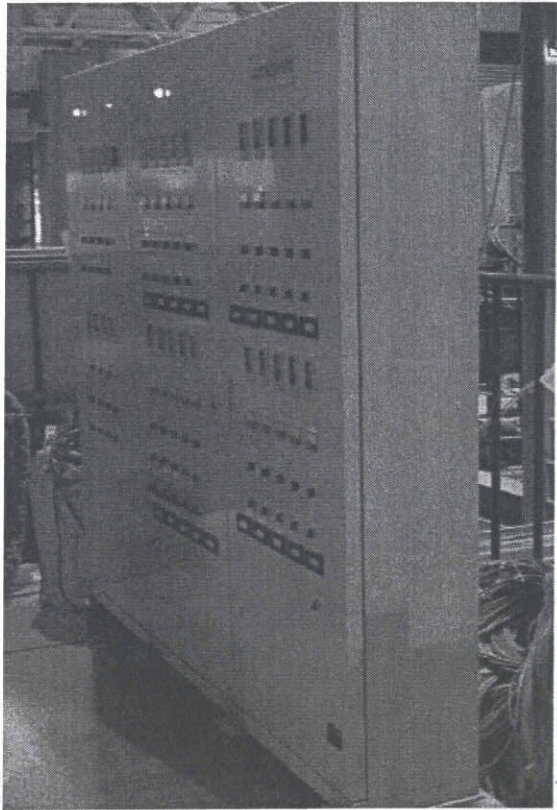
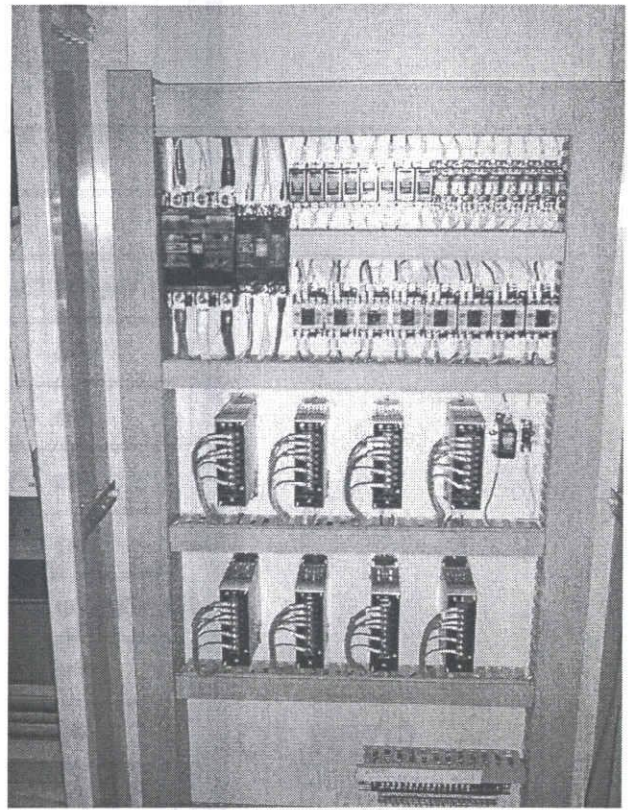


Figure 2.11 Photograph of back of heated plate (rear cover close)





(a) outside



(b) inside

Figure 2.12 Photographs of temperature controller system

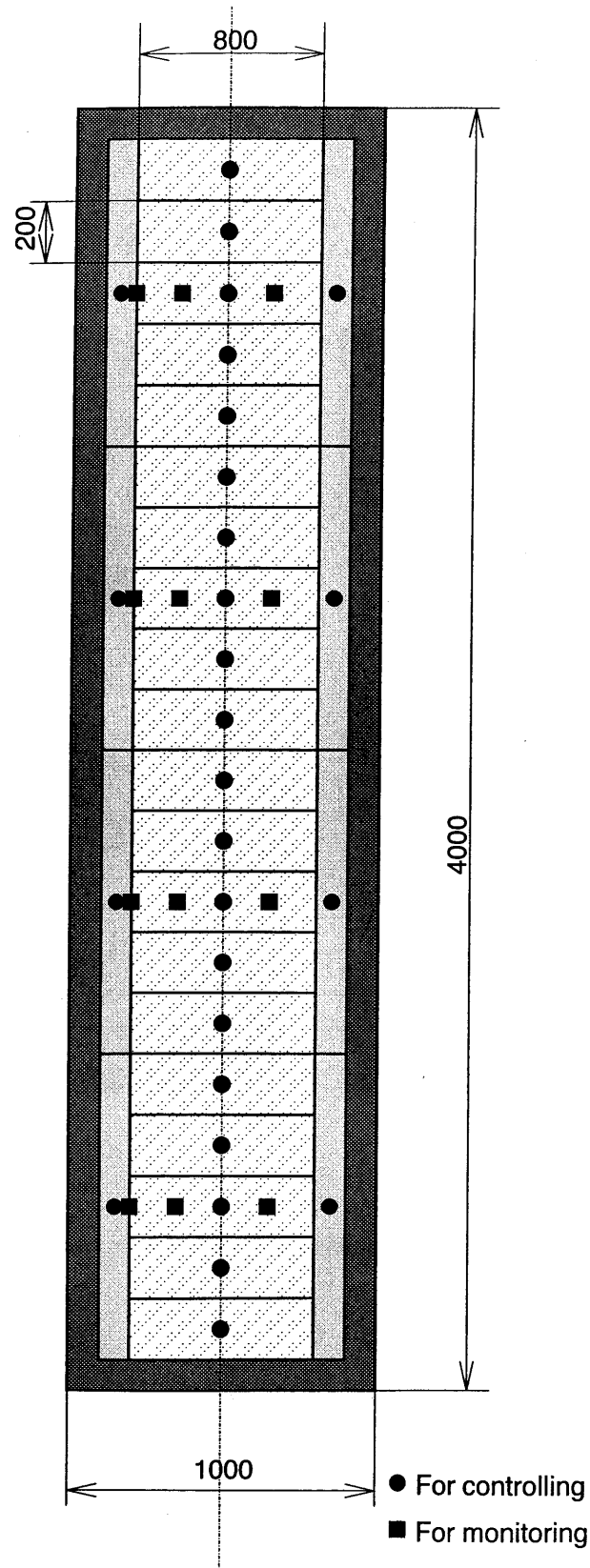


Figure 2.13 Locations of thermocouples for measuring surface temperature of heated plate



Heated surface

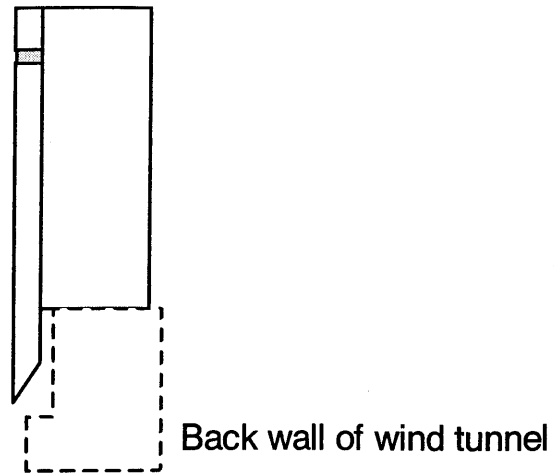


Figure 2.14 Details near leading edge of plate

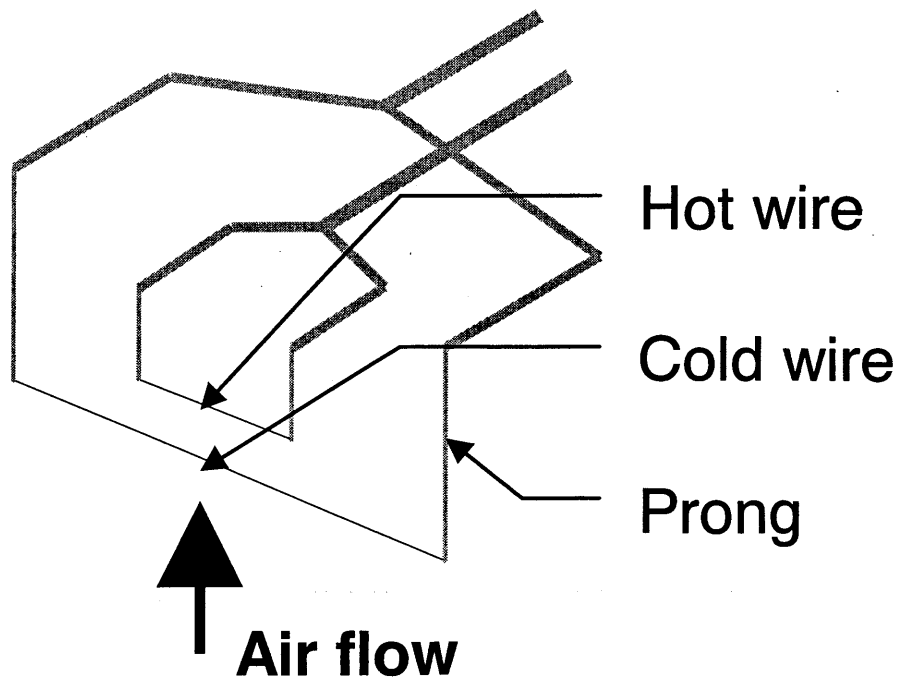


Figure 2.15 Schematics of hot and cold wire probe

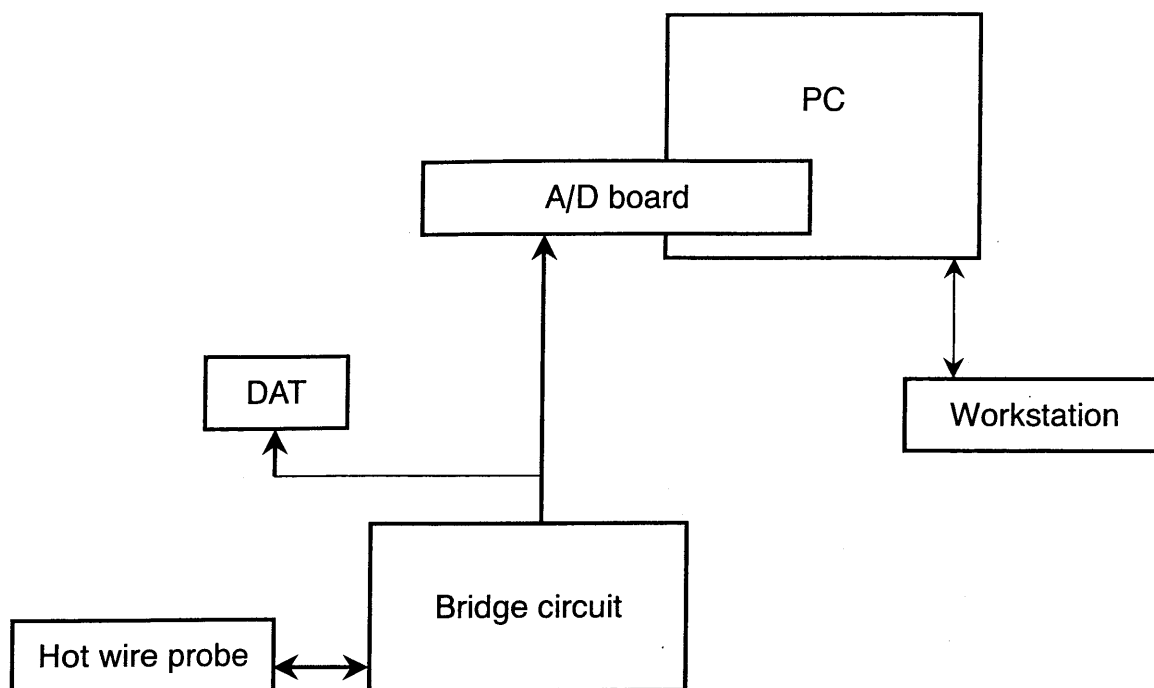


Figure 2.16 Hot wire measurement system

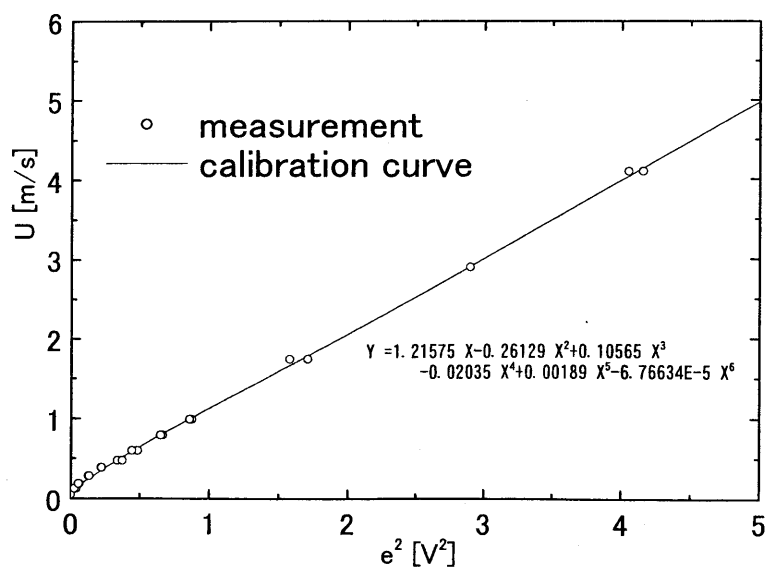


Figure 2.17 Example of calibration curve

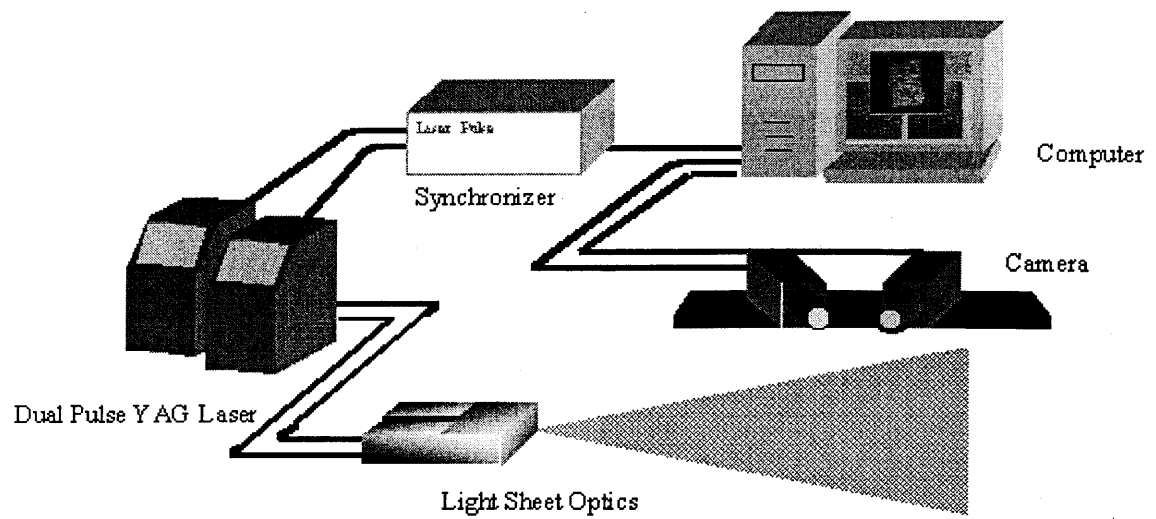
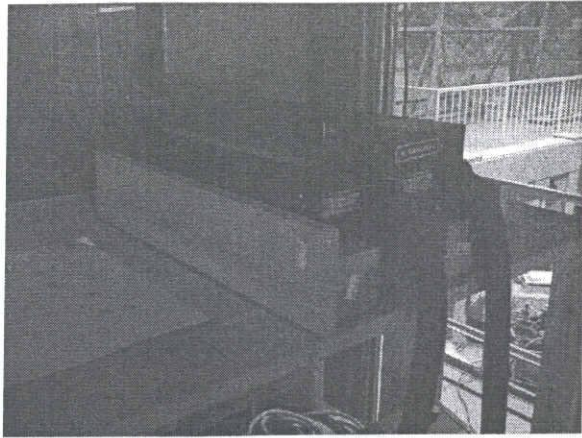
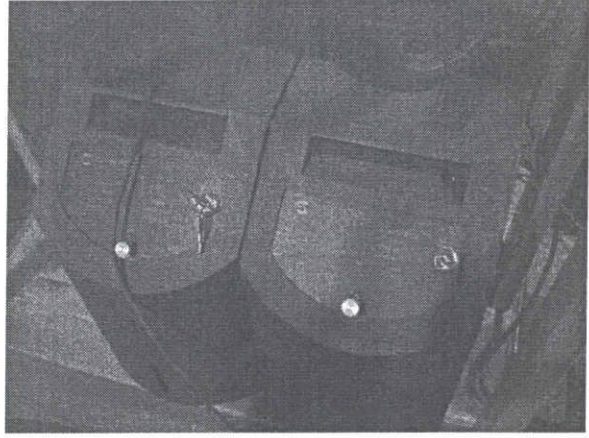


Figure 2.18 Schematics of PIV measurement system



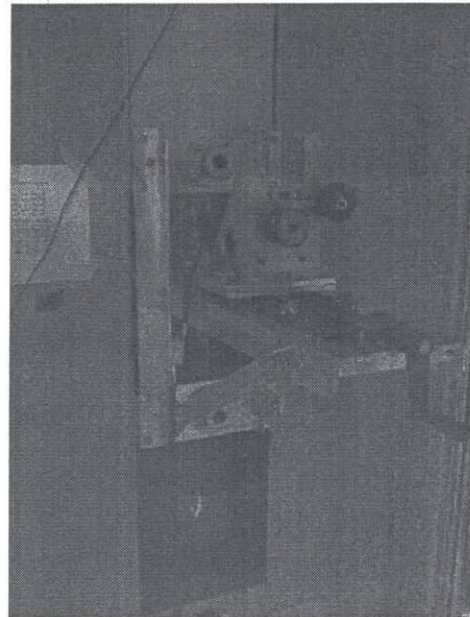
(a) YAG-LASER



(b) timing controller



(c) CCD camera



(d) particle feeder

Figure 2.19 Photographs of PIV system



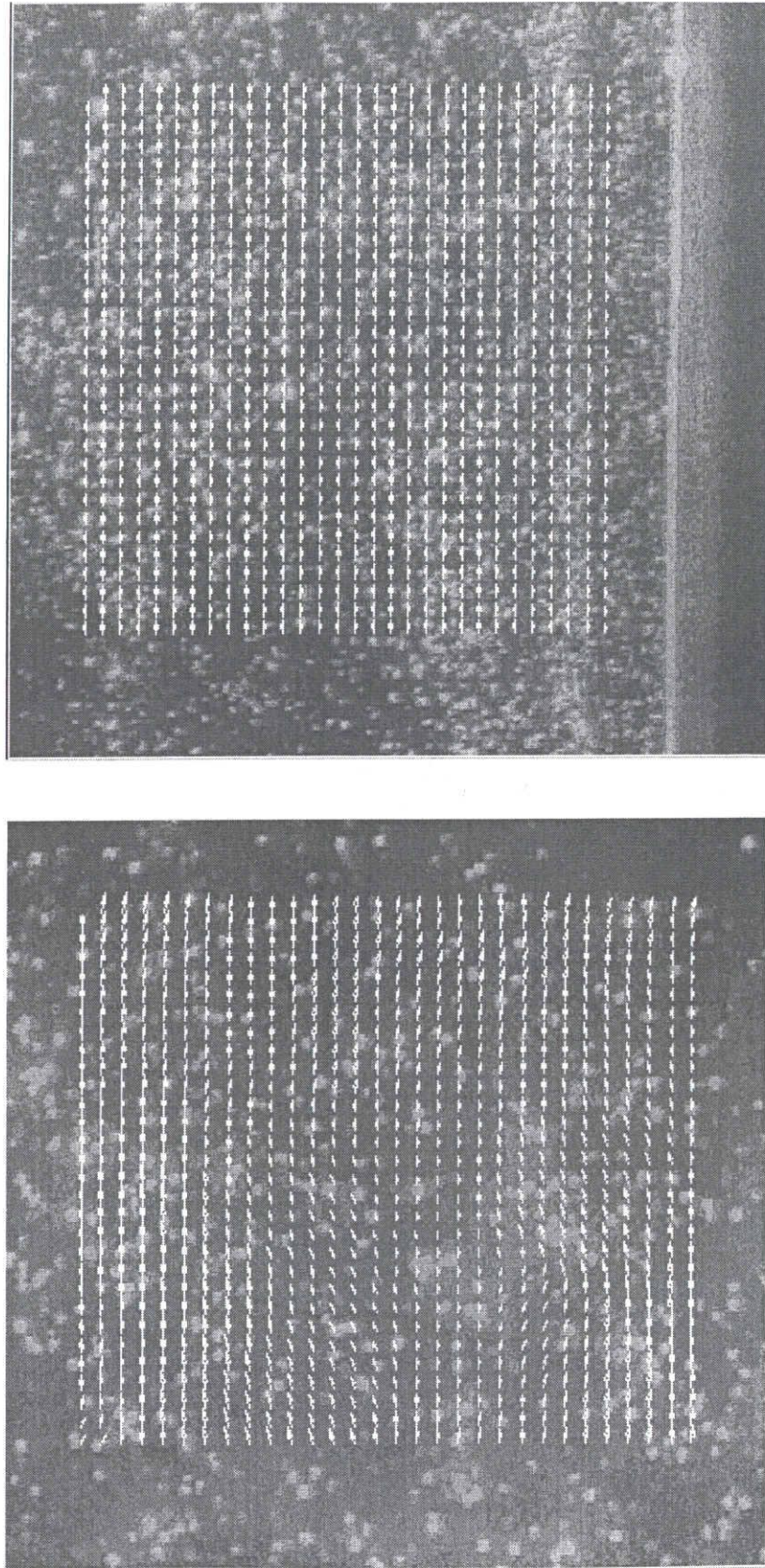


Figure 2.20 Examples of visualized images and calculated velocity vectors

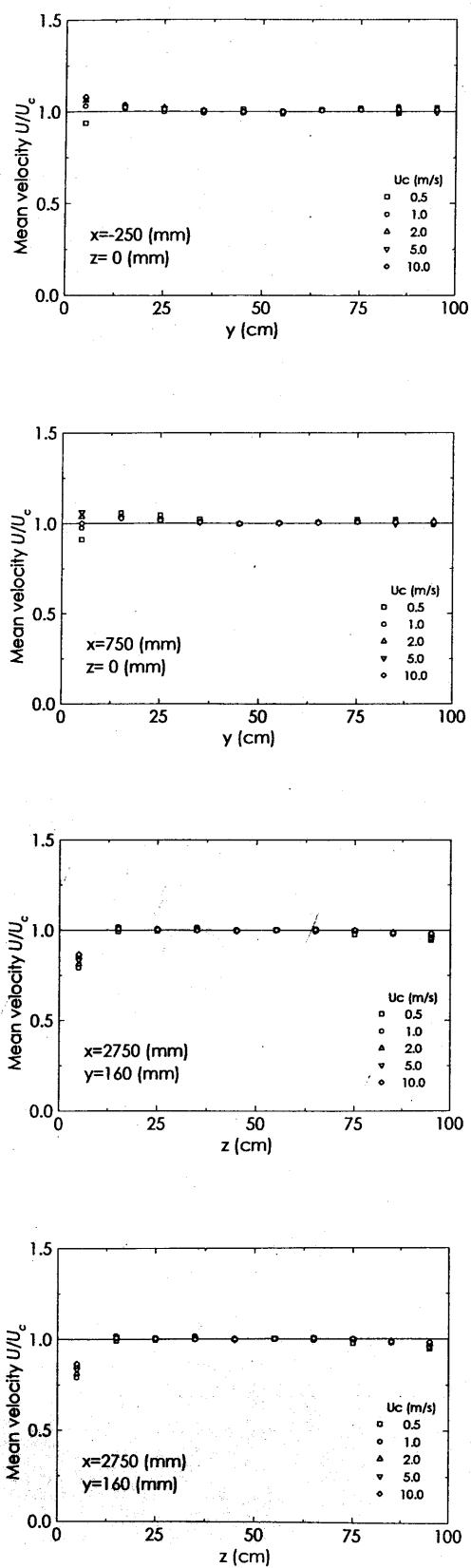


Figure 2.21 Freestream velocity profiles in test section

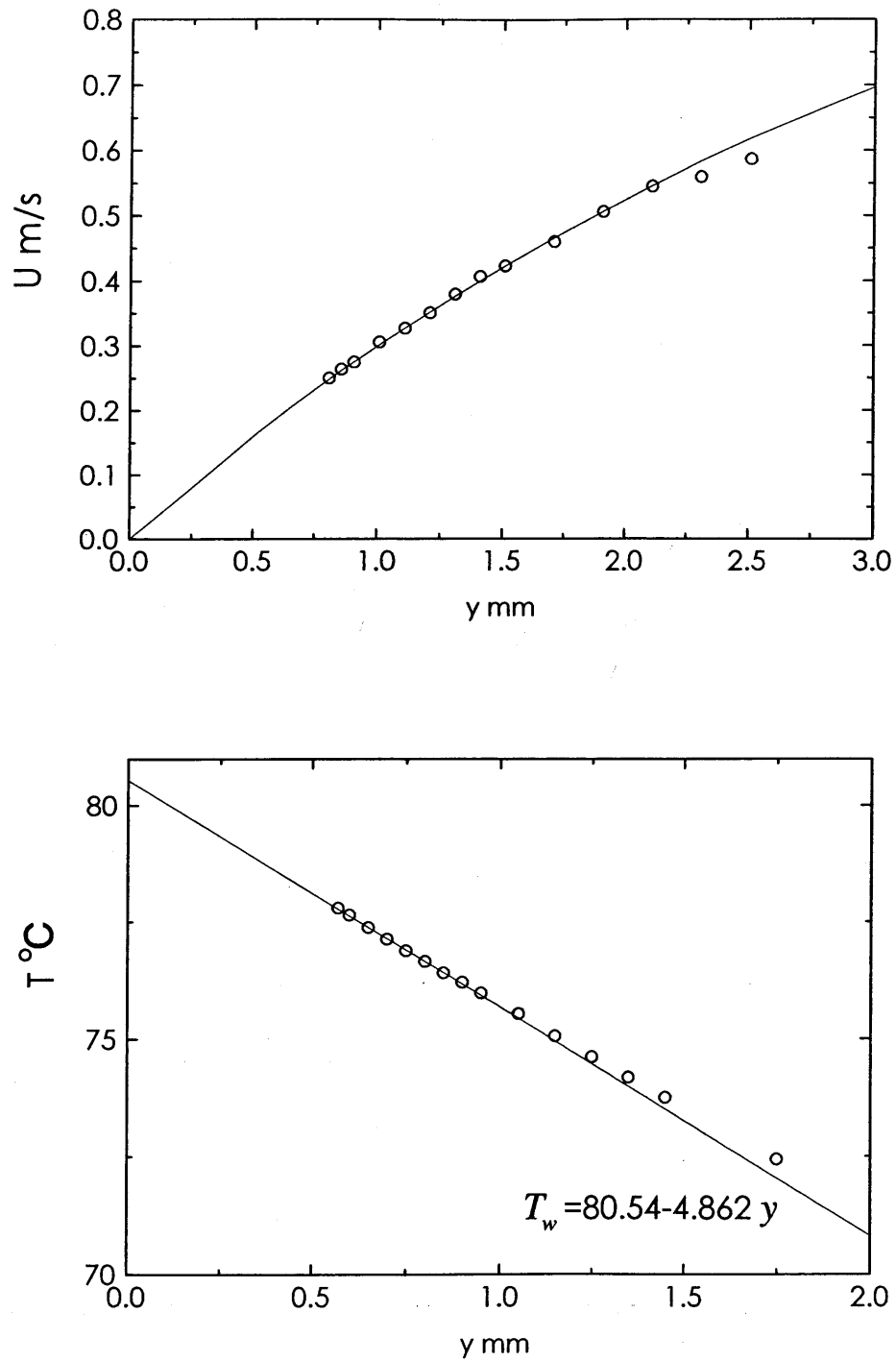


Figure 2.22 Mean velocity and temperature profiles near wall measured with hot and cold wires





# Chapter 3

## BASIC TURBULENT STATISTICS

### 3.1 Local Heat Transfer Rate

The variations in mean and turbulent quantities of the velocity and thermal fields with change in the turbulent boundary layer from natural convection to combined convection due to the introduction of freestream velocity were examined. The heat transfer rates were estimated from temperature gradients near the wall as described in Chap. 2. Local Nusselt numbers  $N_{ux}$  for various Grashof numbers are shown in Fig. 3.1. The value of  $N_{ux}$  is normalized with that of turbulent pure natural convection  $(N_{ux})_n$  (Tsuji and Nagano, 1988a), and  $Grx / Rex^3$  is taken as the coordinate.

It should be noted that for constant  $Grx$ , a decrease in  $Grx / Rex^3$  implies an increase in freestream velocity. On the other hand, if  $Grx / Rex^3$  and the thermal condition are constant, the change in  $Grx$  corresponds to that in  $x$ . Carey and Gebhart (1983) have suggested in their results over a range of local Richardson numbers  $Rix (= Grx / Rex^2)$  that it is difficult to determine the  $x$ -location of the initial instability occurrence for given thermal and fluid conditions because the value of  $Rix$  depends on the downstream distance  $x$ .

A drastic reduction in  $N_{ux}$  with increasing freestream velocity is observed, i.e.,  $N_{ux} / (N_{ux})_n$  decreases to about 0.4 at a value of  $Grx / Rex^3$  for a given  $Grx$ . When attention is paid to  $Grx / Rex^3 \simeq 10^{-3}$ ,  $N_{ux} / (N_{ux})_n$  decreases with decreasing  $Grx$  and takes the smallest

value at  $Grx = 1.05 \sim 1.10 \times 10^{11}$ . This signifies that  $Nux$  still remains at a high value in the region downstream of the location where the  $Nux$  reduction occurs with increasing freestream velocity.

A decrease in  $Nux$  with increasing freestream velocity in the combined-convection boundary layer along a vertical plate is also observed in the experiments with air of Hall and Price (1970), and Inagaki and Kitamura (1988). In their experiments, however, the minimum value of  $Nux / (Nux)_n$  remained at about 0.75, and the  $Nux$  reduction was not so abrupt as in the present experiment. The discrepancy between both results may be attributed to differences in the experimental setup and conditions. In their experiments, a test section with a small area was used and relatively large disturbances were involved in the freestream, which yielded a transition Reynolds number of a remarkably small value for pure forced convection. We made an effort to control freestream disturbances, and thus it is considered that the essential characteristics of the turbulent combined-convection boundary layer appeared more clearly.

## 3.2 Mean Velocity and Temperature Profiles

The changes in the streamwise mean velocity and mean temperature profiles in the boundary layer for  $Grx = 3.30 \sim 3.58 \times 10^{11}$  and  $Grx / Rex^3 = \infty \sim 3.75 \times 10^{-5}$  (corresponding to the freestream velocity of  $0 \sim 1.1$  m/s) are shown in Figs. 3.2 and 3.3, respectively. The mean velocity  $U$ , the mean temperature  $T$ , and the distance from the wall  $y$  are normalized as the similarity variables used for the laminar natural-convection boundary layer. Since  $Grx$  and  $x$  are almost constant, the abscissa  $\eta (= (y / x)Grx^{1/4})$  is directly proportional to the distance from the wall. As seen in these figures, the mean velocity and temperature profiles markedly change with the introduction of freestream velocity. With increasing freestream velocity, the thickness of the velocity and thermal boundary layers decreases, and the maximum mean velocity increases and its location approaches the wall. At  $Grx / Rex^3 =$

$1.65 \times 10^{-4}$ , the dimensionless value of the maximum mean velocity which is 0.41 at  $Grx / Rex^3 = 1.15 \times 10^{-4}$  reaches 0.58 with a slight increase in freestream velocity, at which point a sudden decrease in the local heat transfer rate occurs, as shown in Fig. 3.1. Thus, the change in  $Nux$  is closely related with those in the mean velocity and mean temperature.

For  $Grx / Rex^3 = 3.75 \times 10^{-5}$ , the laminar combined-convection boundary layer was calculated numerically, and the profiles of velocity and temperature are plotted by solid lines in Figs. 3.2 and 3.3, respectively. The measurements conform well to the calculated results for the laminar boundary layer. Judging from the behavior of turbulent quantities to be discussed below, it is concluded that the combined-convection boundary layer changes from turbulent to laminar with a slight increase in freestream velocity, and that the location of the transition to the turbulent boundary layer shifts farther downstream.

Krishnamurthy and Gebhart (1989) reported that the transition to turbulence in the combined-convection boundary layer was fairly delayed in comparison with that in pure natural convection. In addition, recently, Abu-Mulaweh, Chen and Armaly (2000) also measured the turbulent quantities with a laser Doppler velocimeter and a cold-wire anemometer, and obtained a similar conclusion. Therefore, such a laminarization of the combined-convection boundary layer may be regarded as a phenomenon caused by the delay of transition.

### 3.3 Intensities of Velocity and Temperature Fluctuations and Turbulent Heat Flux

Figure 3.4 shows the intensity profiles of streamwise velocity fluctuation  $u$  normalized by the maximum mean velocity  $U_m$  in the transition from turbulence to laminar. In the turbulent natural-convection boundary layer, the maximum intensity of velocity fluctuation occurs at a location  $\eta \simeq 25$  beyond the maximum mean velocity location  $\eta \simeq 3$ . This intensity profile is peculiar to the turbulent natural-convection boundary layer (Tsuji and Nagano, 1988a;

1988b). With the addition of freestream velocity ( $Grx / Rex^3 = 4.68 \times 10^{-4}$ ), the intensity of the velocity fluctuation begins to decrease in the entire boundary layer region, although the profile is similar to that in the natural-convection boundary layer.

In the range of  $Grx / Rex^3 = 1.65 \times 10^{-4} \sim 1.05 \times 10^{-4}$ , the intensity profile varies remarkably in accordance with the changes in the local heat transfer rate and mean velocity profile, as mentioned previously. At  $Grx / Rex^3 = 1.65 \times 10^{-4}$ , a fluctuation intensity larger than that in pure natural convection appears at the maximum mean velocity location ( $\eta \simeq 1.5$ ). Moreover, at  $Grx / Rex^3 = 1.15 \times 10^{-4}$  and  $1.05 \times 10^{-4}$ , the intensity profile of the velocity fluctuation decreases and takes two peaks with an infinitesimal value near the maximum mean velocity location. The occurrence of such a two-peak profile was also observed for different  $Grx$  values. In the initial phase of the transition in combined convection, it is confirmed by the linear instability analysis of Carey and Gebhart (1983) and the experiment of Krishnamurthy and Gebhart (1989) that the intensity of the velocity fluctuation has two peaks, with an infinitesimal value at the maximum mean velocity location. Therefore, the appearance of a fluctuation intensity profile having two peaks clearly characterizes the transition of the combined-convection boundary layer.

With a further increase in freestream velocity ( $Grx / Rex^3 = 3.75 \times 10^{-5}$ ), the intensity of the velocity fluctuation becomes extremely small with the laminarization of the boundary layer. As the freestream velocity becomes sufficiently large ( $Grx / Rex^3 < 10^{-6}$ ), the boundary layer changes again to turbulence, and the turbulent characteristics of forced convection appear.

In general, turbulent energy is mainly produced through mean shear motion. However, in the combined-convection boundary layer, the intensity of the velocity fluctuation decreases despite a mean velocity gradient that is larger than in turbulent pure natural convection, as shown in Fig. 3.2. It has been found that the near-wall turbulence structure of natural convection differs significantly from those of forced convection (Tsuji and Nagano, 1992a). The occurrence of laminarization and the peculiar intensity profile of the velocity

fluctuation with the addition of freestream velocity will also reveal the inherent difference between the structures of natural and forced convection.

The changes in the intensity of temperature fluctuation  $t$  with the transition from turbulence to laminar are shown in Fig. 3.5, being normalized by the temperature difference between the surface temperature  $T_w$  and the ambient temperature  $T_\infty$ . The intensity of temperature fluctuation varies rapidly with the increase in freestream velocity, keeping step with the change in the velocity fluctuation intensity. The increasing and decreasing tendencies in the maximum intensity of temperature fluctuation have a close resemblance to those of the velocity fluctuation. At  $Grx / Rex^3 = 4.68 \times 10^{-4}$ , the intensity profile of the temperature fluctuation shows no great difference from that in pure natural convection. However, with increasing  $Grx / Rex^3$ , the temperature fluctuation intensity decreases, and the location of the maximum intensity gradually approaches the maximum mean velocity location. At  $Grx / Rex^3 = 3.75 \times 10^{-5}$ , the intensity of the temperature fluctuation as well as that of the velocity fluctuation becomes extremely small. Thus, the two-peak profiles did not appear in the temperature fluctuation intensity.

Figure 3.6 shows the streamwise turbulent heat flux  $\overline{uT}$ , which represents the turbulent generation due to the buoyancy, normalized by the maximum mean velocity and the temperature difference. The turbulent heat flux in the natural-convection boundary layer shows a positive peak at the maximum mean velocity location and takes small negative values near the wall. With the addition of freestream velocity ( $Grx / Rex^3 = 4.68 \times 10^{-4}$ ),  $\overline{uT}$  decreases at the maximum mean velocity location and increases in the negative value near the wall. The value of  $Nux$ , however, remains that of pure natural convection. At  $Grx / Rex^3 = 1.65 \times 10^{-4}$ , the value of  $\overline{uT}$  increases again at the maximum mean velocity location, whereas the negative value of  $\overline{uT}$  decreases near the wall. Then, the value of  $Nux$  becomes larger than that in turbulent pure natural convection, as seen in Fig. 3.1. With a further increase in freestream velocity ( $Grx / Rex^3 = 1.05 \times 10^{-4}$ ), the profile of turbulent heat flux takes a zero crossing at the maximum mean velocity location from negative values near the

wall to positive values. At  $Gr_x / Re_x^3 = 3.75 \times 10^{-5}$ , the  $\overline{u\tau}$  value also becomes almost zero in the entire boundary layer region.

As mentioned above, turbulent quantities observed in the combined-convection boundary layer suddenly change with a slight increase in freestream velocity. It seems to be very difficult to correctly predict such a behavior of turbulent combined convection with existing turbulence models. Although the accumulation of experimental data for turbulent combined convection remains paramount, some improvement in turbulence models will be also required.

### 3.4 Waveforms and Spectra of Velocity and Temperature Fluctuations

Figures 3.7 display the waveforms of velocity fluctuation  $u$  and temperature fluctuation  $t$  measured at the near-wall location where the mean velocity becomes about half the maximum mean velocity, at the maximum mean velocity location, and at the location in the outer region where the mean velocity becomes a middle value between the maximum and freestream velocities, respectively. In the case of turbulent pure natural convection, long-period waves indicating large-scale fluid motion are dominant in both the velocity and thermal fields. Though the waveforms at  $Gr_x / Re_x^3 = 4.68 \times 10^{-4}$  are still similar to those of pure natural convection, large-amplitude and high-frequency waveforms appear at  $Gr_x / Re_x^3 = 1.65 \times 10^{-4}$ , which correspond to the temporal increases in the intensities of velocity and temperature fluctuations near the wall, as shown in Figs. 3.4 and 5. With a further increase in freestream velocity, the waveforms become smaller in amplitude, vary from random to harmonic with a specific frequency, and almost disappear at  $Gr_x / Re_x^3 = 3.75 \times 10^{-5}$ .

Figure 3.8 depicts the power spectra of velocity and temperature fluctuations, which are observed at the near-wall (solid line), at the maximum mean velocity location (broken line), and at the location in the outer region (dotted line), respectively. In the pure natural-

convection boundary layer, fluctuations of several Hz are observed near the wall, and a large-scale fluid motion of a frequency lower than 1 Hz dominates in the outer region. With a slight addition of a freestream, the scale of fluid motion begins to change. At  $G_{rx} / R_{ex}^3 = 4.68 \times 10^{-4}$ , the low frequency fluctuation suddenly decays, and the fluctuations in the frequency range of 1 to 10 Hz become evident over the whole boundary-layer region. As the freestream velocity increases ( $G_{rx} / R_{ex}^3 = 1.65 \times 10^{-4}$ ), the frequency of the most energetic fluctuation shifts toward the higher frequency region. Then, the spectrum at the maximum mean velocity location assembles at a specific frequency of 9 Hz. When laminarization is approached ( $G_{rx} / R_{ex}^3 = 1.05 \times 10^{-4}$ ), spectrum peaks appear at the fundamental frequency of 9 Hz and its harmonic, which may imply that the linear fluid motions control the boundary layer.

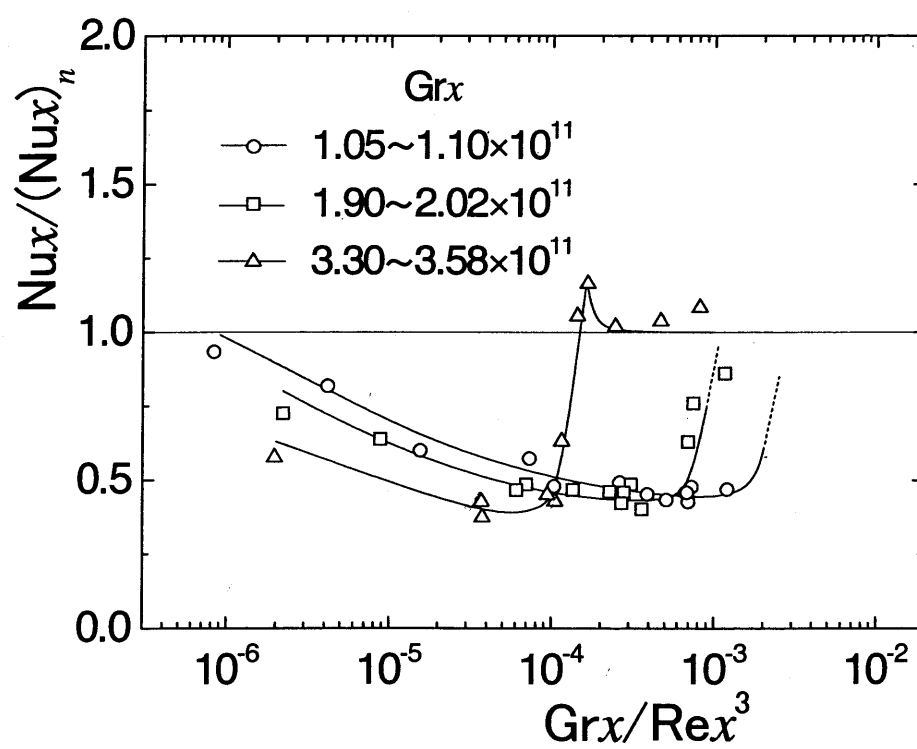
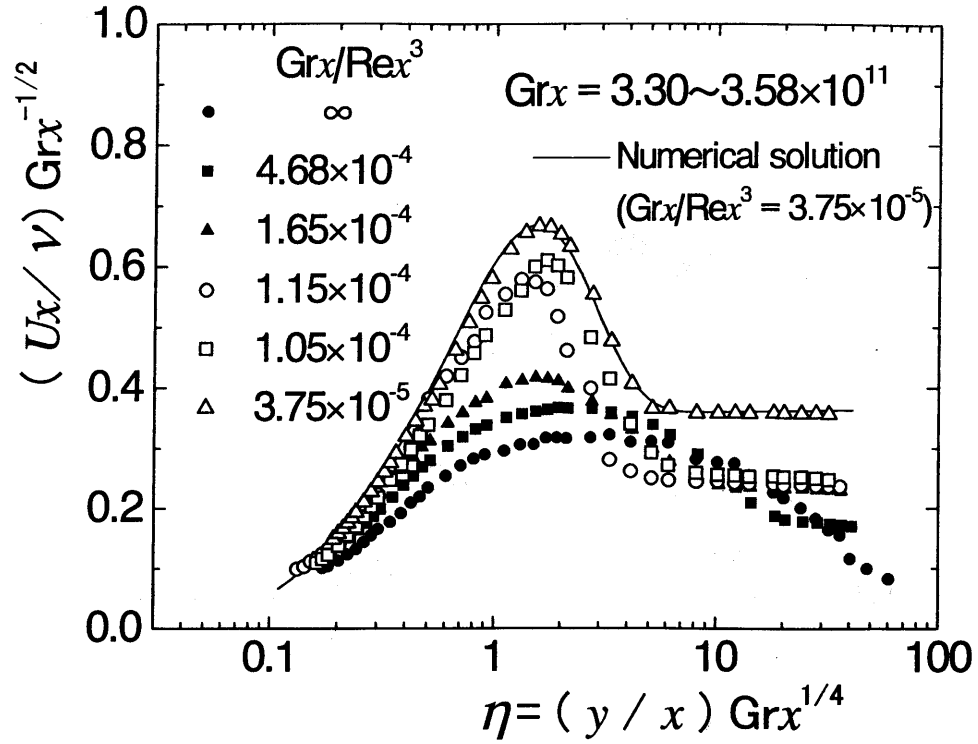
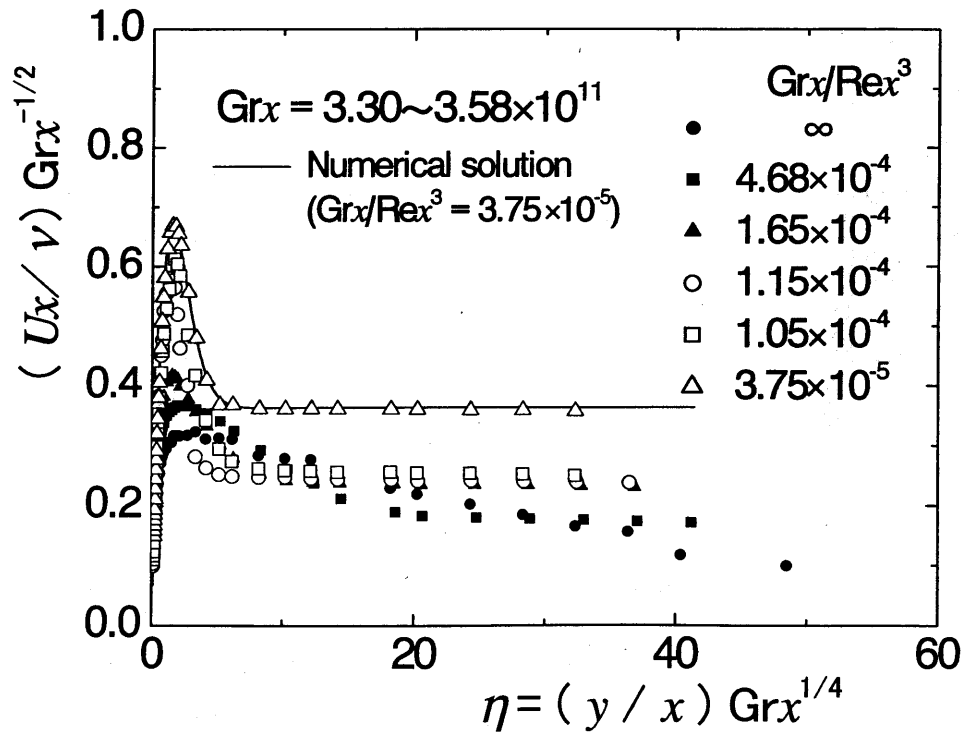


Figure 3.1 Local heat transfer rates of turbulent combined-convection boundary layer



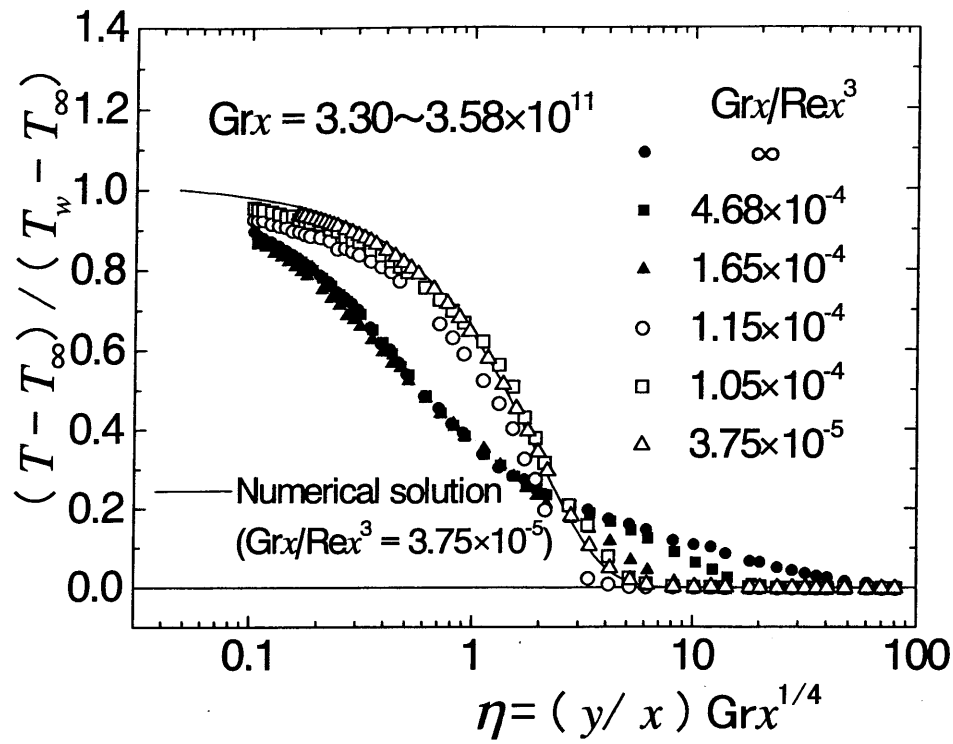


(a) semi-logarithmic scale

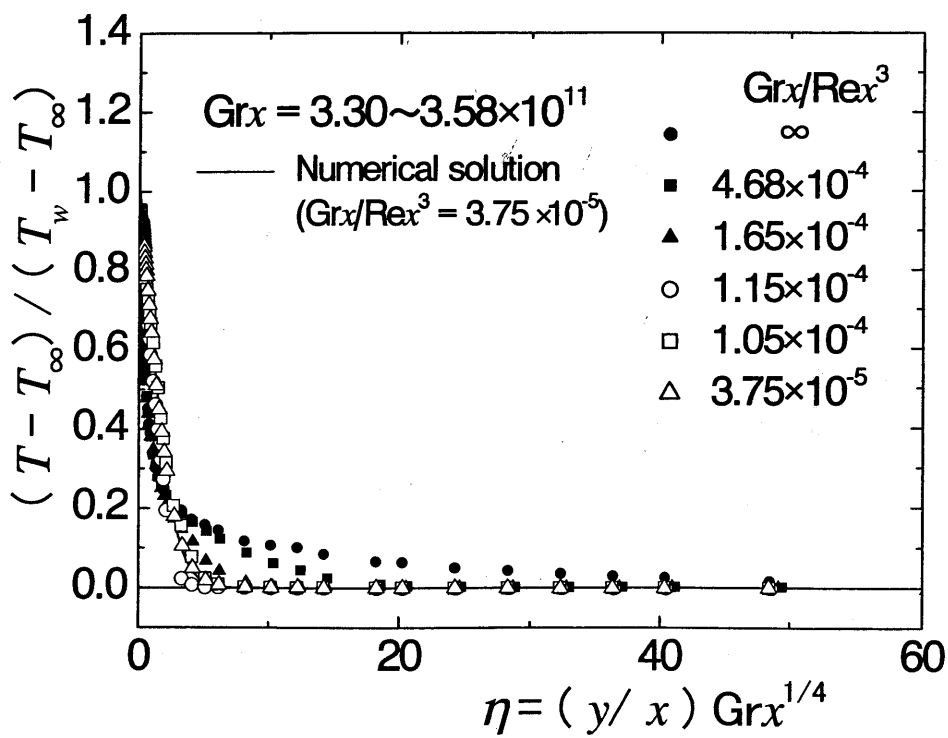


(b) linear scale

Figure 3.2 Change in mean velocity profile with increase in aiding freestream velocity

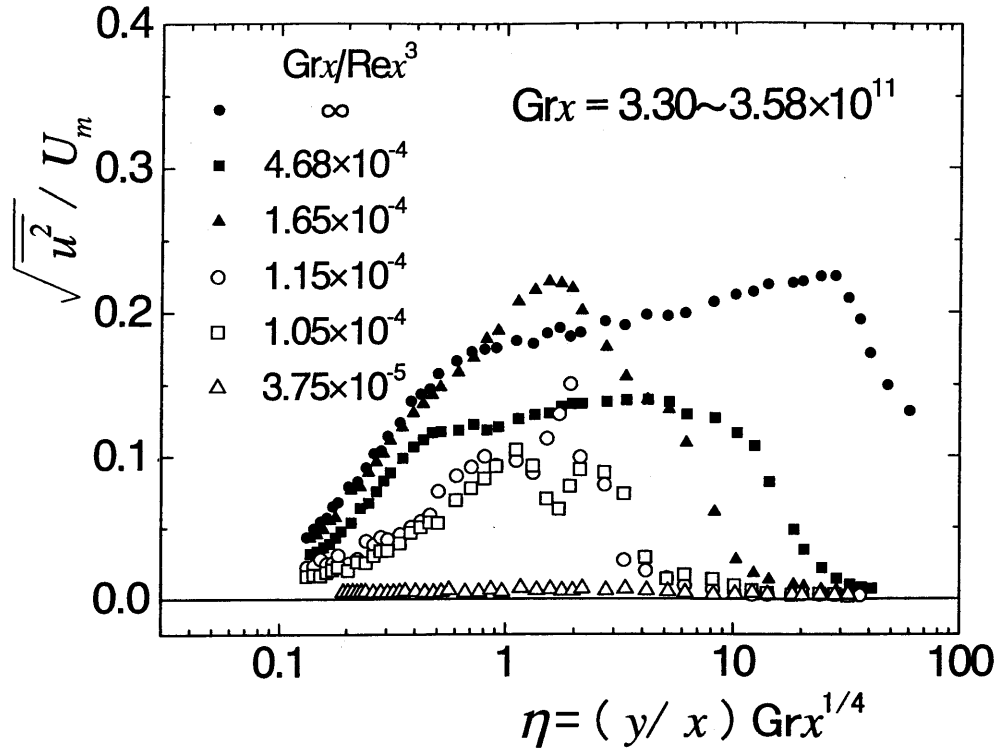


(a) semi-logarithmic scale

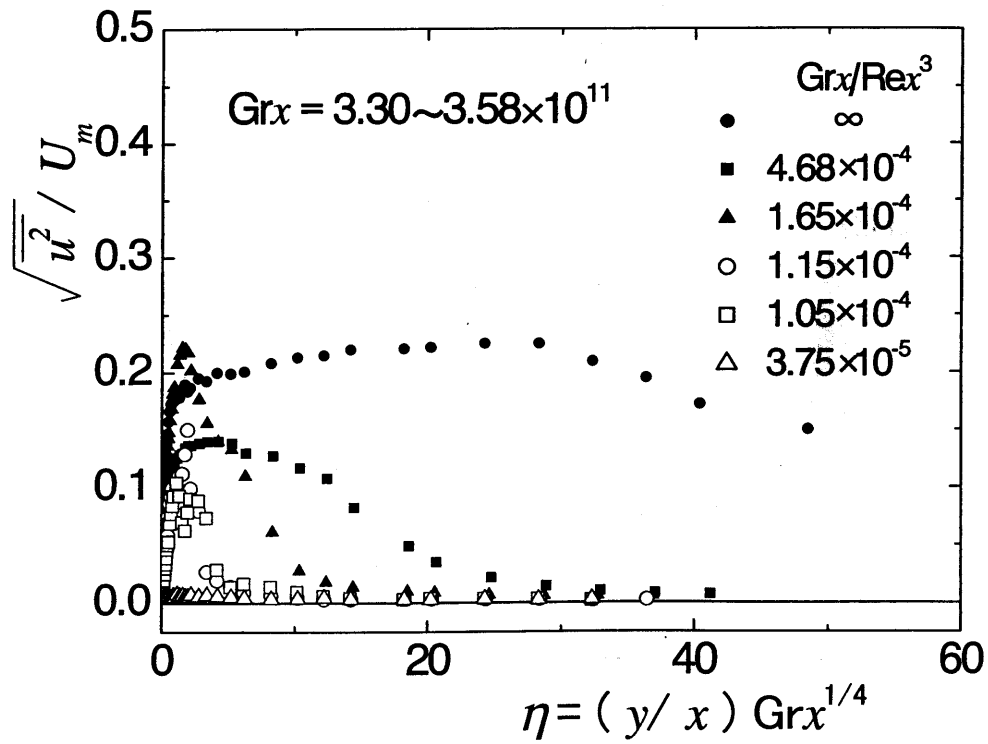


(b) linear scale

Figure 3.3 Change in mean temperature profile with increase in aiding freestream velocity

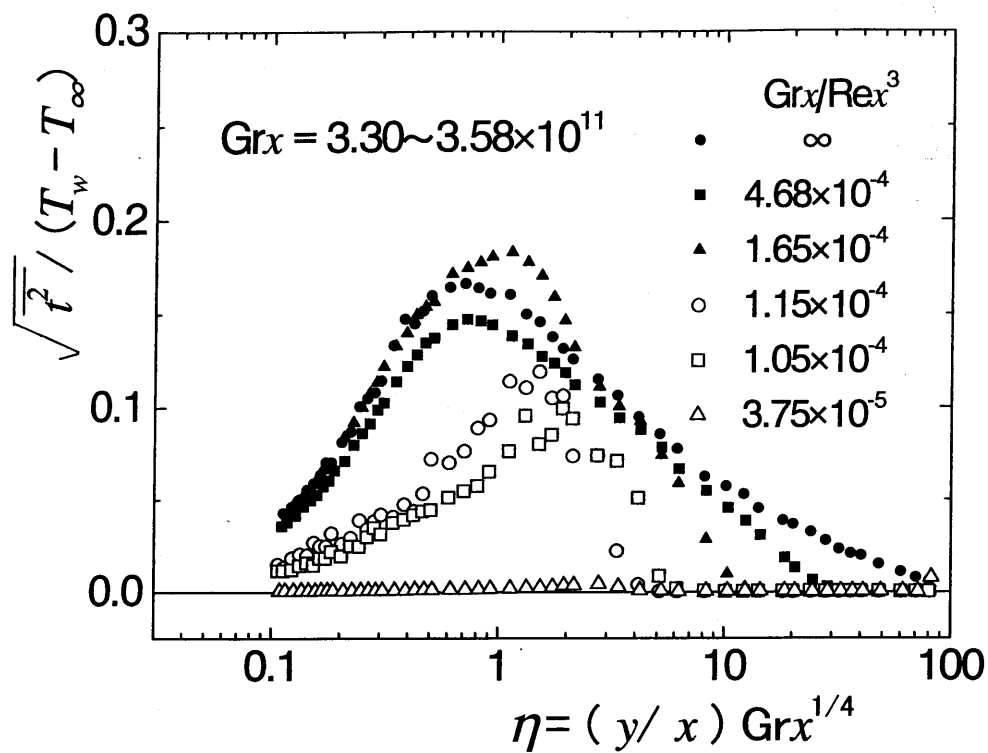


(a) semi-logarithmic scale

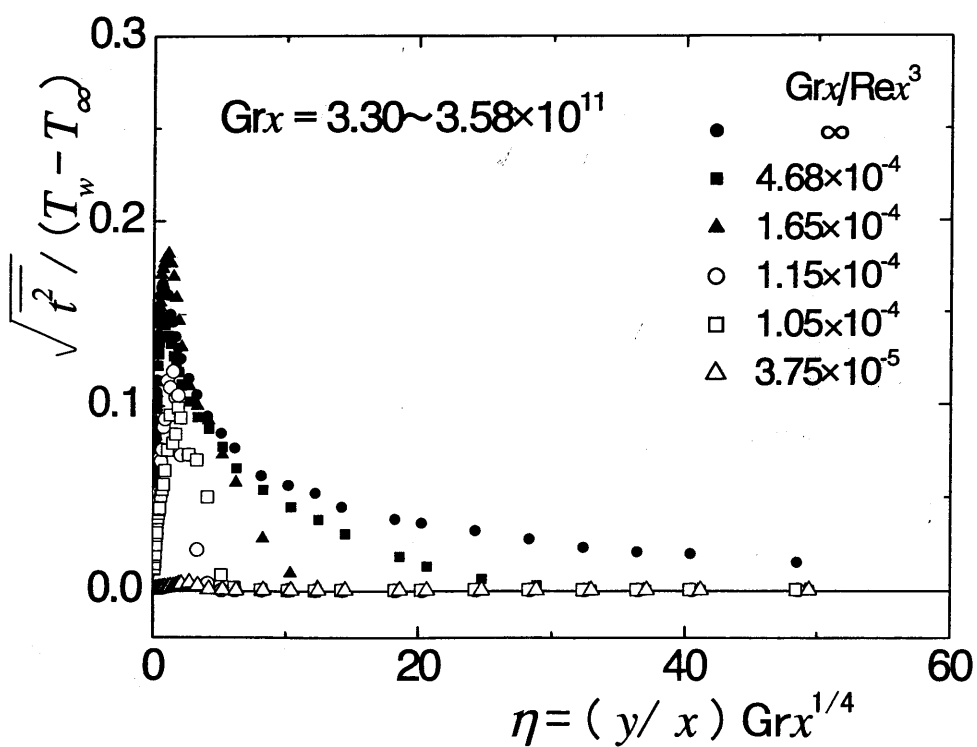


(b) linear scale

Figure 3.4 Change in intensity of streamwise velocity fluctuation with increase in aiding freestream velocity

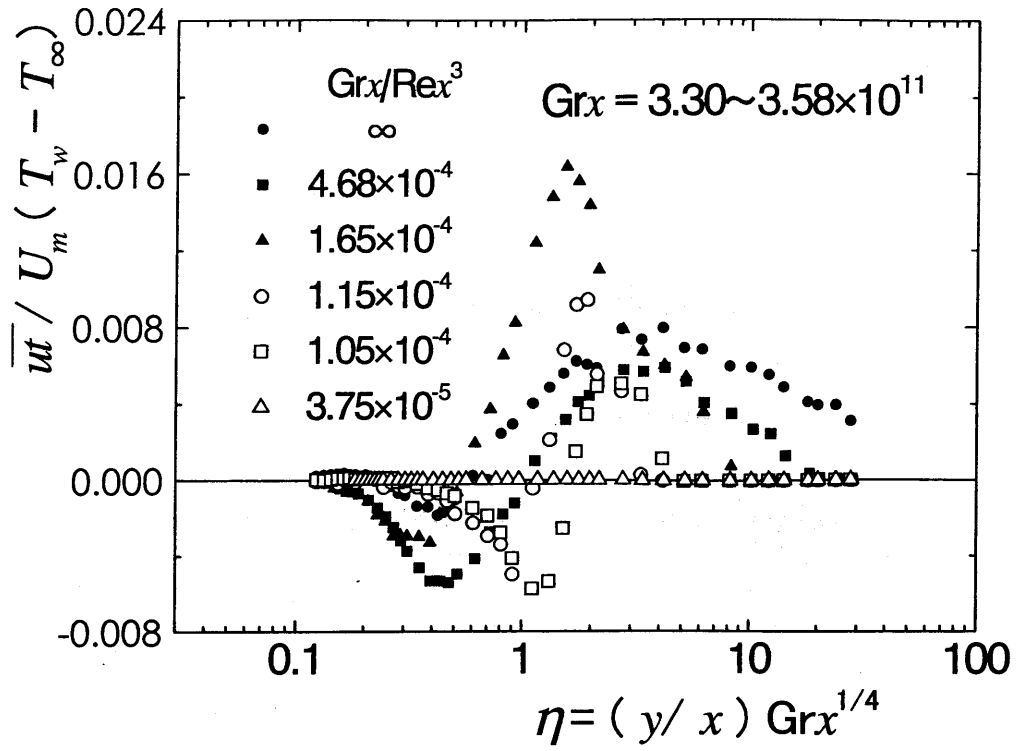


(a) semi-logarithmic scale

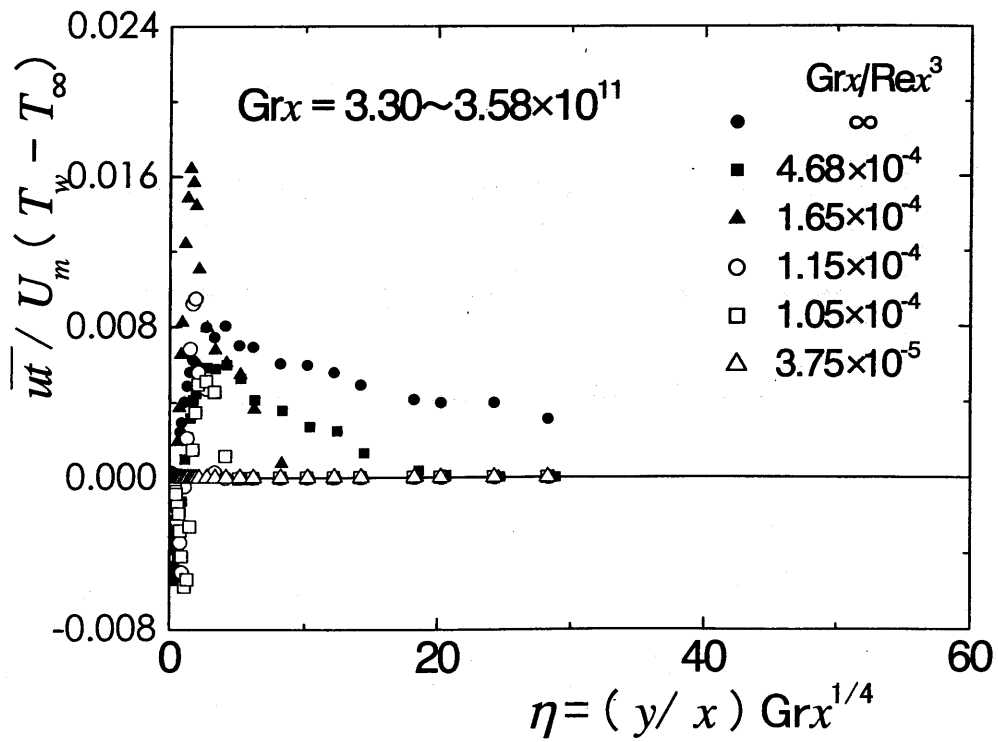


(b) linear scale

Figure 3.5 Change in intensity of temperature fluctuation with increase in aiding freestream velocity

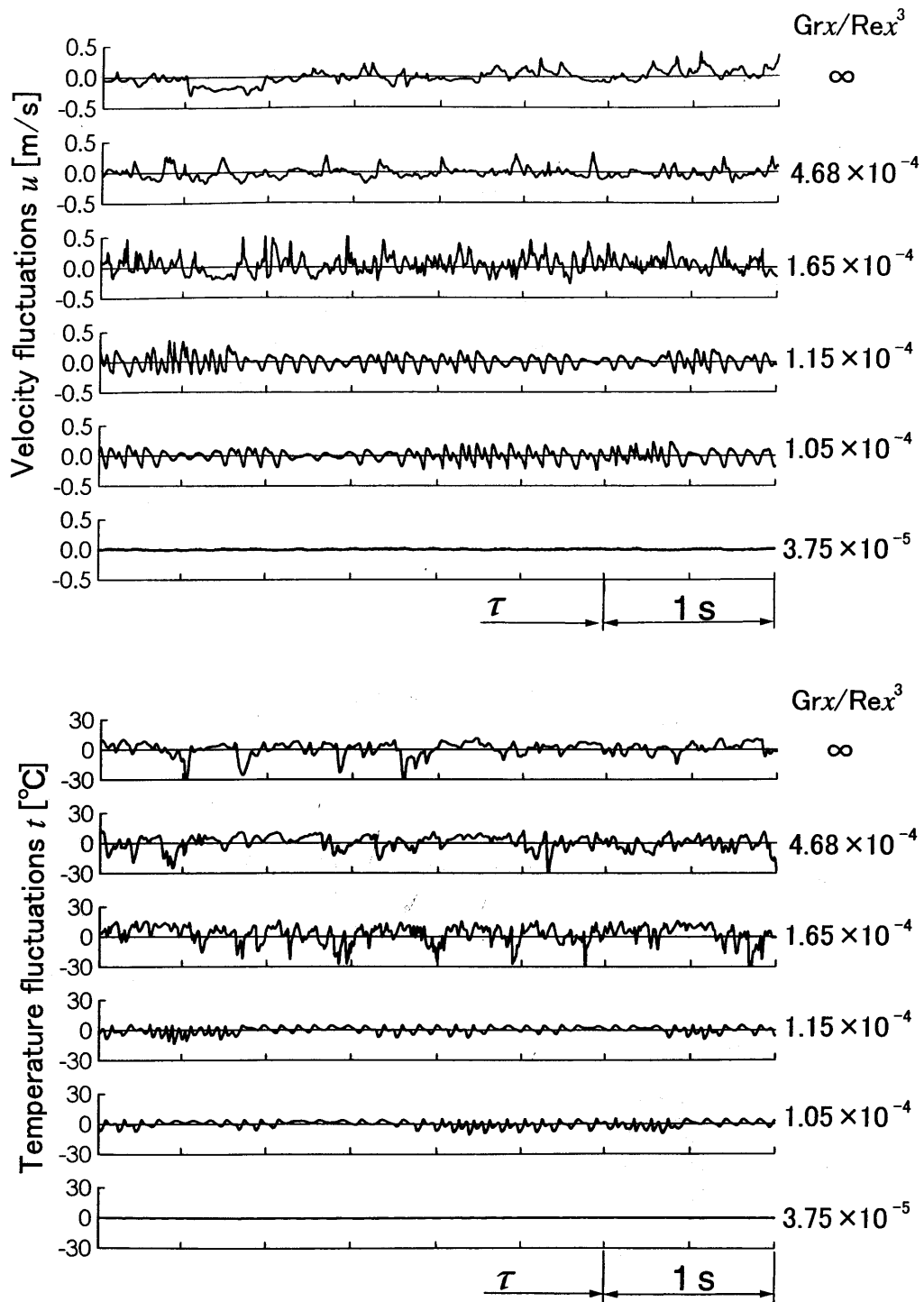


(a) semi-logarithmic scale



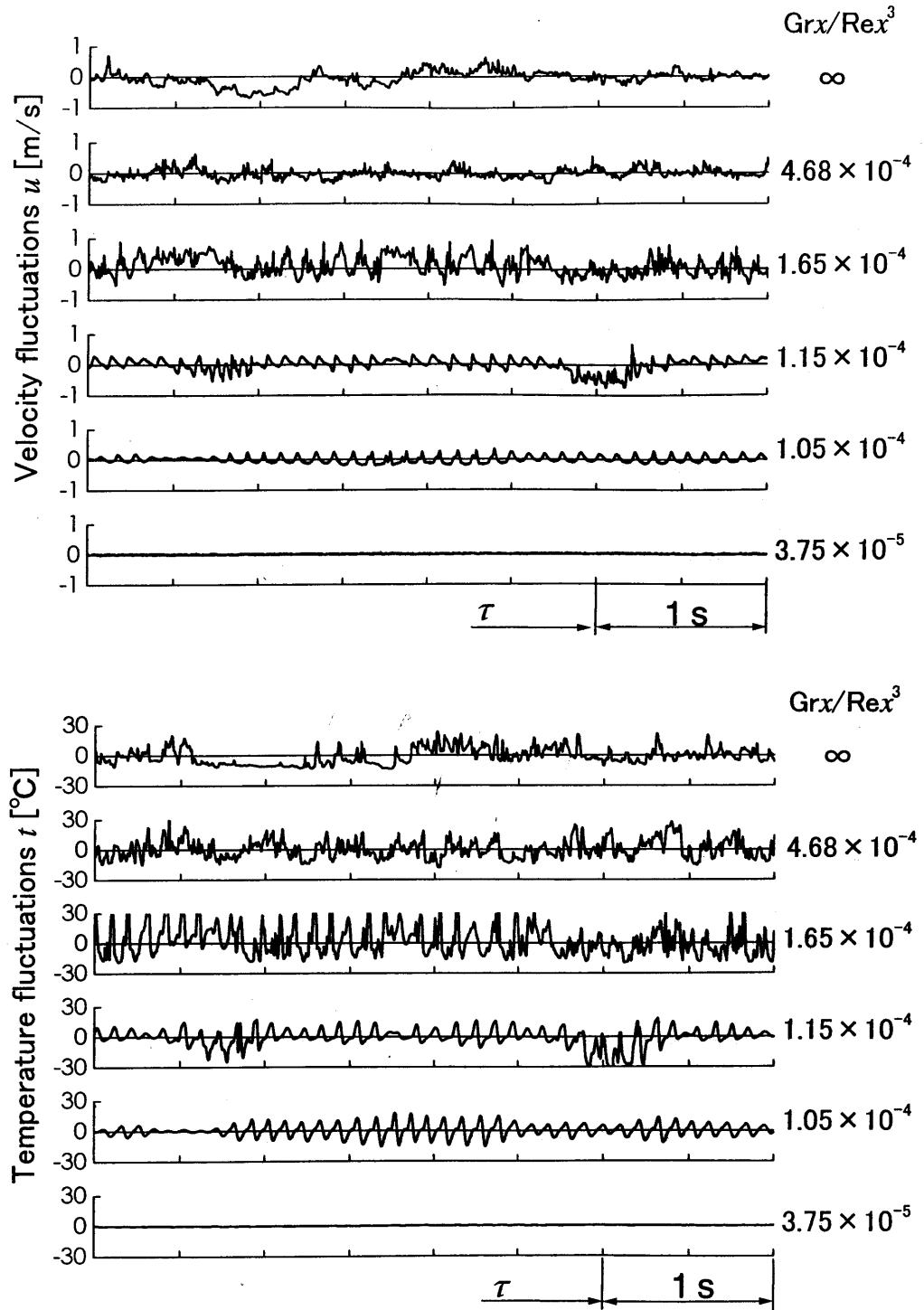
(b) linear scale

Figure 3.6 Change in turbulent heat flux with increase in aiding freestream velocity



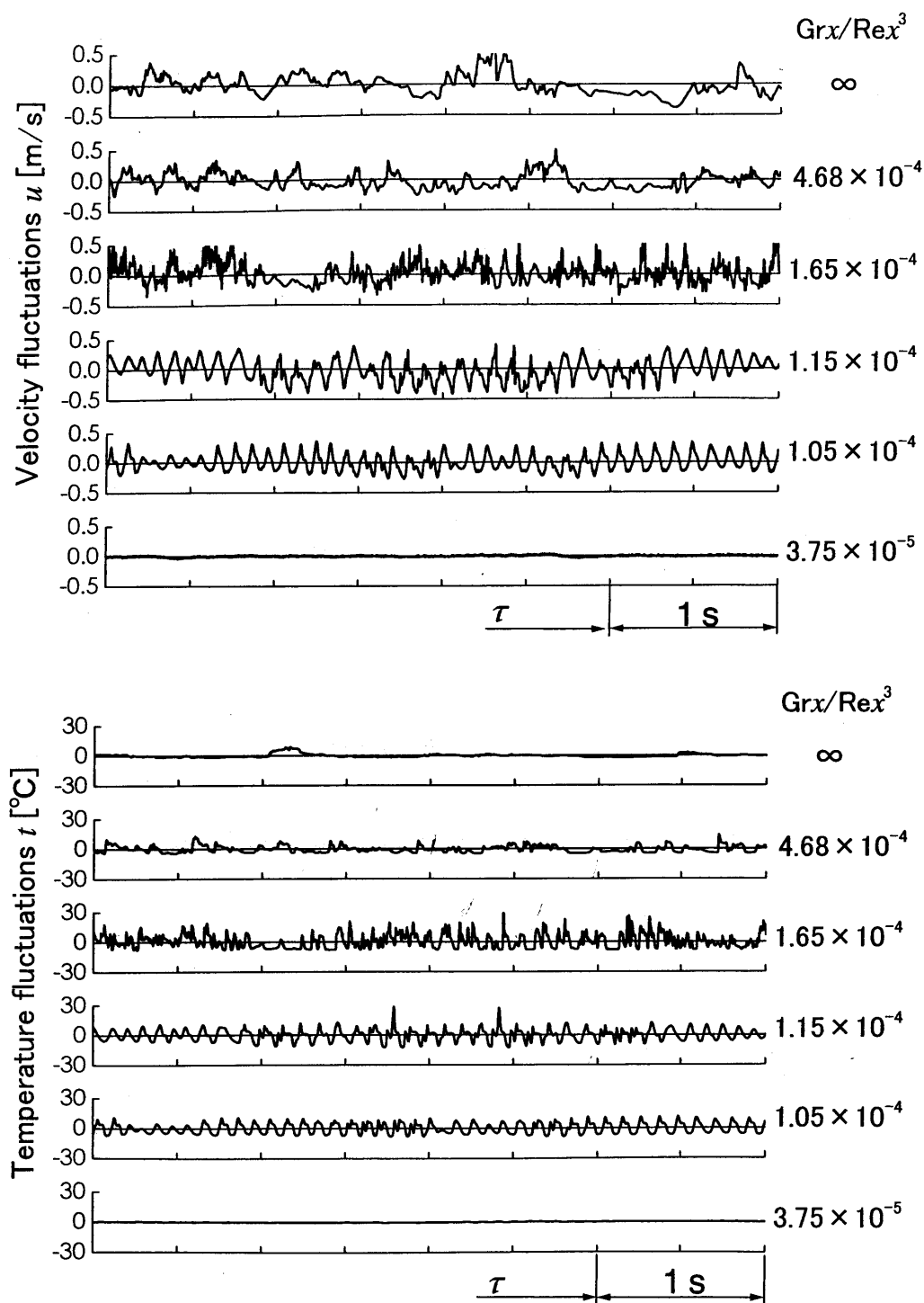
(a) near-wall location

Figure 3.7 Waveforms of velocity and temperature fluctuations (1/3)



(b) maximum mean velocity location

Figure 3.7 Waveforms of velocity and temperature fluctuations (2/3)



(c) location in outer region

Figure 3.7 Waveforms of velocity and temperature fluctuations (3/3)



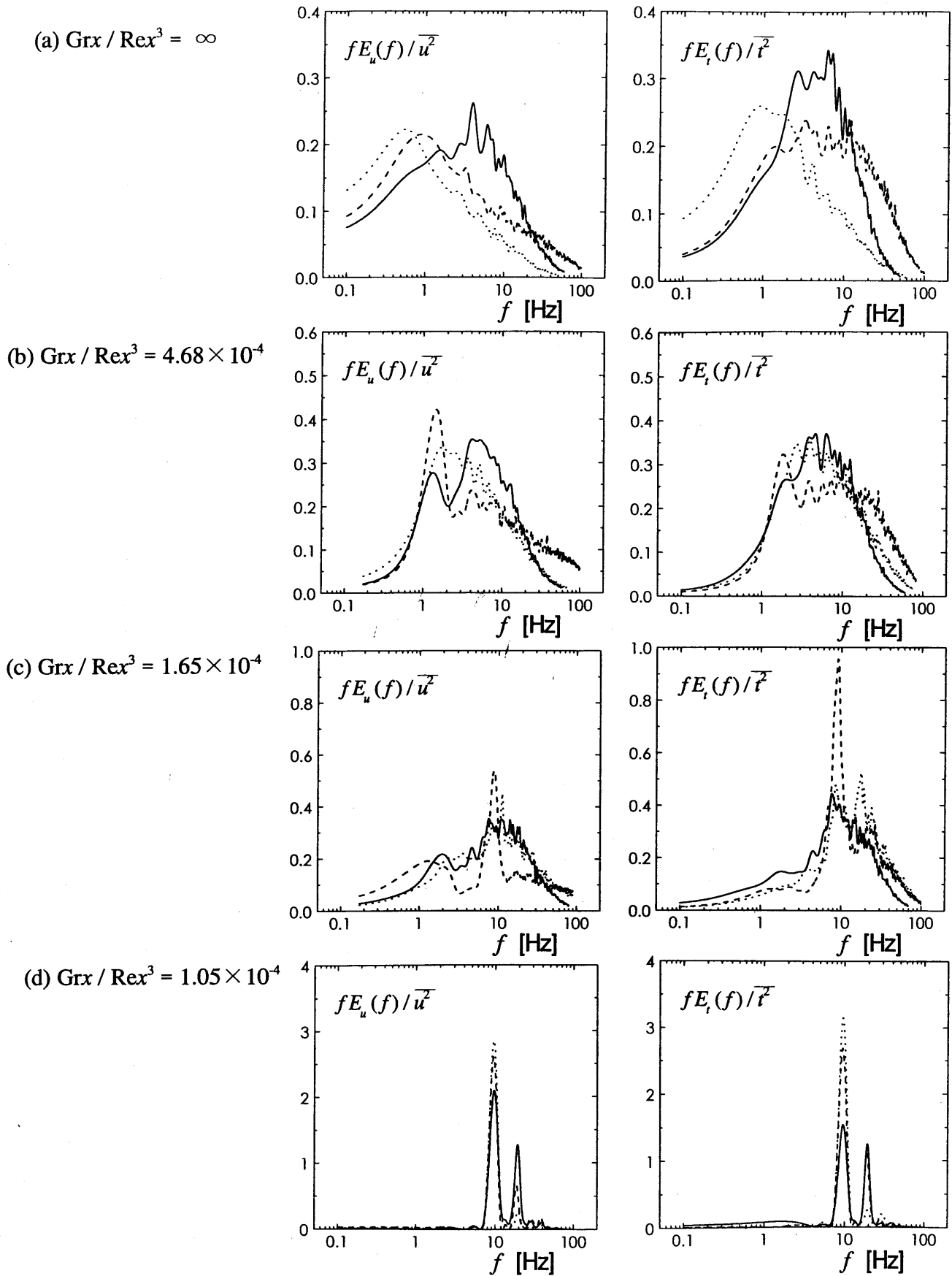


Figure 3.8 Power spectra of velocity and temperature fluctuations



## Chapter 4

# REGIMES OF BOUNDARY LAYER FLOWS

### 4.1 Criterion for Reduction in Heat Transfer Rate

Since the local heat transfer rate of the boundary layer rapidly decreases with the delay of transition to turbulence, a firm grasp of the thermal and flow conditions leading the turbulent boundary layer to a laminar one is very important to correctly estimate the heat removal capability by combined convection. The variations in local Nusselt numbers,  $N_{ux}$ , and wall shear stresses  $\tau_w$  with an increasing freestream velocity are shown in Figs 4.1 and 4.2. The heat transfer rate  $h$  and wall shear stress  $\tau_w$  were estimated from velocity and temperature gradients very near the wall, as described in Chap.2. Figure 4.1 presents these values against the local Richardson number  $Rix (= Grx / Rex^2)$  using the similarity variable for forced convection laminar boundary layers, and Figure 4.2 presents these values normalized with those for the pure turbulent natural-convection boundary layer (Tsuji and Nagano, 1988a) against the coordinate  $Grx / Rex$ . Also shown in Fig. 4.1 is the numerical result of Patel, Armaly and Chen (1998) for  $N_{ux}$  of the combined convection laminar boundary layer, which is represented by the solid line. It is quite evident from the figures that the parameter  $Grx / Rex$  gives good correlations for both  $N_{ux}$  and  $\tau_w$  and is suitable for evaluating the beginning point of laminarization of the boundary layer due to an increase in freestream velocity. The

effect of the freestream on  $Nux$  differs from that on  $\tau_w$ , which is attributed to a lack of analogy between heat and momentum transfer in the natural-convection boundary layer (Tsuji and Nagano, 1988a). At  $Grx / Rex \simeq 3 \times 10^6$ ,  $Nux / (Nux)_n$  suddenly decreases to about 0.4 at a given value of  $Grx / Rex$ , whereas  $\tau_w / (\tau_w)_n$  increases without indicating an obvious reduction in spite of the laminarization of the boundary layer.

On the other contrary, the values of  $Rix$  indicating the reduction in  $Nux$  depend on the value of  $Grx$ : this reduction of  $Grx = 1.90 \sim 2.22 \times 10^{11}$  occurs at  $Rix = 30 \sim 60$ . When  $Grx = 3.30 \sim 3.59 \times 10^{11}$ ,  $Nux$  decreases in the range of  $Rix = 10 \sim 20$ . This indicates that the similarity based on  $Rix$  is no longer useful for the turbulent boundary layer, while for the laminar boundary layer, the flow regime can be identified as natural, combined and forced convection, based on the value of  $Rix$ .

Figure 4.3 shows the change in the measured maximum intensity of temperature fluctuation  $(\sqrt{t^2})_m$  with the laminarization of the boundary layer from turbulence to laminar due to an increase in the freestream velocity. The maximum temperature fluctuation is normalized by the temperature difference between the surface temperature  $T_w$  and the ambient temperature  $T_\infty$ , and the  $Grx / Rex$  is taken as the abscissa. In spite of the introduction of a freestream, the maximum temperature fluctuation initially remains constant. Then, at  $Grx / Rex \simeq 3 \times 10^6$ , the temperature fluctuation decays exponentially with an increase in the freestream, and the value of  $(\sqrt{t^2})_m / (T_w - T_\infty)$  decreases to about  $10^{-3}$ , which is less than 1/100 of that for pure turbulent natural convection. At this value of  $Grx / Rex$ , a sudden decrease in  $Nux$  occurs as shown in Fig. 4.2.

Consequently, it was presumed that the relation  $Grx / Rex \simeq 3 \times 10^6$  ( $Grx > 10^{11}$ ) may be a good guideline for predicting the occurrence of a laminarization of the turbulent combined-convection boundary layer.

## 4.2 Grx-dependency of Turbulent Statistics

In Chapter 3, it was revealed that the turbulent characteristics of the combined-convection boundary layer are different in several respects from those in both natural and forced convection. Here, concentrating on the data at  $Grx / Rex \simeq 3 \times 10^6$ , we examined the turbulent statistics of the combined-convection boundary layer for different Grashof numbers ( $Grx = 1.95 \sim 1.98 \times 10^{11}$  and  $3.28 \sim 3.59 \times 10^{11}$ ).

The intensity profiles of the streamwise velocity fluctuation  $u$  with an increasing freestream velocity are shown in Fig. 4.4. The intensity of the velocity fluctuation  $u$  is normalized by the maximum mean velocity  $U_m$ , and a similarity variable  $\eta = (y / x) Grx^{1/4}$  for the laminar natural-convection boundary layer is used as the dimensionless distance from the wall, which is suitable for scaling the flow field near the wall in the turbulent natural-convection boundary layer (Tsuji and Nagano, 1989). In pure natural convection ( $Grx / Rex = \infty$ ), the maximum intensity of velocity fluctuation occurs beyond the maximum mean velocity location ( $\eta \simeq 3$ ). With the introduction of a freestream ( $Grx / Rex = 3.92 \times 10^6$  for  $Grx \simeq 3.5 \times 10^{11}$ ), the boundary layer thickness becomes thinner and the location of the maximum velocity approaches the wall, and simultaneously the intensity of the velocity fluctuation begins to decrease. As the freestream velocity increases, a similar change in the intensity profiles for different  $Grx$  is observed. At  $Grx / Rex = 2.73 \times 10^6$  for  $Grx \simeq 3.5 \times 10^{11}$  and  $Grx / Rex = 3.08 \times 10^6$  for  $Grx \simeq 2 \times 10^{11}$ , the maximum fluctuation intensities are attained at the location of the maximum mean velocity ( $\eta \simeq 1.5$ ), and these values become larger than those for pure natural convection. Then, at  $Grx / Rex = 2.35, 2.25 \times 10^6$  for  $Grx \simeq 3.5 \times 10^{11}$  and  $Grx / Rex = 2.40 \times 10^6$  for  $Grx \simeq 2 \times 10^{11}$ , the intensity profiles of fluctuations show two peaks with an infinitesimal value near the maximum mean velocity location, with a rapid decay in the fluctuation over the entire boundary-layer region. This profile characterizes a laminarization of the turbulent combined-convection boundary layer (Carey and Gebhart, 1983; Krishnamurthy and Gebhart, 1989). A further increase in the

freestream velocity results in the disappearance of the velocity fluctuation with the laminarization of the boundary layer.

Figure 4.5 presents the change in the intensity of the temperature fluctuation  $t$  normalized by the temperature difference between the surface temperature  $T_w$  and the ambient temperature  $T_\infty$  with an increasing freestream velocity. Regardless of  $Gr_x$  values, the increasing and decreasing tendencies of the maximum intensity of the temperature fluctuation closely resemble those of the velocity fluctuation: the maximum intensity of the temperature fluctuation decreases with the introduction of a freestream, and as the freestream velocity increases, the maximum value initially increases and then rapidly decreases as the freestream velocity increases.

The change in the cross-correlation coefficients  $R_{ut}$  between velocity and temperature fluctuations is presented in Fig. 4.6. The profile of  $R_{ut}$  also varies remarkably due to the laminarization of the boundary layer, and the peculiar profile is observed at  $Gr_x / Re_x \simeq 3 \times 10^6$ . Independently of  $Gr_x$ , the different sign of  $R_{ut}$  alternately appears with  $y$  and the maximum absolute value of  $R_{ut}$  becomes almost unity. Since the waveforms of the velocity fluctuation  $u$  and temperature fluctuation  $t$  vary from random to harmonic with a specific frequency in the laminarization of the boundary layer, as described in Chap. 3, this profile of  $R_{ut}$  implies that velocity and temperature fluctuations have the same frequency with different phases. The estimated phase difference between velocity and temperature fluctuations approximately coincides with that determined by a linear stability analysis for the transition of the laminar combined-convection boundary layer (Carey and Gebhart, 1983).

The power spectra of velocity and temperature fluctuations measured at  $Gr_x = 1.95, 1.98 \times 10^{11}$  are shown in Fig. 4.7. A change in these spectra with the laminarization of the boundary layer is similar to that measured at  $Gr_x = 3.28 \sim 3.59 \times 10^{11}$ , as shown in Fig. 3.8, i.e., at  $Gr_x / Re_x \simeq 3 \times 10^6$ , spectrum peaks appear at the fundamental frequency of 9 Hz and its harmonic, indicating that the linear fluid motions control the boundary layer.

### 4.3 Regimes of Boundary Layer Flows

The classification of boundary layer flows is very important for engineering applications. Patel, Armaly and Chen (1998) proposed a map of the various convection flow regimes by utilizing the numerical results obtained with a low Reynolds-number  $k-\varepsilon$  turbulence model. Following their map, we have made a map based on our experimental results. The boundary layer flows were identified in the following manner: when waveforms are random and the profiles of fluctuation intensities are similar to those in pure natural or pure forced convection, the flow regime is regarded as turbulent; in cases where harmonic waveforms with a specific frequency appear, the flow is regarded as in transition; but the flow is regarded as laminar when the intensities of velocity and temperature fluctuations become almost zero and the profiles of mean velocity and mean temperature coincide with the theoretical ones obtained for the laminar combined-convection boundary layer.

Figure 4.8 depicts the regimes of boundary layer flows in the coordinates  $Re_x$  and  $Gr_x$ . The transition regime corresponds to the region placed between the thick and thin dotted curves. For the laminar region, the flow regime can be identified as natural, combined and forced convection, based on the criterion that  $Nux$  deviates more than 5 % from the calculated values for laminar pure natural and forced convection. This identification is shown with two chain lines (plotted as Richardson number  $Rix = Gr_x / Re_x^2 = 0.0276, 5.97$ ) in Fig. 4.8, which agree well with the result of Patel, Armaly and Chen (1998).

In the turbulent natural-convection boundary layer, the transition occurs at about  $Gr_x = 3 \times 10^9$ , and the turbulent boundary layer develops in the range  $Gr_x > 10^{10}$ . Nevertheless, with the addition of the freestream velocity, the region of laminar combined convection extends to the large  $Gr_x$  region, and the transition is remarkably delayed: the boundary layer for  $Re_x \simeq 2 \times 10^5$  and  $Gr_x \simeq 3 \times 10^{11}$  is still laminar, although the  $Gr_x$  value is 100 times as large as the critical Grashof number in pure natural convection. On the map presented by Patel, Armaly and Chen (1998), the region  $Gr_x > 5 \times 10^9$  for moderate  $Re_x$  is divided into turbulent

combined convection and turbulent natural convection. In practice, however, the laminar combined-convection regime appears in the region regarded as turbulent combined convection, as shown in Fig. 4.8.

With special heed to the laminarization region, the regimes of boundary layer flows, in the coordinates of the local Reynolds number  $Re_x$  and local Grashof number  $Gr_x$ , are shown in Fig. 4.9. Even though  $Gr_x$  is quite large, the turbulent combined-convection flow changes to laminar with an increase in the freestream velocity. As shown in this figure, the transition region indicated with hatches lies in the relation  $Gr_x \propto Re_x$  under the present experimental conditions. Therefore, the Richardson number  $Rix (= Gr_x / Re_x^2)$ , which is generally used to classify the regimes of buoyancy flows, may be not effective in correlating the laminarization of the turbulent combined-convection boundary layer.

From these results for  $Nux$ , turbulent statistics, and the regimes of the boundary layer flows, it is found that the criterion for the beginning of the reduction in heat transfer rate due to the laminarization of the boundary layer may be determined by the relation  $Gr_x / Re_x \simeq 3 \times 10^6$  for  $Gr_x > 10^{11}$ . A comparison of the regimes of the boundary layer, which is identified by the value of  $Nux$ , obtained in the present experiment and those of other researchers is shown in Fig. 4.10. Noticeable discrepancies in the criteria for estimating the value of  $Nux$  are seen. Hall and Price (1970) conducted an experiment and concluded that the heat transfer rate became minimum when the freestream velocity was of the same order of magnitude as the maximum mean velocity in the turbulent natural-convection boundary layer. In addition, they also estimated that this condition can be expressed as  $Rix \doteq 10$ . Kitamura and Inagaki (1987) also made a similar report for the condition of the minimum heat transfer rate. In the present experiment, a rapid reduction in the heat transfer rate was observed at a rather small freestream velocity of about half or two-thirds of the maximum mean velocity. The discrepancy between the present results and those of these earlier studies may be ascribed to the differences in the experimental setup and conditions. In their experiments, test sections with small areas were used and relatively large disturbances were involved in the



freestream, which yielded a substantially small transition Reynolds number value even for pure forced convection. In fact, they did not observe an obvious laminarization of the boundary layer, though velocity fluctuations were suppressed to some extent. Thus, the occurrence of  $Nux$  reduction was not so abrupt as that observed in the present experiment and the minimum value of  $Nux / (Nux)_n$  remained at about 0.75. It is considered that the present results, obtained by controlling freestream disturbances to the lowest level possible, more accurately reveal the essential characteristics of the turbulent combined-convection boundary layer.

Patel, Armaly and Chen (1998) numerically investigated the heat transfer characteristics of the combined-convection boundary layer with a low Reynolds number  $k-\epsilon$  turbulence model. They classified various flow regimes and suggested that, with a deterioration of  $Nux$ , turbulent natural convection changed to turbulent combined convection under the condition of  $Re_x = 0.00174 Gr_x^{0.615}$  ( $Gr_x > 5 \times 10^9$ ). However, this criterion gives a reduction in  $Nux$  at a quite small  $Re_x$  and a laminarization of the boundary layer could not be predicted, which may reveal a deficiency in existing turbulence models.

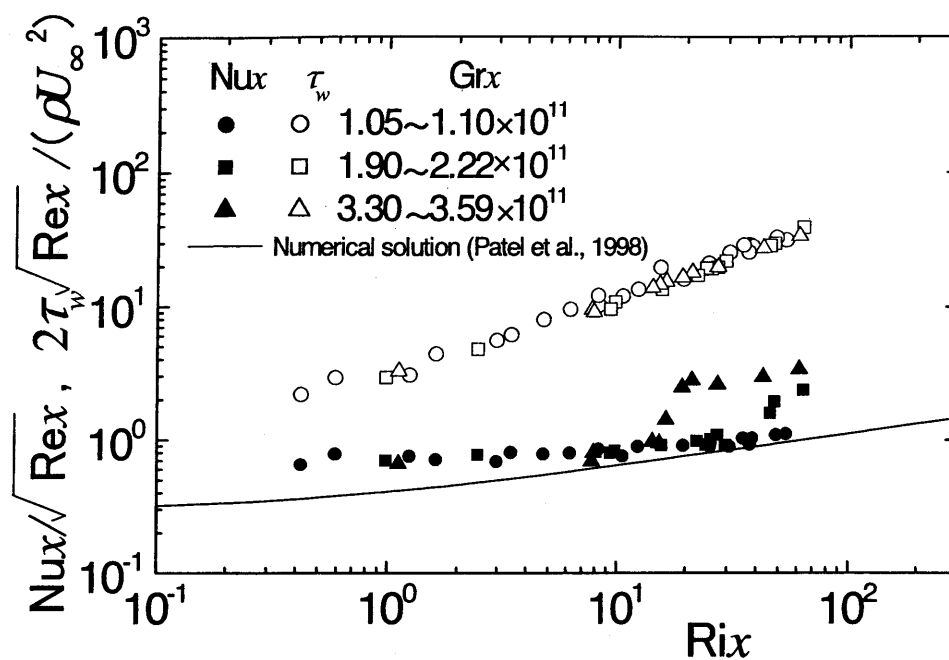


Figure 4.1 Heat transfer rates and wall shear stresses with  $Rix$

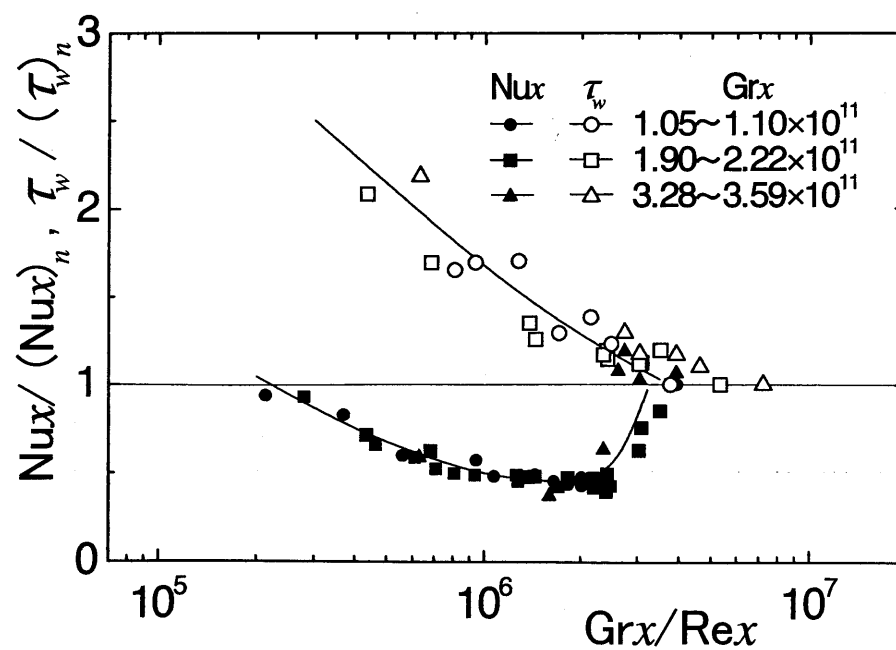


Figure 4.2 Heat transfer rates and wall shear stresses with  $Grx / Rex$

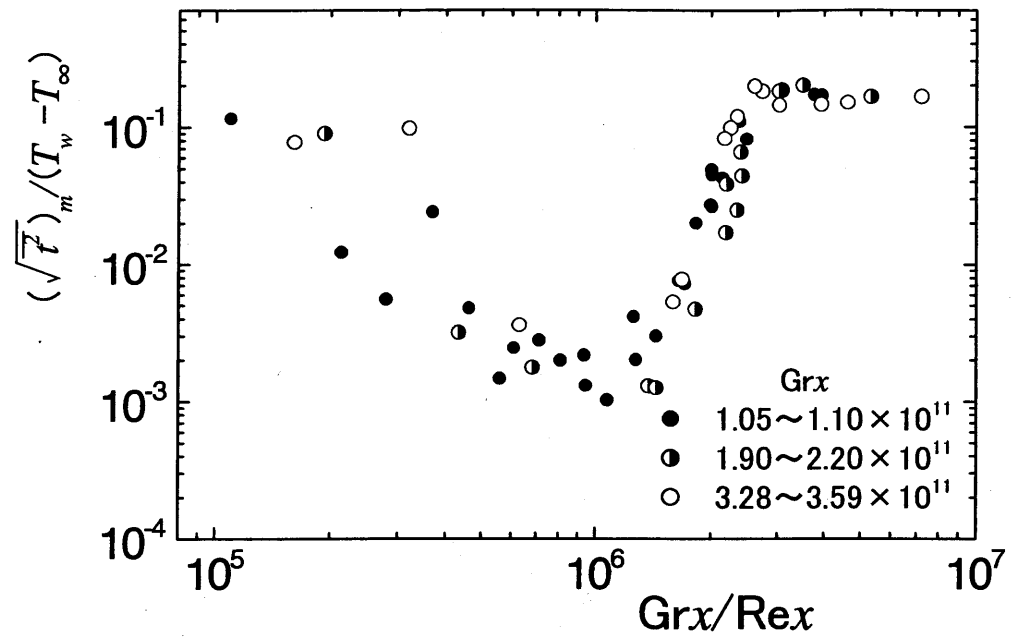


Figure 4.3 Maximum values of temperature fluctuations with  $Grx / Rex$

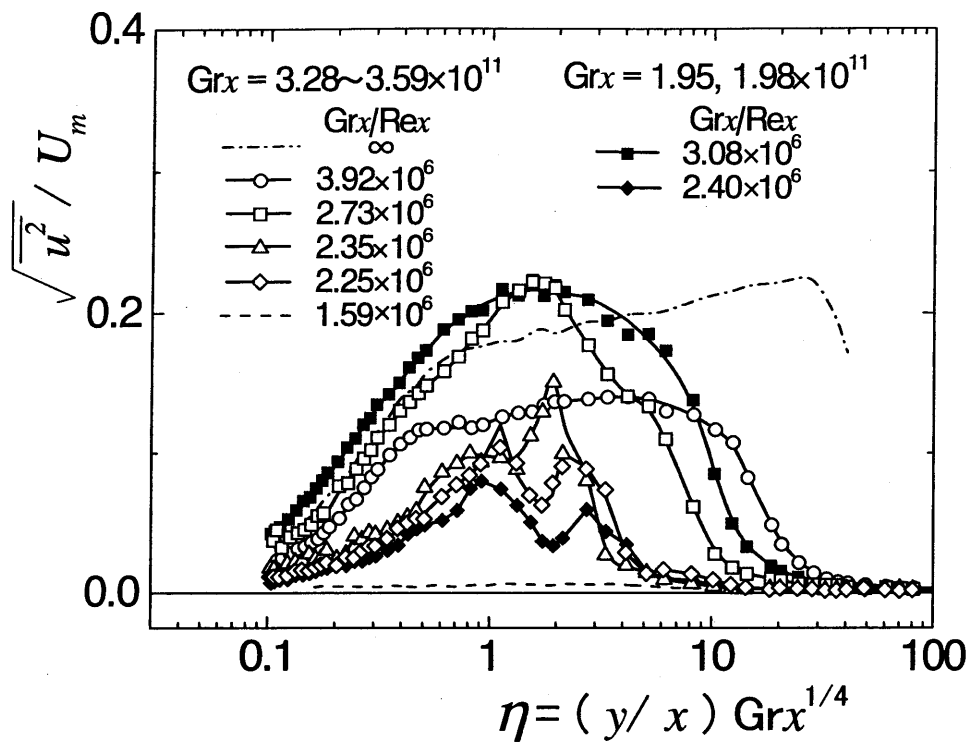


Figure 4.4 Intensities of streamwise velocity fluctuation for different Grashof numbers

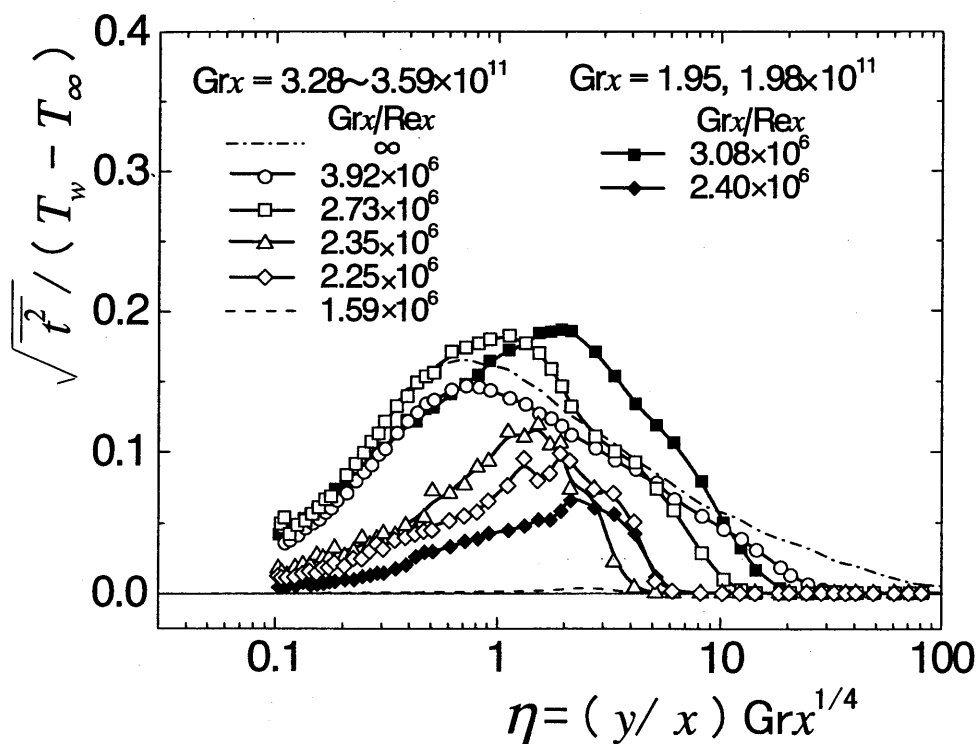


Figure 4.5 Intensities of temperature fluctuation for different Grashof numbers

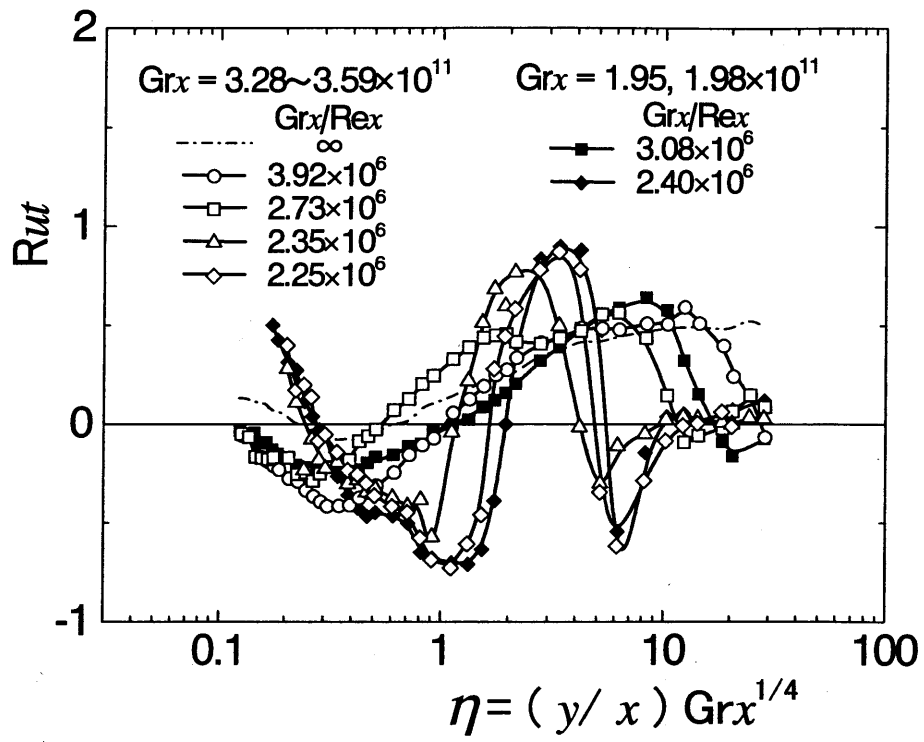
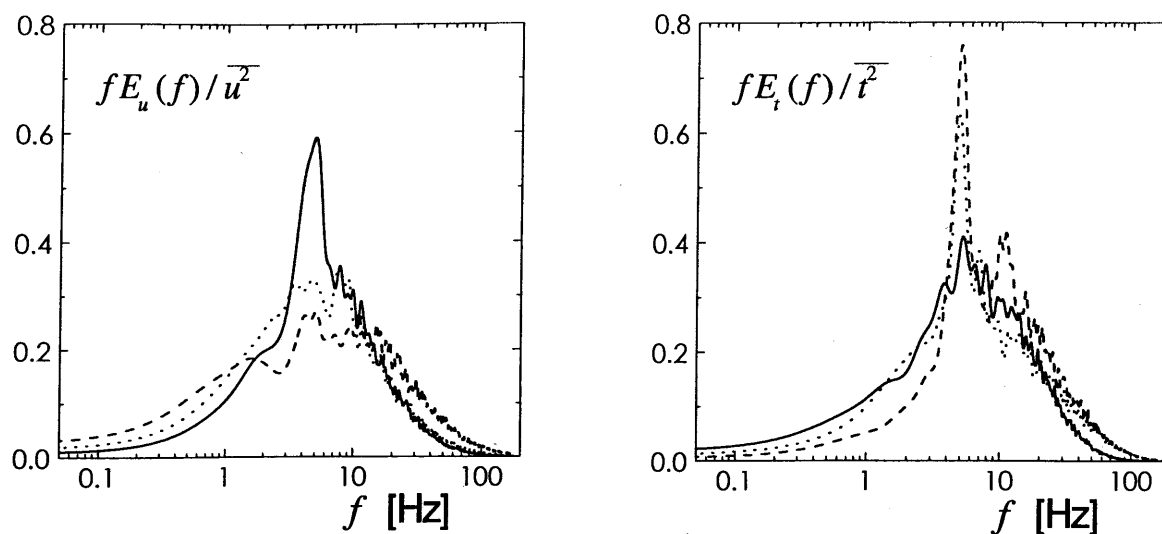
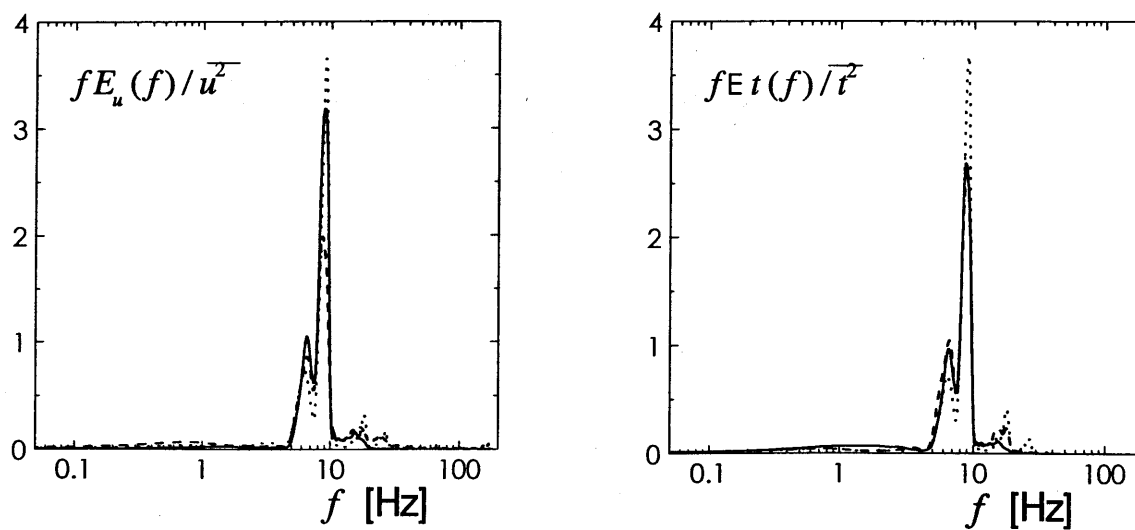


Figure 4.6 Cross-correlation coefficients between velocity and temperature fluctuations for different Grashof numbers



(a)  $Grx/Rex = 3.08 \times 10^6$



(b)  $Grx/Rex = 2.40 \times 10^6$

Figure 4.7 Power spectra of velocity and temperature fluctuations

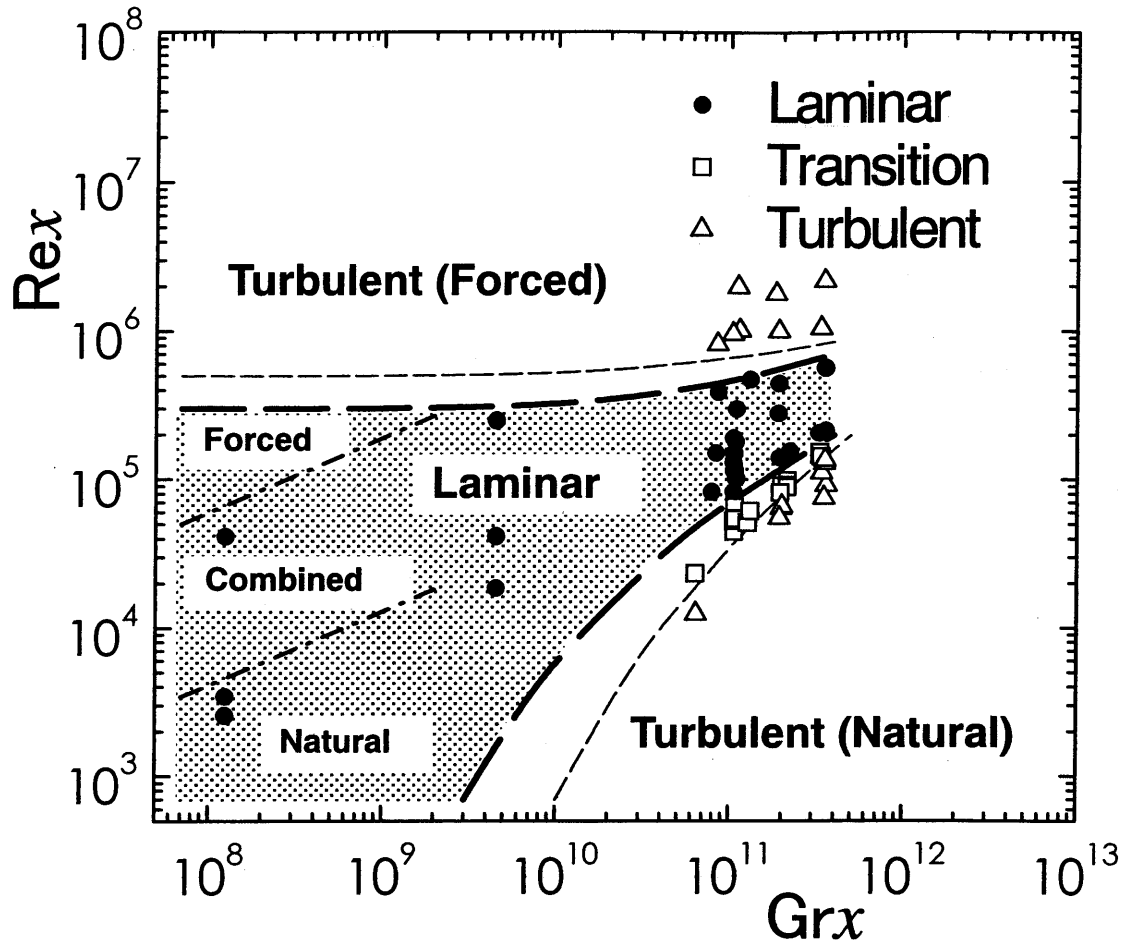


Figure 4.8 Regimes of boundary layer flows

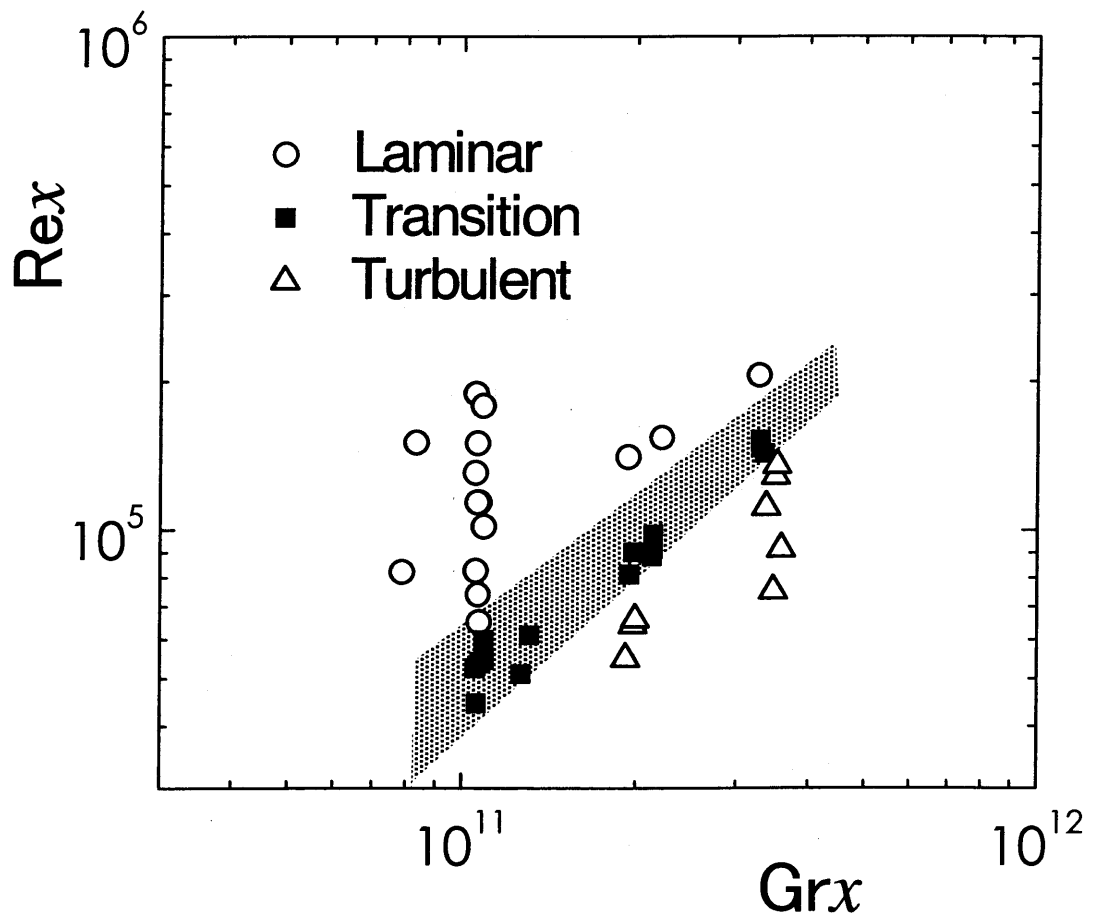


Figure 4.9 Regimes of boundary layer flows at high  $Gr_x$  numbers



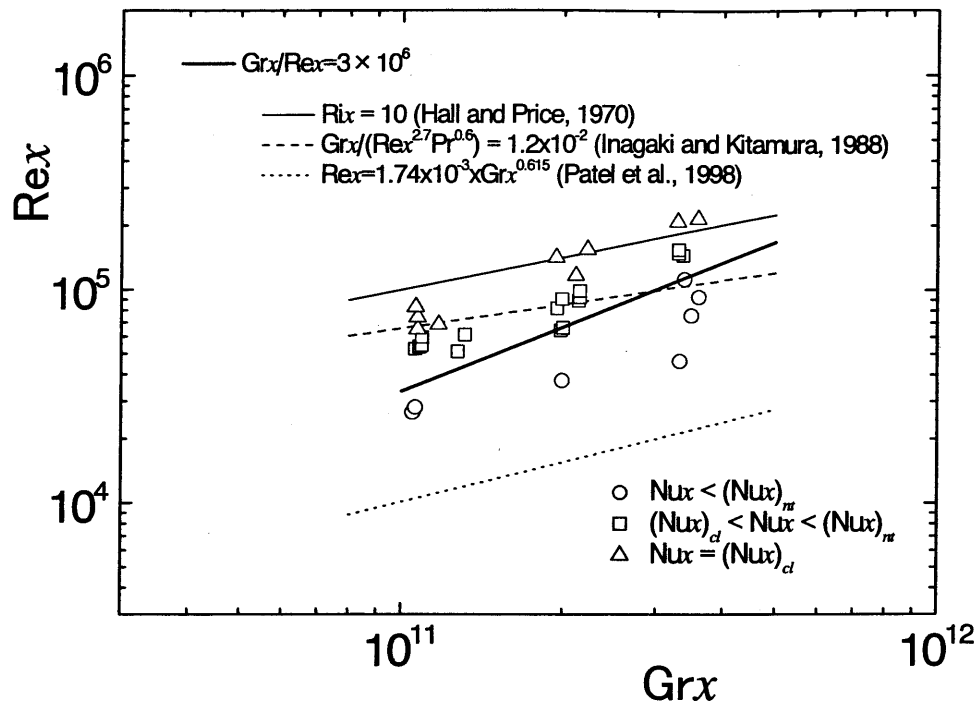


Figure 4.10 Comparison of convective heat transfer regimes



# Chapter 5

## STRUCTURAL CHARACTERISTICS

### 5.1 Skewness and Flatness Factors

The high order turbulent behavior in the boundary layer was examined to gain a firm grasp of the stabilizing effect of the freestream on the combined-convection boundary layer. The change in skewness factors  $S(u)$  and  $S(t)$  and the flatness factors  $F(u)$  and  $F(t)$ , which are third- and fourth-order moments of velocity and temperature fluctuations, respectively, are presented in Fig. 5.1. These factors are definitely different from those for the Gaussian probability distribution, and the factors for pure natural convection agree closely with measurements by Tsuji and Nagano (1988b). The effect of freestream sensitively appears in the velocity field. As freestream velocity increases, the mean velocity profile in the boundary layer markedly varies as shown in Fig. 3.2. Simultaneously,  $S(u)$  shifts toward positive while the velocity fluctuation has a probability distribution close to Gaussian ( $S(u) \simeq 0$  and  $F(u) \simeq 3$ ) over a wide range of the natural-convection boundary layer. Near the wall,  $F(u)$  becomes substantially higher than in pure natural convection, which indicates more intermittent fluctuations. On the other hand, the changes in  $S(t)$  and  $F(t)$  profiles are relatively small. All the skewness factors  $S(t)$  of temperature fluctuation become negative near the wall ( $\eta < 1$ ) and positive in the outer layer ( $\eta > 1$ ), and all the flatness factors  $F(t)$  near the wall and the outer edge of the boundary layer exceed a value of 3. These profiles of

skewness and flatness factors characterize high- and low-temperature fluid motions encompassing the whole boundary-layer region as observed in the natural-convection boundary layer (Tsuji, Nagano and Tagawa, 1992a; Tsuji and Nagano, 1996). Thus, the large-scale structure in the outer layer, which is strongly connected with the generation of turbulence in the natural-convection boundary layer, seems to be also maintained in the combined-convection boundary layer despite the addition of a freestream.

## 5.2 Fluid Motion in Outer Region

Fluid motions in the outer layer of the combined-convection boundary layer at  $Gr_x/Rex = 3.44 \times 10^6$  for  $Gr_x = 1.1 \times 10^{11}$  were investigated with PIV measurements. An example of velocity vectors in the  $(x-y)$  plane is shown in Fig. 5.2. The strong upward flow appears near the wall, which implies that the boundary layer flow is dominated by the buoyancy. The large-scale fluid motion is observed in the whole boundary layer, and the boundary layer thickness changes in the mean flow direction. Figure 5.3 shows instantaneous signals of velocity fluctuations  $u$  and  $v$  together with the Reynolds shear stresses  $uv$  normalized by the relevant fluctuation intensities. The form of the signals changes with the distance from the wall  $\eta$ . As the outer edge of the boundary layer is approached, long-period signals become notable, while high-frequency signals appear at the location of maximum mean velocity. Intermittent occurrences of strong positive  $u$  motion, which concern the profiles of skewness and flatness factors shown in Fig. 5.1, simultaneously induce  $v$  and  $uv$  motions of large positive values. Such fluid motions generate turbulent energy, since the mean velocity gradient in the outer layer is negative.

Figure 5.4 shows instantaneous fluctuation velocity fields in the  $(x-y)$  plane captured at  $uv > 0$ ,  $uv \sim 0$  and  $uv < 0$ , marked with arrows in Fig. 5.3. The features of the motion of each fluid are strikingly different. When  $uv$  takes a positive value, it is frequently observed that a large-scale fluid motion with a high speed moves from the maximum mean velocity location

toward the edge of the boundary layer. Compared with such a fluid motion, the scale of the fluid motion at  $uv < 0$  is quite small and the occurrence of large amplitude fluctuations is limited to the region around the maximum mean velocity location. This result demonstrates that the scale of the outward fluid motion with a high speed contributing to the generation of turbulence is distinctly larger than that of other fluid motions.

Figure 5.5 demonstrates the temporal variation in instantaneous streamwise velocity profile in the boundary layer when turbulent energy is generated. Over the entire boundary layer, the velocity profile is initially lower than the time-averaged velocity and then increases with time. Such changes in the velocity field from a low-speed flow to a high-speed flow can be regarded as fluid motions responding to the large-scale structure in the thermal field, which are observed in the turbulent natural-convection boundary layer (Tsuji, Nagano and Tagawa, 1992a; Tsuji and Nagano, 1996), because the cross-correlation coefficient between streamwise velocity and temperature fluctuations takes a high value of about 0.6 in the outer layer of the combined-convection boundary layer, as shown in Fig. 4.6.

### 5.3 Structure of Velocity Field in Near-Wall Region

The velocity field in the near-wall region was then examined with PIV for the turbulent combined-convection boundary layer. The experiments were carried out under the uniform surface temperature  $T_w = 52.0\text{ }^\circ\text{C}$  and freestream velocity  $U_\infty = 0.08\text{ m/s}$ . The ambient fluid temperature  $T_\infty$  was  $29.5\text{ }^\circ\text{C}$ , and the local Reynolds number  $Re_x$  and local Grashof number  $Gr_x$  were  $1.39 \times 10^4$  and  $6.44 \times 10^{10}$ , respectively. The distributions of turbulent quantities in the velocity field are shown in Fig. 5.6. The intensities of velocity fluctuations  $u$ ,  $v$  and the Reynolds shear stress  $\overline{uv}$  are normalized by the maximum mean velocity  $U_m$ , and a similarity variable  $\eta = (y/x) Gr_x^{1/4}$  for the laminar natural-convection boundary layer is used as the dimensionless distance from the wall, which is suitable for scaling the flow field near the wall in the turbulent natural-convection boundary layer (Tsuji and Nagano, 1989).

The features of each profile are similar to those observed in the turbulent natural-convection boundary layer (Tsuji and Nagano, 1988a, b). The maximum intensities of  $u$  and  $v$  occur beyond the maximum mean velocity location ( $\eta \simeq 2$ ), and the Reynolds shear stress  $\overline{uv}$  also takes a maximum value in the outer layer. It should be noted that, despite the increase in mean velocity gradient near the wall,  $\overline{uv}$  of combined-convection becomes positive at the maximum mean velocity location and almost zero at the near-wall region.

Figure 5.7 presents instantaneous signals of velocity fluctuations  $u$  and  $v$ . A large-scale fluid motion frequently appears, and at almost the same time an accelerating ( $u > 0$ ) or decelerating ( $u < 0$ ) flow appears in the whole visualized region. However, no signals of  $u$  and  $v$  suggesting intermittent bursts, as seen in the forced convection boundary layer, could be recognized for the turbulent combined-convection boundary layer.

An example of instantaneously fluctuating velocity vectors in the ( $x$ - $y$ ) plane is demonstrated in Fig. 5.8. Even in the near-wall region where the mean velocity gradient takes a positive value, the invasion of low-speed fluid ( $u < 0$ ,  $v < 0$ ) is frequently observed. Such a fluid motion may be the origin of the peculiar  $\overline{uv}$  profile measured in the near-wall region.

Instantaneous vectors consisting of velocity fluctuations  $u$  and  $w$  observed near the wall ( $\eta = 0.87$ ,  $y = 5.0$  mm) are shown in Fig. 5.9. The decelerating flow is observed in the whole-visualized region, but non-uniformity in the spanwise direction exists. The time series of instantaneous vectors consisting of velocity fluctuations  $u$  and  $w$  observed near the wall ( $\eta \simeq 0.70$ ,  $y = 4.0$  mm) are shown in Fig. 5.10. In the ordinary boundary layer, turbulence generation is associated with the quasi-coherent structure near the wall, such as low- and high-speed streaks (Kim, Moin and Moser, 1987). However, no streaky structure could be recognized in any visualized fluid motions with PIV for the turbulent combined-convection boundary layer.

Figure 5.11 shows the two-point correlations in the velocity field. The spanwise spatial correlation coefficient decreases monotonously with increasing  $\Delta z$  and does not take negative

infinitesimal values, which may indicate the existence of low and high speed streaks.

Tsuji, Nagano and Tagawa (1992a), and Tsuji and Nagano (1996) concluded through their experiments with a thermocouple rake and flow visualization using a smoke-wire technique that low- and high-speed streak structures and intermittent bursts, as seen in forced convection, did not exist near the wall in the turbulent natural-convection boundary layer. Velocity vectors and two-point correlations obtained for the combined-convection boundary layer also suggest a lack of such quasi-coherent structures in the near-wall region. As seen from these results, the near-wall turbulence production through the mean shear stress significantly differs between combined and forced convection. Thus, the laminarization of the combined-convection boundary layer may be caused by such differences in structures. Namely, the large-scale structure in the outer region plays a predominant role in turbulence generation, whereas no quasi-coherent structure as seen in forced convection exists in the near-wall region. Therefore, a slight increase in uniform freestream added at the outer edge of the boundary layer may restrict the large-scale vortex motions that serve to maintain turbulence in the outer layer, and bring on a laminarization of the boundary layer.

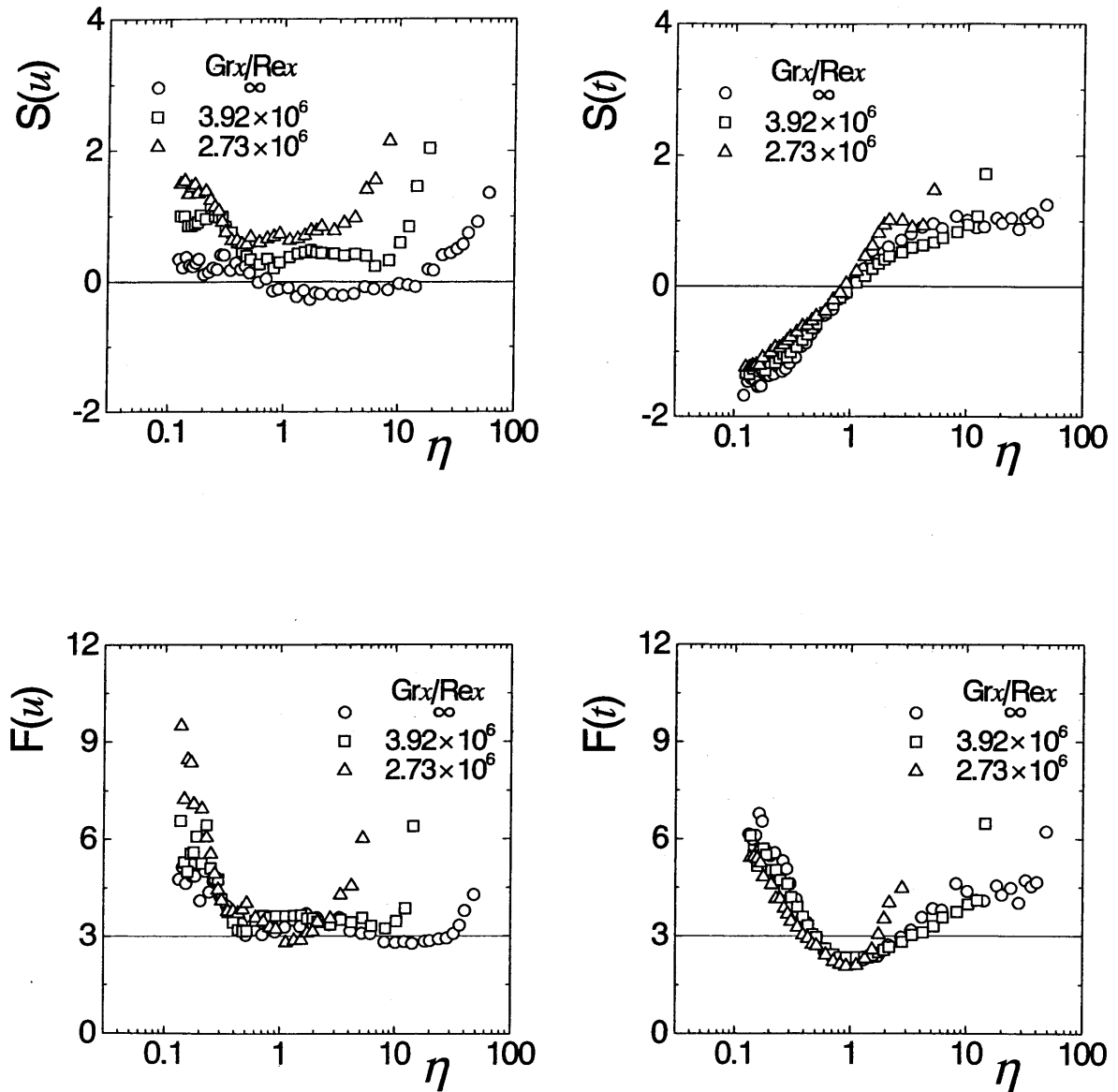


Figure 5.1 Change in skewness and flatness factors of velocity and temperature fluctuations



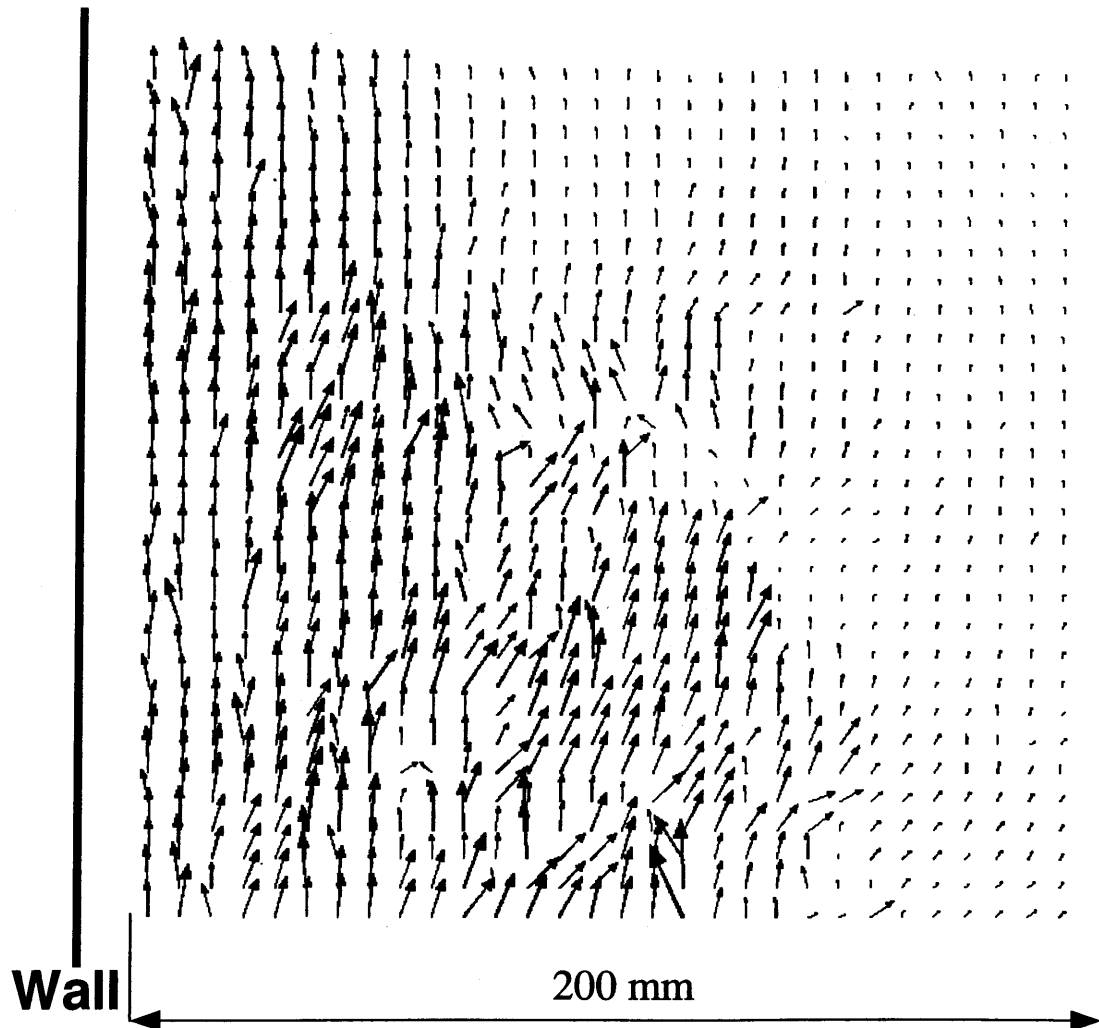


Figure 5.2 Example of instantaneous velocity vectors

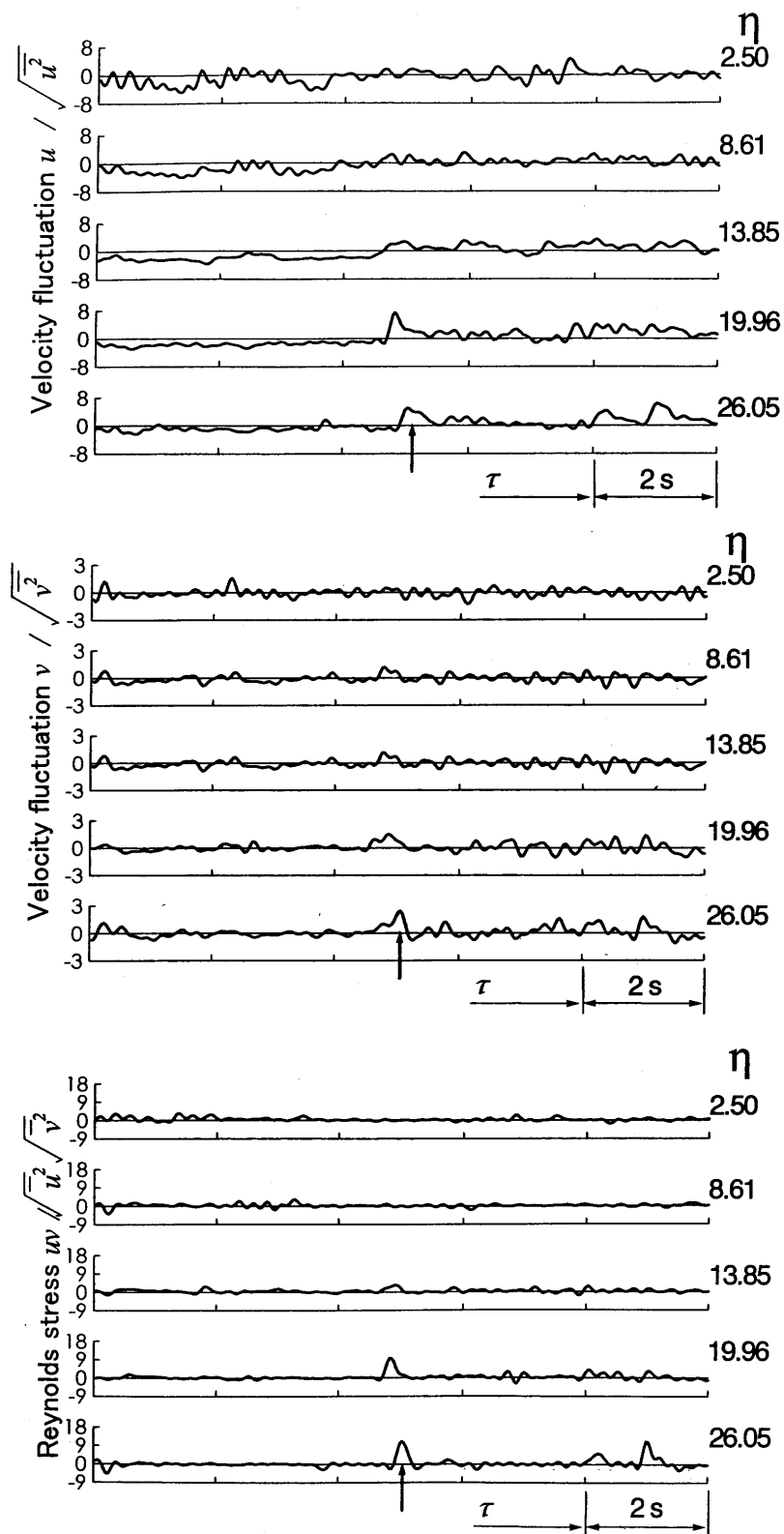


Figure 5.3 Signal traces of velocity fluctuations  $u$  and  $v$ , and Reynolds stresses  $uv$  in combined-convection boundary layer

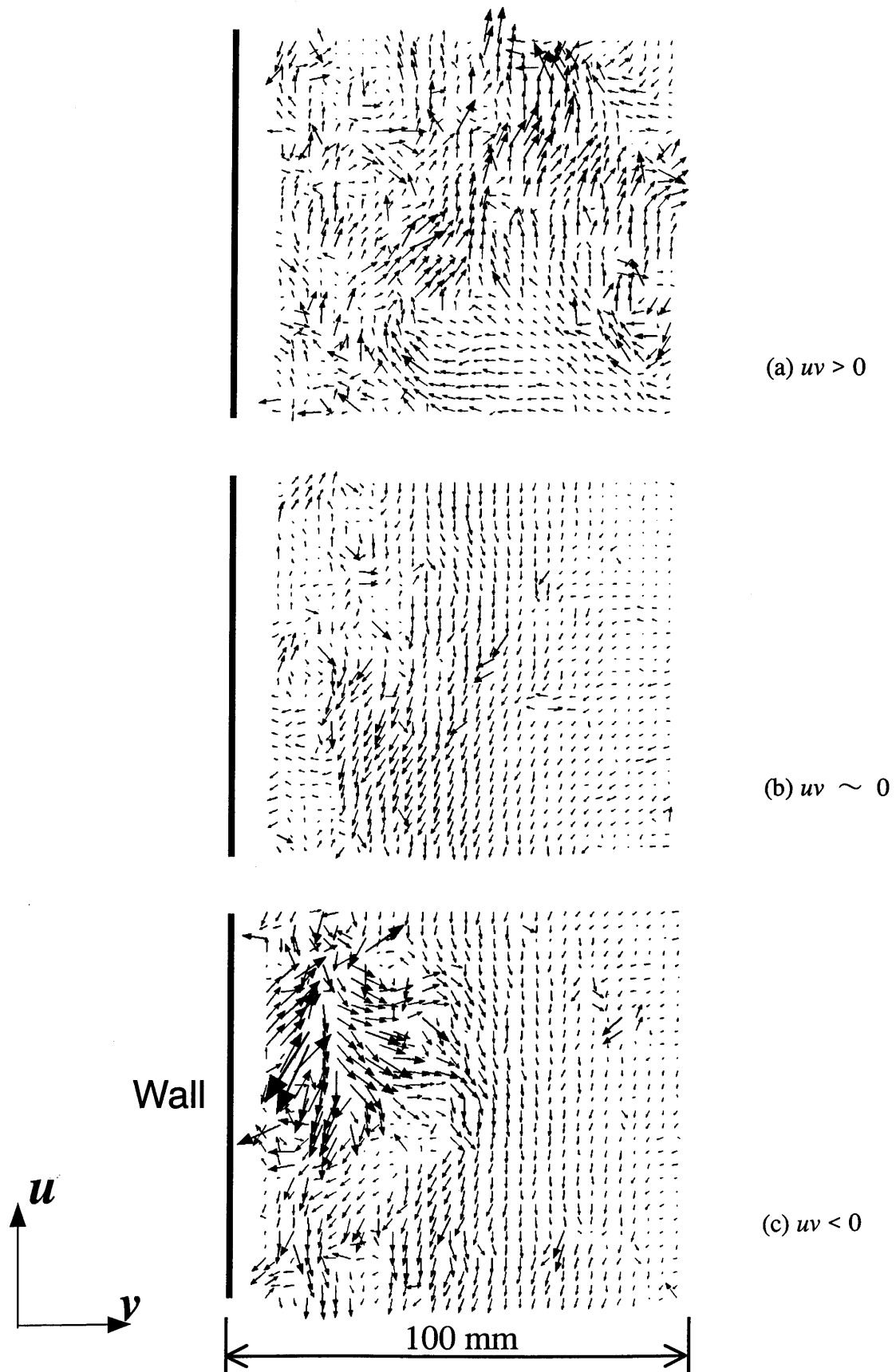


Figure 5.4 Velocity fluctuation vectors in  $(x-y)$  plane

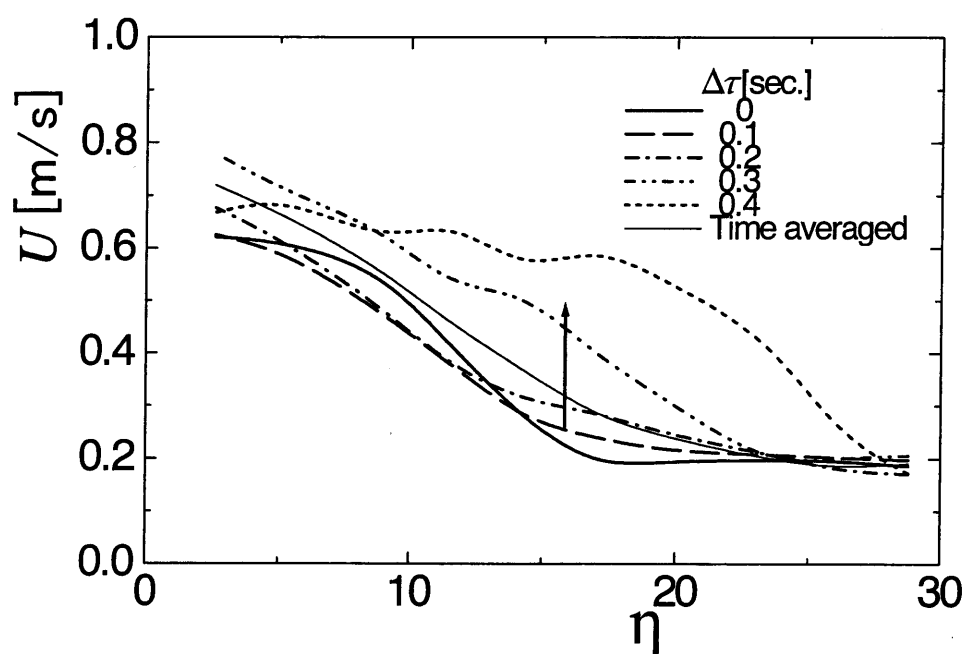


Figure 5.5 Temporal variation of instantaneous streamwise velocity profiles in  $(x-y)$  plane

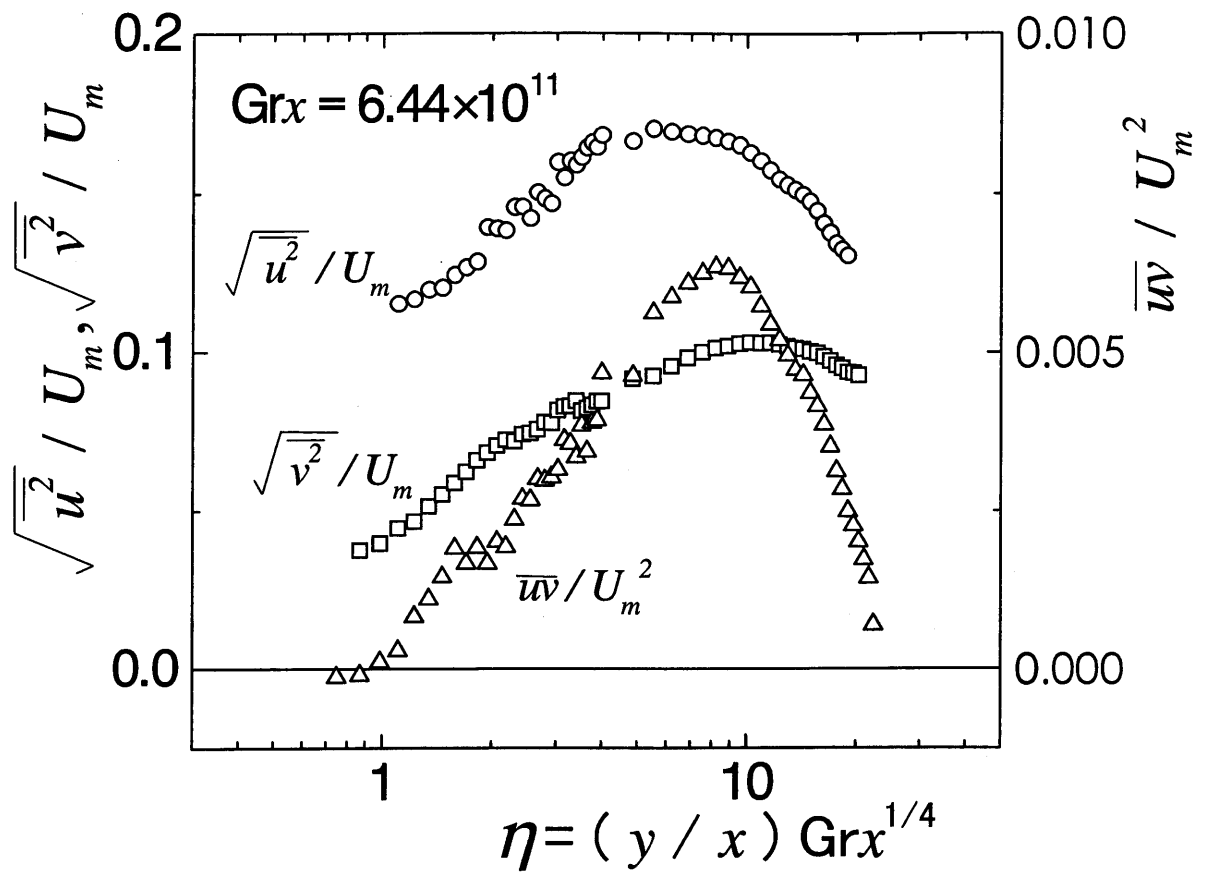


Figure 5.6 Distributions of turbulent quantities near wall

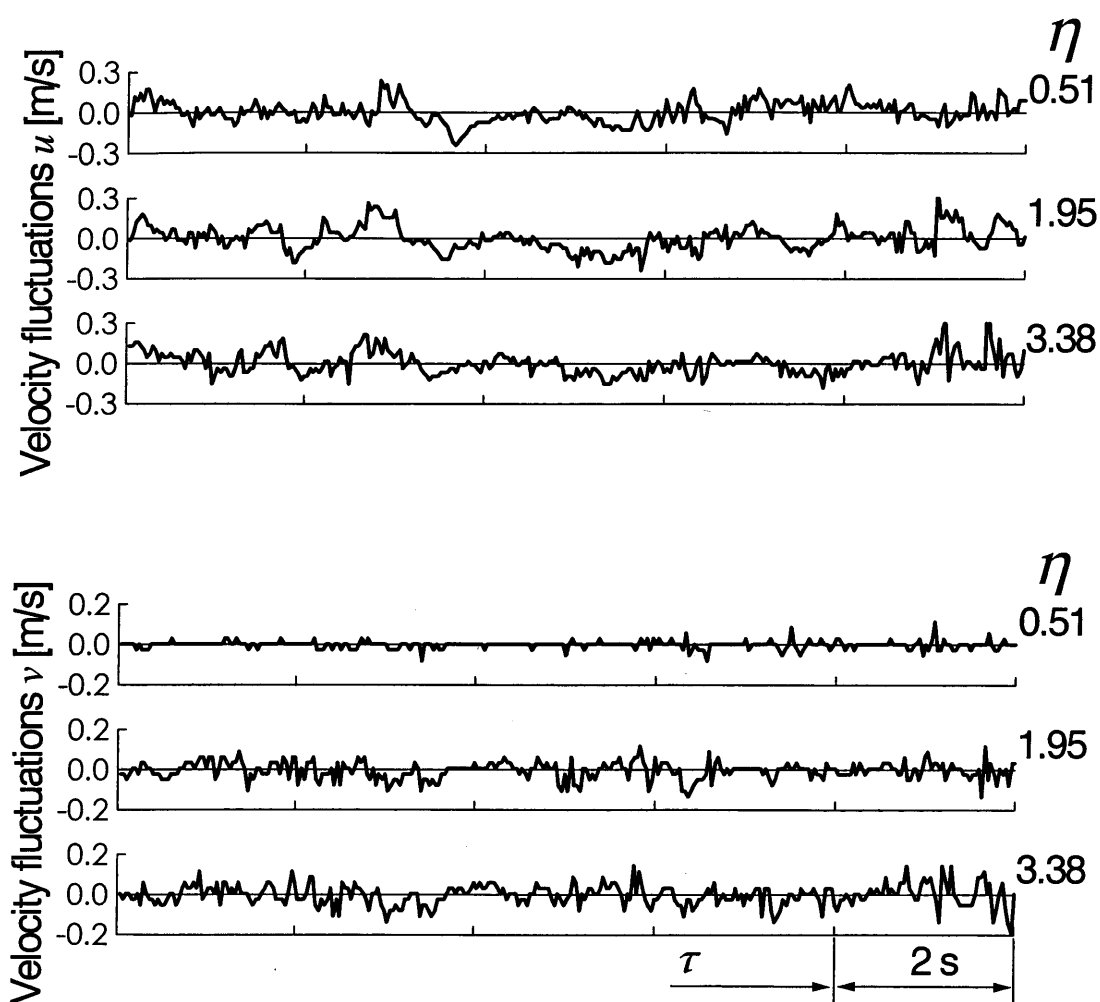


Figure 5.7 Signal traces of velocity fluctuations  $u$  and  $v$

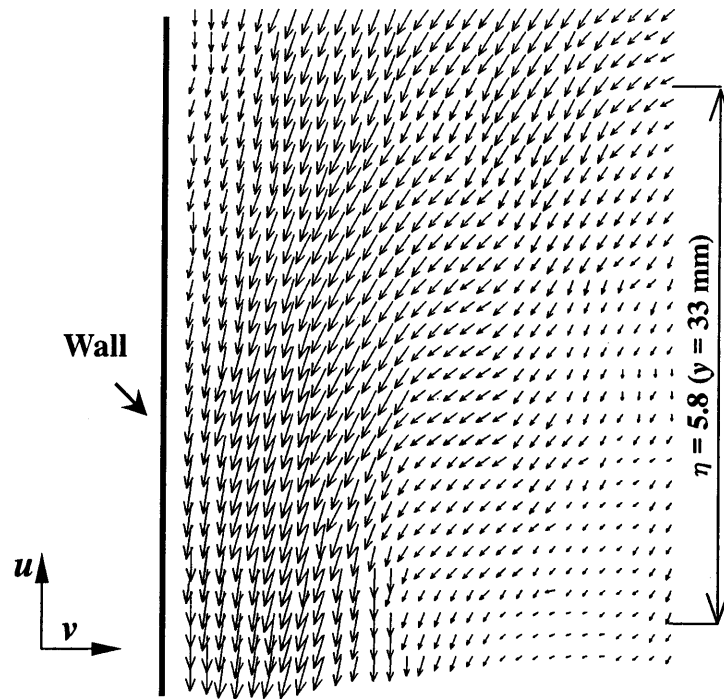


Figure 5.8 Example of velocity fluctuation vectors in  $(x - y)$  plane

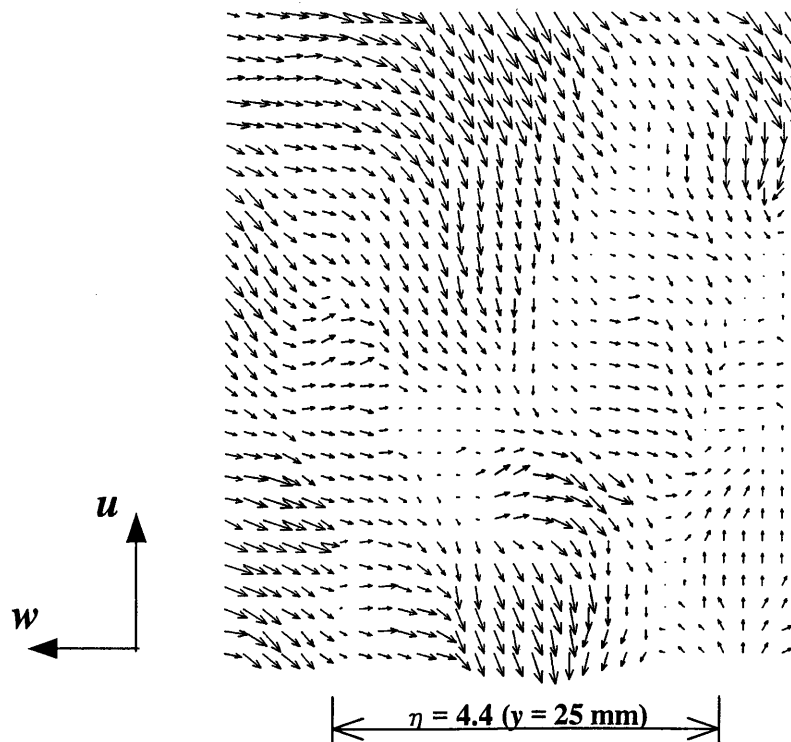


Figure 5.9 Velocity fluctuation vectors near wall in  $(x - z)$  plane

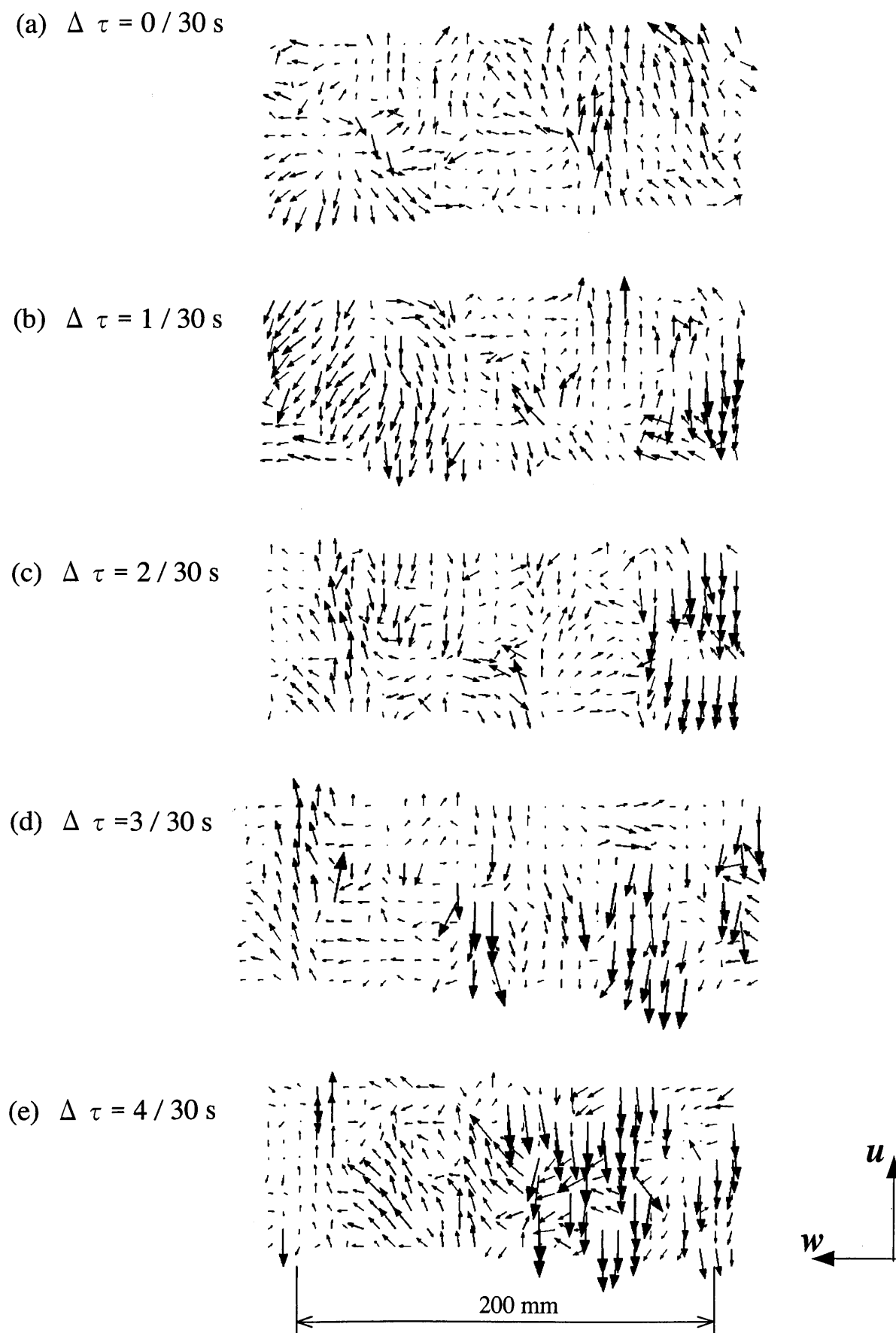


Figure 5.10 Temporal variation of velocity fluctuation vectors near wall in  $(x - z)$  plane



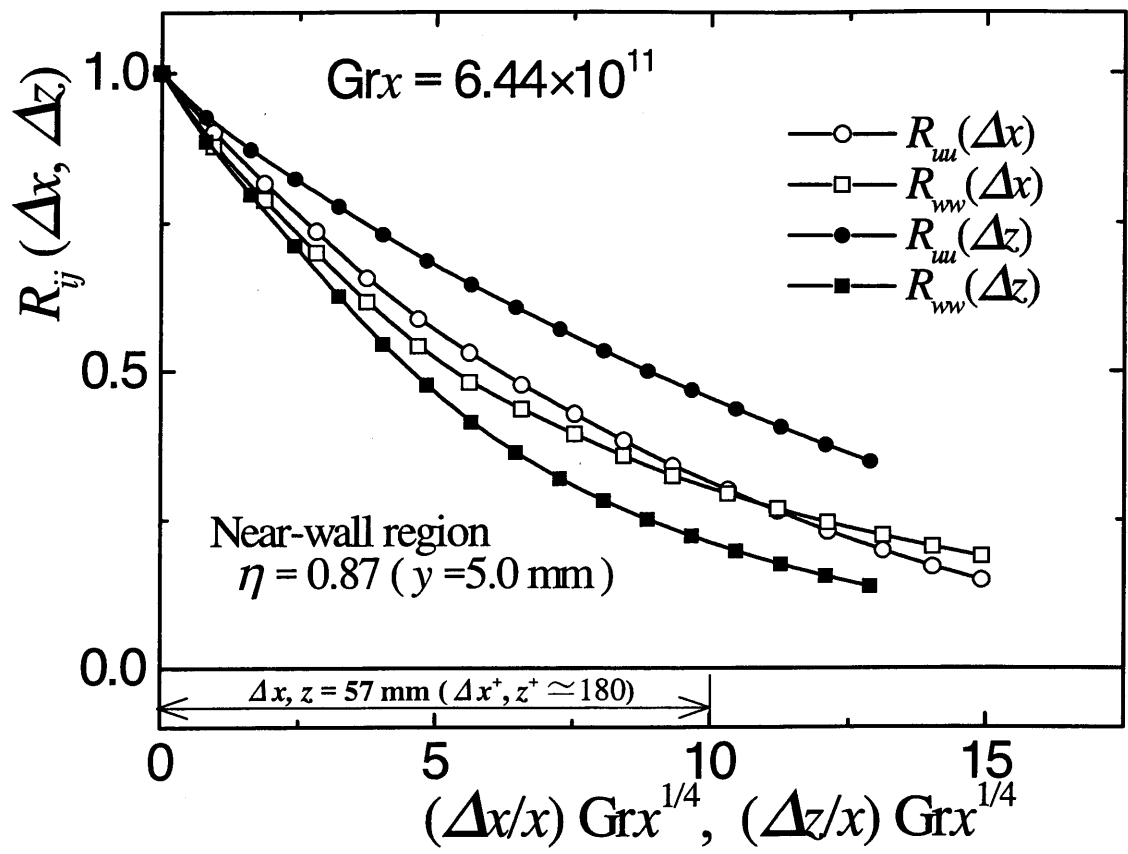


Figure 5.11 Two-point correlations in near-wall velocity field



# Chapter 6

## LINEAR STABILITY ANALYSIS

### 6.1 Stability Equations

To explain the experimental results, a linear stability analysis was conducted of the combined-convection boundary layer along a vertical isothermal heated plate in air ( $Pr = 0.71$ ). With the Boussinesq-approximated governing equations for thermally-driven flows, a decomposition of instantaneous velocity, pressure and temperature into mean and disturbance components leads to the equations for the base flow and disturbances.

The introduction of the boundary layer theory yields equations for the base flow:

$$\frac{\partial U}{\partial x} + \frac{\partial V}{\partial y} = 0 \quad (6.1)$$

$$U \frac{\partial U}{\partial x} + V \frac{\partial U}{\partial y} = \nu \frac{\partial^2 U}{\partial y^2} + g\beta(T - T_\infty) \quad (6.2)$$

$$U \frac{\partial T}{\partial x} + V \frac{\partial T}{\partial y} = \alpha \frac{\partial^2 T}{\partial y^2} \quad (6.3)$$

which are subject to the following boundary conditions:

$$U = V = 0, \quad T = T_w \quad \text{at } y = 0 \quad (6.4)$$

$$U = U_\infty, \quad T = T_\infty \quad \text{at } y \rightarrow \infty \quad (6.5)$$

A similarity solution for the above equations (6.1)–(6.5) does not exist. Therefore, using the finite volume method (Patankar, 1980), the profiles of mean velocity and mean temperature in the boundary layer were numerically determined.

For disturbances, linear equations may be obtained by omitting terms higher than the second order of magnitude. Upon introducing a stream function, assumptions of two-dimensionality and periodic disturbances, the disturbance stream function  $\phi$ , and the temperature disturbance  $t$  are expressed as:

$$\phi = \phi(y) \exp[i(\gamma x - \omega \tau)] \quad (6.6)$$

$$t = \theta(y) \exp[i(\gamma x - \omega \tau)] \quad (6.7)$$

After eliminating pressure fluctuation, the residual equations in terms of disturbance amplitude functions  $\phi(y)$  and  $\theta(y)$  are obtained:

$$\begin{aligned} \left( U - \frac{\omega}{\gamma} \right) (\phi' - \gamma^2 \phi) + \left( \frac{\partial^2 V}{\partial x \partial y} - \frac{\partial^2 U}{\partial y^2} \right) \phi \\ = \frac{1}{i\gamma} \left[ \nu (\phi'''' - 2\gamma^2 \phi'' + \gamma^4 \phi) - V (\phi''' - \gamma^2 \phi') + \left( \frac{\partial^2 V}{\partial x^2} - \frac{\partial^2 U}{\partial x \partial y} \right) \phi' + g\beta\theta' \right] \end{aligned} \quad (6.8)$$

$$\left( U - \frac{\omega}{\gamma} \right) \theta - \frac{\partial T}{\partial y} \phi = \frac{1}{i\gamma} \left[ \alpha (\theta'' - \gamma^2 \theta) - V \theta' - \frac{\partial T}{\partial x} \phi' \right] \quad (6.9)$$

where the prime denotes differentiation with respect to  $y$ . The boundary conditions are:

$$\phi = \phi' = \theta = 0 \quad \text{at } y = 0, \infty \quad (6.10)$$

According to Eqs. (6.6) and (6.7), solutions to the set of equations, (6.8) and (6.9), with  $\text{Im}(\omega) > 0$  represent an unstable condition. This means that the amplitudes of disturbances grow exponentially with time.

## 6.2 Numerical Solution of Eigenvalue Problem

Equations (6.8) and (6.9) were solved by collocation method (Orzag and Kells, 1980; Tanaka, Tsuji and Nagano, 1994) as an eigenvalue problem. The coordinate transformation to the Gauss-Lobatto point was applied:

$$y = \frac{y_m}{2} (1 - X_j) \quad (6.11)$$

$$X_j = \cos \frac{\pi j}{N} \quad (j = 1, \dots, N) \quad (6.12)$$

The disturbances may be expressed by trial functions including Chebyshev polynomials (Tanaka, Tsuji and Nagano, 1994) and satisfying the boundary conditions, Eq. (6.10) :

$$\phi(y) = \sum_{n=0}^N \phi_n (1 - X_j^2)^2 T_n(X_j) \quad (6.13)$$

$$\theta(y) = \sum_{n=0}^N \theta_n (1 - X_j^2) T_n(X_j) \quad (6.14)$$

Substituting Eqs. (6.13) and (6.14) into Eqs. (6.8) and (6.9) yields the simultaneous algebraic equations:

$$A\vec{X} = \lambda B\vec{X} \quad (6.15)$$

where

$$\vec{X} = (\phi_0, \phi_1, \dots, \phi_N, \theta_0, \theta_1, \dots, \theta_N)^T, \quad \lambda = \omega/\gamma$$

For the calculation of Eq. (6.15), the QR matrix eigenvalue algorithm was adopted, and the eigenvectors and eigenvalues were determined. The number of collocation points was 128,

and the computational domain for the base flow was three times as large as the boundary layer thickness.

Stability analyses for various flow fields were carried out to verify the numerical accuracy of the present method. The neutral stability curve for the pure natural-convection boundary layer along a vertical plate agreed well with that obtained by Tanaka, Tsuji and Nagano (1994), and the critical Reynolds number and eigenvalues for plane Poiseuille flow also coincided with those reported by Orzag and Kells (1980).

## 6.3 Results and Discussions

Since the similarity profile does not hold for the base flow of the combined-convection boundary layer, unique neutral stability curve cannot be obtained. Therefore, the parameter  $Grx / Rex^3$ , which depends not on  $x$  but on the freestream velocity and thermal conditions, was used in the present study. As previously mentioned in Chapter. 3, the decrease in  $Grx / Rex^3$  corresponds to the increase in freestream velocity under the constant thermal condition, and the  $x$ -dependency is contained in the  $Grx$  number.

Figure 6.1 depicts the neutral stability curves for the natural-convection and combined-convection boundary layers. In the figure, the non-dimensional wave number  $\gamma^* [= \gamma x / (Grx / 4)^{1/4}]$  is taken as the ordinate. The neutral curve for pure natural convection agrees closely with that calculated by Tanaka, Tsuji and Nagano (1994). A noticeable change in the neutral curve arises from the increase in freestream velocity. When introducing a weak freestream ( $Grx / Rex^3 = 10^{-3}$ ) in the high wave number region, the neutral curve shifts toward an extremely higher Grashof number, while it remains at a low Grashof number for the low-wave number region. This result agrees well with that of Carey and Gebhart (1980). Then, with increasing freestream velocity, the neutral curve entirely shifts toward the higher  $Grx$  region, and the critical Grashof number  $Grx_{crit.}$  for combined convection becomes much higher than that for natural convection.

In Fig. 6.2, the mean velocity profiles for natural convection and combined convection are compared. The mean velocity  $U$  and the distance from the wall  $y$  are normalized with the similarity variables used for the laminar natural-convection boundary layer. The effect of the freestream on the mean velocity profile is marked in the outer layer. The mean velocity gradient is reduced in the outer layer but increases near the wall with the addition of the freestream. Consequently, the inflection point of the mean velocity profile almost disappears. It is well known that the presence of an inflection point of mean velocity brings out the instability of the boundary layer, and that the maximum disturbance occurs near the inflection point (Krishnamurthy and Gebhart, 1989). In addition, as described in Chapter 5, a large-scale vortex plays an important role in turbulence generation for the combined-convection boundary layer. Thus, the change in the mean velocity profile in the outer layer with increasing freestream velocity seems to be one of the causes of the laminarization of the boundary layer.

The critical Grashof number  $Gr_{x_{crit}}$  determined by linear stability analysis is plotted against the coordinate  $Grx / Rex^3$  in Fig. 6.3. As seen in Fig. 6.1, the critical Grashof number is independent of  $Grx/Rex^3$  for an extremely weak freestream. In addition, with increasing freestream velocity ( $Grx / Rex^3 < 10^{-3}$ ), the critical Grashof number increases exponentially. Thus, it is found that both experimental and analytical results indicate the sudden delay of the transition region due to the freestream effect. Then, for  $Grx / Rex^3 < 10^{-3}$ , the unstable fluctuations indicating the transition of the boundary layer from laminar to turbulent arise at  $Rix = 0.56$ . Certainly, there is an indication that, under limited experimental conditions, the  $Rix$  number is a good parameter for predicting the beginning of the transition (Krishnamurthy and Gebhart, 1989). These results may be ascribable to the fact that the heat and fluid flow characteristics of the laminar combined-convection boundary layer can be correlated with the Richardson number  $Rix$  (Gryzagoridis, 1975; Sammakia, Carey and Gebhart, 1985; Patel, Armaly and Chen, 1998). Therefore, as long as the linear stability analysis is based on the laminar boundary layer, it is natural that a transition behavior correlated with the Richardson

number will be obtained.

These results may be very useful in understanding why the laminarization of the boundary layer occurs with an increasing freestream velocity. Such an analysis for the combined-convection boundary layer was also conducted by Carey and Gebhart (1983), and it was concluded that even a weak-aiding freestream suppressed the amplification of disturbances in air along a vertical heated plate. In their study, however, the base flow was determined as a perturbation of pure natural convection, and the freestream velocity was restricted so as not to exceed the maximum velocity of natural convection at the nose of the neutral curve to ensure the accuracy of the base flow solution, i.e., their analysis concerns only a very weak freestream. Indeed, a significant difference in the neutral stability curve obtained does not appear, and there is no change in the critical Grashof number between natural convection and combined convection. In the present analysis, as previously mentioned, the profiles of mean velocity and temperature in the boundary layer were obtained by directly solving the partial differential equations for the base flow by the finite volume method. Then, a linear analysis was performed over a wide range of freestream velocities and the change in the neutral stability curve for combined convection can be observed in the present analysis.

On the other hand, it has been revealed through our experiments that the laminarization of the turbulent combined-convection boundary layer occurs at a rather small freestream velocity of about a half or two thirds of the maximum mean velocity, and that the relation  $Gr_x / Re_x \simeq 3 \times 10^{-6}$  is a good guideline showing the occurrence of a laminarization, as described in Chap. 4. Namely, there exists a noticeable quantitative discrepancy between the experimental and theoretical results, i.e., the calculated critical Grashof number is appreciably smaller than that recognized by the decay of temperature fluctuations.

For this circumstance, the measured cross-correlation coefficients  $R_{ut}$  between velocity and temperature fluctuations, shown in Fig. 6.4, are discussed here. The profile of  $R_{ut}$  varies remarkably with increasing freestream velocity, and the peculiar profiles appear in accordance with the laminarization of the boundary layer. However, a similar profile is observed for



$Gr_x / Re_x^3 = 1.05 \times 10^{-4}$  and  $Gr_x = 3.30 \times 10^{11}$  and for  $Gr_x / Re_x^3 = 3.68 \times 10^{-4}$  of  $Gr_x = 1.95 \times 10^{11}$ , and a different sign of  $R_{\theta}$  alternately appears with  $y$  and the maximum absolute value of  $R_{\theta}$  almost approaches unity. This indicates that velocity and temperature disturbances have the same frequency with different phases. Unfortunately, such an  $R_{\theta}$  profile cannot be discussed in the context of the present linear stability analysis because periodic disturbances for velocity and temperature fluctuations are assumed. Recently, Moresco and Healey (2000) suggested the importance of the effects of spatio-temporal disturbance on the stability properties. In addition, it is indicated that the stability in the whole boundary layer region of natural convection may not be directly connected with a local stability (Polymeropoulos and Gebhart, 1967; Knowles and Gebhart, 1968; Dring and Gebhart, 1969; Tanaka, Tsuji and Nagano, 1994). Indeed, in the case of pure natural convection, the critical Grashof number obtained by linear stability analysis becomes distinctly smaller than that measured in the experiment.

Thus, it seems to be very difficult to correctly predict the laminarization of the boundary layer for combined convection using a simple linear analysis, and more advanced stability analyses will be required for the quantitative prediction of the critical Grashof number and for detailed information on the laminarization of the boundary layer.

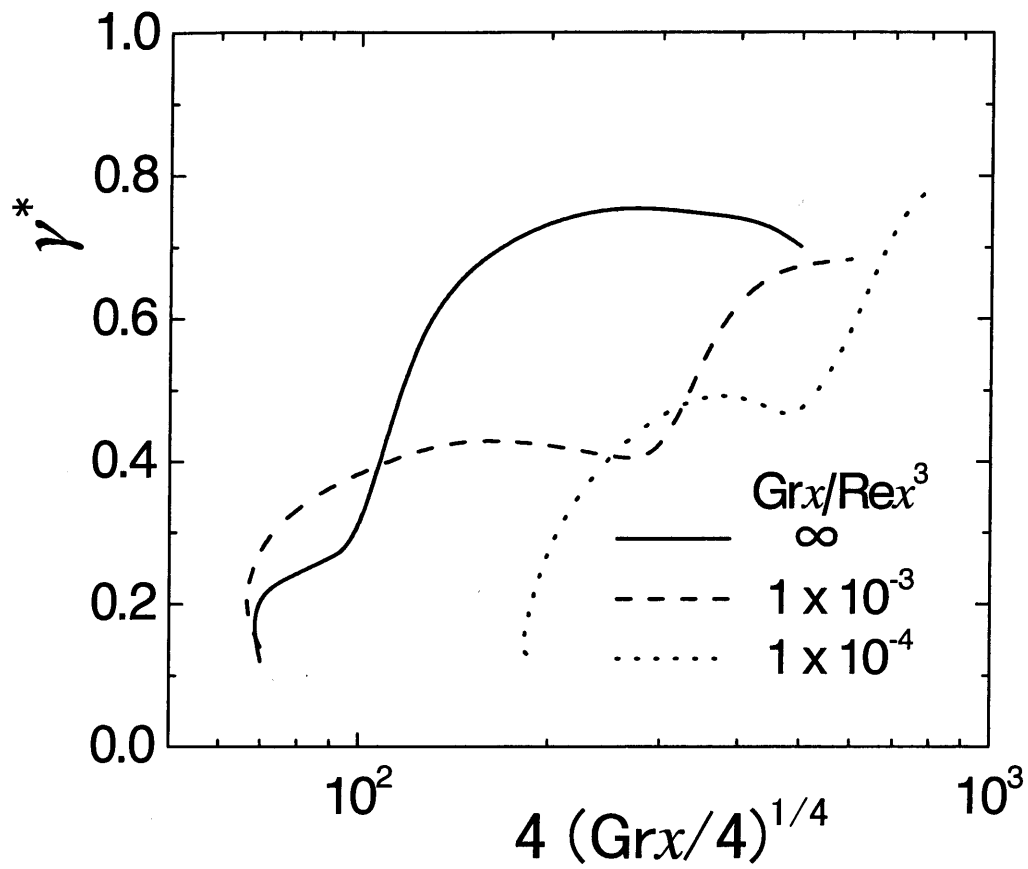


Figure 6.1 Neutral curves for natural convection and combined convection

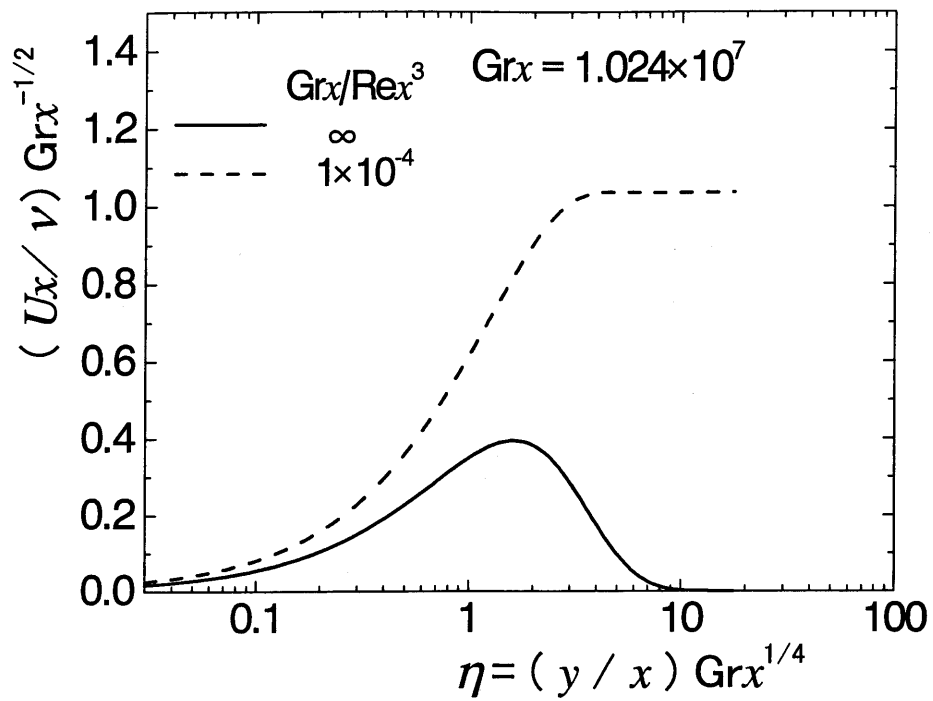


Figure 6.2 Comparison of mean velocity profiles for natural convection and combined convection

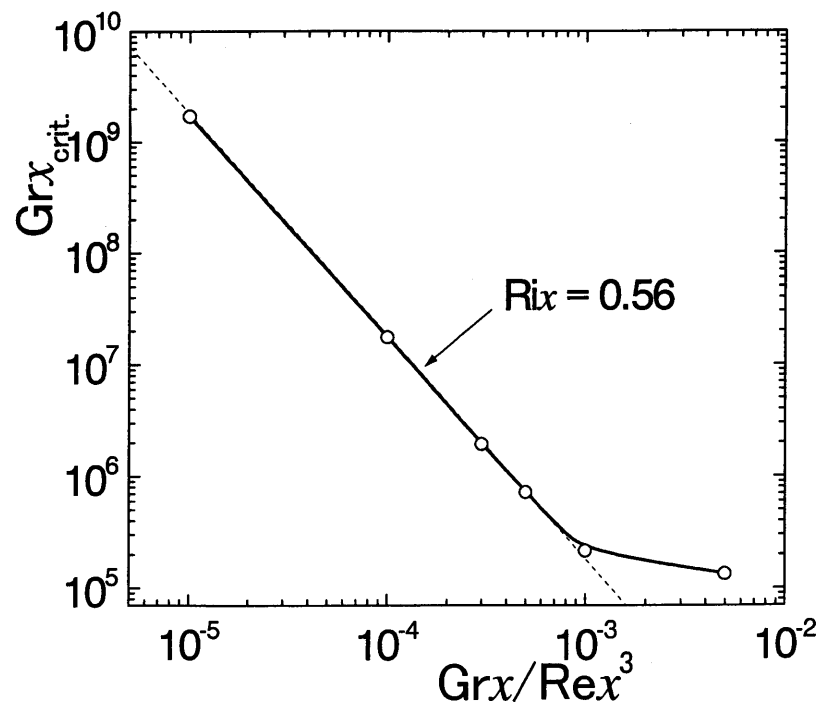


Figure 6.3 Critical Grashof number

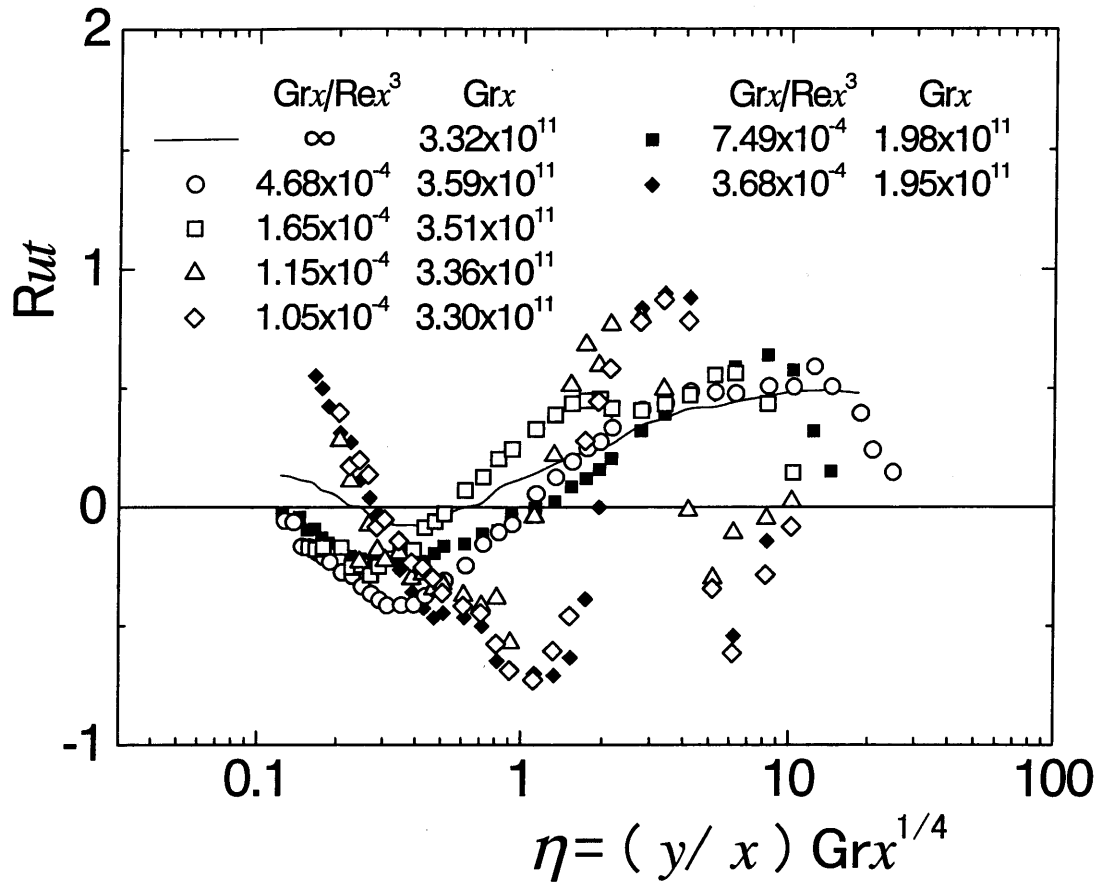


Figure 6.4 Cross-correlation coefficients between velocity and temperature fluctuations measured with hot and cold wires

# Chapter 7

## CONCLUSIONS

Fluid flow and heat transfer characteristics in the turbulent combined-convection boundary layer along a vertical isothermally-heated plate in air have been investigated experimentally and theoretically.

In Chapter 3, the heat transfer rate and turbulent statistics of the boundary layer have been measured with normal hot and cold wires, paying close attention to the near-wall region. The results may be summarized as follows.

- 1) A drastic reduction in  $N_{ux}$  is observed in combined convection with a slight increase in freestream velocity, and the value of  $N_{ux}$  decreases to about 40 % of that in turbulent natural convection. This behavior of  $N_{ux}$  is due to the boundary layer transition from turbulent to laminar, and the transition location is displaced in the region farther downstream of that observed in pure natural convection. As the freestream velocity becomes sufficiently large, the boundary layer changes again to turbulent having the characteristics of forced convection
- 2) With an increase in freestream velocity, the velocity and temperature fluctuations become smaller in amplitude and change from random to harmonic at a specific frequency, and an intensity profile of velocity fluctuation with two peaks appears.

In Chapter 4, the turbulent statistics of the boundary layer for different Grashof numbers were discussed. The results may be summarized as follows.

- 1) As the freestream velocity increases, the local heat transfer rate suddenly decreases due to the transition from turbulent to laminar, whereas the wall shear stress monotonously increases.
- 2) A similar change in the turbulent quantities appears independently of local Grashof number.
- 3) The regimes of boundary layer flows are classified based on the experimental results. With increasing freestream velocity, the region of laminar combined convection extends to the large  $Gr_x$  region far from the critical Grashof number in pure natural convection.
- 4) The flow and heat transfer characteristics with a laminarization of the turbulent combined-boundary layer are correlated with the unique parameter  $Gr_x / Re_x$ , and the laminarization occurs at  $Gr_x / Re_x \simeq 3 \times 10^6$  for  $Gr_x > 10^{11}$ .

In Chapter 5, measurements with normal hot and cold wires and particle image velocimetry (PIV) have been conducted to investigate the spatio-temporal structures of the turbulent combined-convection boundary layer. The results may be summarized as follows.

- 1) For the turbulent combined-convection boundary layers, the large-scale fluid motions in the outer region play a predominant role in turbulence generation, while quasi-coherent structures as observed in the ordinary boundary layers do not exist in the near-wall.
- 2) An increasing freestream restricts large-scale fluid motions in the outer layer, so that turbulence generation is suppressed and the boundary layer becomes laminar.

In Chapter 6, the laminarization process in the turbulent combined-convection boundary layer due to increased freestream velocity air was investigated in a linear stability analysis and

hot wire measurements. The results may be summarized as follows.

- 1) Although a quantitative discrepancy exists between the experiment and the analysis, the drastic delay in the transition location with increasing freestream velocity, which gives rise to the laminarization of the boundary layer, can be well explained by the stability analysis.
- 2) Upon adding freestream at the edge of the boundary layer, the mean velocity gradient at the outer region is reduced, and the inflection point of the mean velocity profile almost disappears.
- 3) The laminarization characteristics of the boundary layer are very sensitive to experimental conditions such as a freestream disturbance. Thus, it seems very difficult to correctly predict the laminarization from turbulent to laminar for combined convection using a linear stability analysis.





# BIBLIOGRAPHY

- Abdelmecuid, A. M., and Spalding, D. B., 1979. Turbulent flow and heat transfer in pipes with buoyancy effects. *J. Fluid Mech.* **94**, 383-400.
- Abu-Mulaweh, H. I., Chen, T. S., and Armaly, B. F., 2000. Effects of stream velocity on turbulent natural convection flow along a vertical plate. *Experimental Heat Transfer Journal* **13**, 183-195.
- Bradshaw, P., 1965. The effect of wind-tunnel screens on nominally two-dimensional boundary layers. *J. Fluid Mech.* **22**, 679-687.
- Carey, V. P., and Gebhart, B., 1983. The stability and disturbance amplification characteristics of vertical mixed convection flow. *J. Fluid Mech.* **127**, 185-201.
- Celata, G. P., Annibale F., Chiaradia, A., and Cumo, M., 1998. Upflow turbulent mixed convection heat transfer in vertical pipes. *Int. J. Heat Mass Transfer* **41**, 4037-4054.
- Chao, B. T., Chen, S. J., and Yao, L. S., 1983. Mixed convection over a vertical zircaloy plate in steam with simultaneous oxidation. *Int. J. Heat Mass Transfer* **26**, 73-82.
- Cheesewright, R., and Doan, K. S., 1978. Space-time correlation measurements in a turbulent natural convection boundary layer. *Int. J. Heat Mass Transfer* **21**, 911-921.
- Chen, T. S., Armaly, B. F., and Ali, M. M., 1987. Turbulent mixed convection along a vertical flat plate. *Trans. ASME J. Heat Transfer* **109**, 251-253.
- Cotton, M. A., and Jackson, J. D., 1990. Vertical tube air flows in the turbulent mixed convection regime calculated using a low-Reynolds-number  $k-\epsilon$  model. *Int. J. Heat Mass Transfer* **33**, 275-285.
- Dracos, T. ed., 1996. *Three-dimensional velocity and vorticity measuring and image analysis*

*techniques*, Kluwer academic pub., Dordrecht.

- Dring, R. P., and Gebhart, B., 1969. An experimental investigation of disturbance amplification in external laminar natural convection flow. *J. Fluid. Mech.* **36**, 447-464.
- Easby, J. P., 1978. The effect of buoyancy on flow and heat transfer for a gas passing down a vertical pipe at low turbulent Reynolds numbers. *Int. J. Heat Mass Transfer* **21**, 791-801.
- Fabris, G., 1978. Probe and method for simultaneous measurements of "true" instantaneous temperature and three velocity components in turbulent flow. *Rev. Sci. Instrum.* **49**, 654-664.
- Fukatsu, R., 1934. *Wind-tunnel experimental method*. Kyoritsusya, Tokyo.
- Gryzagoridis, J., 1975. Combined free and forced convection from an isothermal vertical plate, *Int. J. Heat Mass Transfer* **18**, 911-916.
- Hall, W. B., and Price, P. H., 1970. Mixed forced and free convection from a vertical heated plate to air. *Proc. 4th Int. Heat Transfer Conf.* **4**, NC 3.3.
- Hattori, Y., Kashiwagi, E., Yamakawa, H., and Wataru M., 1995. Experiments of natural convection to evaluate heat transfer in the spent fuel dry storage facilities. *Proc. 3rd Int. Conf. On Nuclear Engineering* **4**, 1927-1932.
- Hattori, Y., Koga, T., Sakamoto, K., Wataru, M., Tanaka, N., and Takeda, H., 1999a. Development of numerical analytical method to estimate heat removal characteristics of cask storage facility system. *Proc. 7th Int. Conf. On Nuclear Engineering*.
- Hattori, Y., Tsuji, T., Nagano Y., and Tanaka, N., 1999b. Characteristics of turbulent combined-convection boundary layer along a vertical heated plate, *Proc. 1st Symp. on Turbulence and Shear Flow Phenomena*, 545-550.
- Hattori, Y., Tsuji, T., Nagano Y., and Tanaka, N., 2000a. Characteristics of turbulent combined-convection boundary layer along a vertical heated plate. *Int. J. Heat and Fluid Flow* **21**, 520 - 525.
- Hattori, Y., Tsuji, T., Nagano Y., and Tanaka, N., 2000b. Effects of freestream on turbulent combined-convection boundary layer along a vertical heated plate, *Proc. 3rd Symp. on Turbulence, Heat and Mass Transfer*, 695-702.
- Hattori, Y., Tsuji, T., Nagano Y., and Tanaka, N., 2000c. Retransition from turbulence to laminar flow in a combined-convection boundary layer along a vertical heated plate, *Proc.*

- 4th JSME-KSME Thermal Engineering Conf., 3-187-3-192.
- Hattori, Y., Tsuji, T., Nagano Y., and Tanaka, N., 2001a. Effects of freestream on turbulent combined-convection boundary layer along a vertical heated plate, *Int. J. Heat and Fluid Flow* **22**, to be published.
- Hattori, Y., Tsuji, T., Nagano Y., and Tanaka, N., 2001b. Turbulent structure of combined-convection boundary layer along a vertical heated plate, *Proc. 2nd Symp. on Turbulence and Shear Flow Phenomena*, accepted.
- Hattori, Y., Tsuji, T., Nagano Y., and Tanaka, N., Characteristics of combined-convection boundary layer along a vertical heated plate. *Trans JSME B*. to be published.
- Hieber, C. A., and Gebhart, B., 1971. Stability of vertical natural convection boundary layers: some numerical solutions. *J. Fluid Mech.* **48**, 625-646.
- Hinze, J. O., 1975. *Turbulence*, 2nd ed., McGraw-Hill, New York.
- Hishida, M., and Nagano, Y., 1978. Simultaneous measurements of velocity and temperature in nonisothermal flows. *Trans. ASME J. Heat Transfer* **100**, 340-345.
- Hoshino, T., and Sawada, T., 1972. Development of a method for measuring rapidly varying gas temperatures and velocities. *Trans. JSME* **38**, 139-147.
- Hu, H., Saga, T., Kobayashi, T., Taniguchi, N., and Segawa, S., 2000. Visualization on the small scale vortices in a jet mixing flow by using hierarchical recursive PIV method. *Proc. 6th JSME Kanto-branch General Meeting*, 173-174.
- Inagaki, T., 1996. The criterion for turbulent combined forced and natural convection in a vertical flow system. *Trans. ASME J. Heat Transfer* **118**, 213-215.
- Inagaki, T., and Kitamura, K., 1987. Turbulent heat transfer of combined forced and natural convection along a vertical flat plate (Prediction of heat transfer using a surface renewal model and visualized data of surface temperature). *Trans. JSME B* **54**, 2508-2514.
- Inagaki, T., and Kitamura, K., 1988. Turbulent heat transfer of combined forced and natural convection along a vertical flat plate (Effect of Prandtl number). *Trans. JSME B* **54**, 2515-2522.
- Incropera, F. P., ed., 1986. Research needs in electronic cooling. *Proc. workshop sponsored by National Science Foundation and Purdue University*.
- Jaluria, Y., 1984. Numerical study of the thermal process in a furnace. *Numerical Heat*

*Transfer* 7, 211-224.

- Kasagi, N., and Nishimura, M., 1997. Direct numerical simulation of combined forced and natural turbulent convection in a vertical plane channel. *Int. J. Heat and Fluid Flow* 13, 88-99.
- Kim, J., Moin, P., and Moser, R., 1987. Turbulence statistics in fully developed channel flow at low Reynolds number. *J. Fluid Mech.* 177, 133-166.
- Kitamura, K., Koike, M., Fukuoka, I., and Saito, T., 1985. Large eddy structure and heat transfer of turbulent natural convection along a vertical flat plate. *Int. J. Heat Mass Transfer* 28, 837-850.
- Kitamura, K., and Inagaki, T., 1987. Turbulent heat and momentum transfer of combined forced and natural convection along a vertical flat plate - Aiding flow. *Int. J. Heat Mass Transfer* 30, 23-41.
- Knowles, C. P., and Gebhart, B., 1968. The stability of the laminar natural convection boundary layer. *J. Fluid Mech.* 34, 657-686.
- Kraus, A. D., and Bar-Cohen, A., 1983. *Thermal analysis and control of electronic equipment*, Hemisphere Pub. Corp., New York.
- Krishnamurthy, R., and Gebhart, B., 1989. An experimental study of transition to turbulence in vertical mixed convection flows. *Trans. ASME J. Heat Transfer* 111, 121-130.
- Loehrke, R. I., and Nagib, H. M., 1976. Control of free-stream turbulence by means of honeycombs: A balance between suppression and generation. *Trans. ASME J. Fluids Engineering*, 342-353.
- Lumley, J. L., 1964. Passage of a turbulent stream through honeycomb of large length-to-diameter ratio. *Trans. ASME J. Basic Engineering*, 218-220.
- Mackawa, H., Kobayashi, M., and Yashiro, K., 1986. Frequency response of a constant-temperature hot-wire to temperature fluctuations. *Trans. JSME B* 53, 2560-2566.
- Makita, H., Mori, S., and Sawada, K., 1992a. Development of high-precision thermo anemometer (1st report, total system and high-frequency phase compensator for the thermometer). *Trans. JSME B* 58, 90-97.
- Makita, H., Sawada, K., and Mori, S., 1992b. Development of high-precision thermo anemometer (2nd report, on a low-frequency phase compensator for a thermometer and

- improvement in spatial resolution). *Trans. JSME B* **58**, 3100-3107.
- Merkin, J. H., 1969. The effect of buoyancy forces on the boundary-layer flow over a semi-infinite vertical flat late in a uniform free stream. *J. Fluid Mech.* **35**, 439-450.
- Morel, T., 1977. Design of two-dimensional wind tunnel contractions. *Trans. ASME J. Fluids Engineering*, 371-378.
- Moresco, B., and Jealey, J. J., 2000. Spatio-temporal instability in mixed convection boundary layers. *J. Fluid Mech.* **402**, 89-107.
- Mucoglu, A., and Chen, T. S., 1978. Wave instability of mixed convection flow along a vertical flat plate. *Numer. Heat Transfer* **1**, 267-283.
- Nakajima, M., Fukui, K., Ueda, H., and Mizushina, T., 1980. Buoyancy effects on turbulent transport in combined free and forced convection between vertical parallel plates. *Int. J. Heat Mass Transfer* **23**, 1325-1336.
- Orzag, S. A., 1971. Accurate solution of the Orr-Sommerfeld stability equation, *J. Fluid Mech.* **50**, 689-703.
- Orzag, S. A., and Kells, L. C., 1980. Transition to turbulence in plane Poiseuille and plane Couette flow, *J. Fluid Mech.* **96**, 159-205.
- Pankhurst , R. C., and Holder, D. W., 1965. *Wind-tunnel technique*, Sir Isaac Pitman & Sons LTD., London.
- Paranthoen, P., Petit, C., and Lecordier, J.C., 1982. The effect of the thermal prong-wire interaction on the response of a cold wire in gaseous flows (air, argon and helium). *J. Fluid Mech.* **124**, 457-473.
- Patankar, S. V., 1980. *Numerical heat transfer and fluid flow*, Hemisphere Pub. Corp.
- Patel, K. Armaly, B. F., and Chen, T. S., 1998. Transition from turbulent natural to turbulent forced convection. *Trans. ASME J. Heat Transfer* **120**, 1086-1088.
- Polymeropoulos, C. E., and Gebhart, B., 1967. Incipient instability in free convection laminar boundary layers. *J. Fluid Mech.* **30**, 225-239.
- Quintiere, J. G., Rinkinen, W. J., and Jones, W. W., 1981. The effect of room openings on fire plume entrainments. *Comb. Sci. and Tech.* **26**, 193-201.
- Rae, W. H., and Pope, A., 1984, *A low-speed wind tunnel testing*, 2nd ed., John Wiley & Sons. Inc. New York.

- Raffel, M., Willert, C., and Kompenhans, J., 1998. *Particle image velocimetry*, Springer-Verlag, Berlin.
- Sakamoto, K., Koga, T., Gomi, Y., Hattori, Y., Wataru, M., and Kashiwagi, E., 1998. Heat removal characteristics of a metal cask storage facility, *J. Atomic Energy Soc. Japan* **40**, 966-977.
- Sakamoto, K., Koga, T., Wataru, M., and Hattori, Y., 2000. Heat removal characteristics of vault storage system with cross flow for spent fuel, *Nuclear Engineering and Design* **195**, 57-68.
- Sammakia, B., Carey, V. P., and Gebhart, B., 1985. Measurements and calculations of transient mixed convection in air, *Int. J. Heat Mass Transfer* **28**, 1837-1846.
- Schlichting, H., 1979. *Boundary-layer theory*, 7th ed., McGraw-Hill, New York. 572.
- Shehata, A. M., 1984. Mean turbulence structure in strongly heated air flows. Ph.D. thesis, University of Arizona.
- Siebers, D. L., 1983. Experimental mixed convection heat transfer from a large, vertical surface in a horizontal flow. Ph.D. thesis, Stanford University.
- Smith, R. R., 1972. Characteristics of turbulence in free convection flow past a vertical plate. Ph. D. thesis, University of London.
- Subramanian, C. S., and Antonia, R. A., 1981. Effect of Reynolds number on a slightly heated Turbulent boundary layer, *Int. J. Heat Mass Transfer* **24**, 1833-1846.
- Tanaka, H., Tsuji, T., and Nagano, Y., 1994. Stability analysis of thermally-driven flows, *Proc. 31th National Heat Transfer Symp. of Japan*, 232-234.
- Tewari, S. S., and Jaluria, Y., 1990. Mixed convection heat transfer from thermal sources mounted on horizontal and vertical surfaces. *Trans. ASME J. Heat Transfer* **112**, 975-987.
- Tsuji, T., and Nagano, Y., 1988a. Characteristics of a turbulent natural convection boundary layer along a vertical flat plate. *Int. J. Heat Mass Transfer* **31**, 1723-1734.
- Tsuji, T., and Nagano, Y., 1988b. Turbulence measurements in a natural convection boundary layer along a vertical flat plate. *Int. J. Heat Mass Transfer* **31**, 2101-2111.
- Tsuji, T., and Nagano, Y., 1989. Velocity and temperature measurements in a natural convection boundary layer along a vertical flat plate. *Exp. Thermal Fluid Sci.* **2**, 208-215.
- Tsuji, T., Nagano, Y., and Tagawa, M., 1992a. Experiment on spatio-temporal turbulent

- structures of a natural convection boundary layer. *Trans. ASME J. Heat Transfer* **114**, 901-908.
- Tsuji, T., Nagano, Y., and Tagawa, M., 1992b. Frequency response and instantaneous temperature profile of cold-wire sensors for fluid temperature fluctuation measurements. *Exp. in Fluids* **13**, 171-178.
- Tsuji, T., and Nagano, Y., 1996. Structural characteristics of a turbulent natural convection boundary layer. *Proc. 2nd China-Japan Work Shop Turbulent Flows*, 277-289.
- Visualization Soc. of Japan ed., 1994. Japanese low speed wind tunnels. *J. Visualization Soc. of Japan* **14**.
- You, J., Yoo, J.Y., and Choi, H., 2000. Direct numerical simulation of turbulent mixed convection in upward and downward heated vertical tubes, *3rd Int. Symp. on Turbulence, Heat and Mass Transfer*, 719-726.
- Zhang, X., and Dutta, S., 1998. Heat transfer analysis of buoyancy-assisted mixed convection with asymmetric heating conditions. *Int. J. Heat Mass Transfer* **41**, 3255-3264.





# APPENDIX A

## TABULATED EXPERIMENTAL DATA

### A.1 Heat Transfer Rate and Wall Shear Stress

Grx/Rex3	Rex	Grx	Rix	Nux	$\tau_w/\rho U_b^2$	Um/Ub	u2m/Ub	t2m/DT
5.59E-03	2.65E+04	1.05E+11	1.48E+02	496.52	5.880	21.880	5.193	1.71E-01
1.21E-03	4.45E+04	1.06E+11	5.36E+01	234.27	6.546	34.298	3.975	1.10E-01
6.76E-04	5.45E+04	1.09E+11	3.68E+01	230.82	7.958	38.904	1.972	4.89E-02
7.01E-04	5.36E+04	1.08E+11	3.76E+01	214.59	7.847	37.670	1.916	4.49E-02
7.33E-04	5.24E+04	1.06E+11	3.84E+01	237.88	7.495	36.375	1.217	2.64E-02
6.86E-04	5.40E+04	1.08E+11	3.70E+01	229.81	7.058	37.040	1.427	2.72E-02
5.13E-04	5.97E+04	1.09E+11	3.06E+01	218.44	8.088	39.531	0.673	2.00E-02
3.91E-04	6.50E+04	1.07E+11	2.54E+01	227.08	7.552	37.727	0.539	7.63E-03
3.91E-04	6.50E+04	1.07E+11	2.54E+01	227.08	7.552	37.727	0.539	7.63E-03
1.04E-04	1.02E+05	1.09E+11	1.06E+01	241.58	8.477	42.560	0.292	1.03E-03
2.64E-04	7.40E+04	1.07E+11	1.95E+01	246.40	7.109	37.868	0.309	3.00E-03
7.31E-05	1.14E+05	1.07E+11	8.31E+00	286.85	8.699	40.613	0.466	1.31E-03
1.56E-05	1.89E+05	1.06E+11	2.96E+00	298.93	10.265	47.904	0.419	1.48E-03
4.18E-06	2.97E+05	1.10E+11	1.24E+00	412.68	10.923	62.300	1.847	2.42E-02
8.31E-07	5.07E+05	1.08E+11	4.21E-01	468.64	17.460	106.564	1.319	1.23E-02

Grx/Rex3	Rex	Grx	Rix	Nux	$\tau_w/\rho U_b^2$	Um/Ub	u2m/Ub	t2m/DT
4.76E-03	2.81E+04	1.06E+11	1.34E+02	578.21	6.09	22.114	5.387	1.73E-01
9.56E-04	5.10E+04	1.27E+11	4.88E+01	247.41	7.49	37.022	3.369	8.23E-02
5.73E-04	6.12E+04	1.31E+11	3.51E+01	255.82	8.40	41.168	2.127	4.26E-02
3.65E-04	6.83E+04	1.17E+11	2.50E+01	245.54	7.86	38.652	0.308	7.21E-03
7.24E-05	1.14E+05	1.06E+11	8.23E+00	284.68	10.32	40.719	0.348	2.18E-03
1.21E-04	1.02E+05	1.29E+11	1.24E+01	284.80	8.57	41.293	1.339	4.14E-03
1.87E-04	8.27E+04	1.06E+11	1.55E+01	263.61	10.36	39.574	0.238	2.02E-03
4.76E-05	1.30E+05	1.06E+11	6.20E+00	289.44	10.07	41.017	0.418	1.99E-03
3.17E-05	1.50E+05	1.06E+11	4.75E+00	304.73	10.32	42.956	1.487	2.79E-03
1.92E-05	1.78E+05	1.09E+11	3.42E+00	341.57	10.18	47.494	1.176	2.46E-03
5.61E-06	2.87E+05	1.33E+11	1.61E+00	381.89	13.06	60.369	3.152	4.81E-03
1.26E-06	4.70E+05	1.31E+11	5.94E-01	540.23	18.38	93.814	1.418	5.56E-03

Grx/Rex3	Rex	Grx	Rix	Nux	$\tau w/\rho$ Ub <sup>2</sup>	Um/Ub	u2m/Ub	t2m/DT
3.81E-03	3.74E+04	1.99E+11	1.43E+02	651.539	6.267	24.816	5.622	0.166
1.17E-03	5.49E+04	1.92E+11	6.39E+01	553.155	7.479	30.864	8.817	0.203
7.49E-04	6.42E+04	1.98E+11	4.81E+01	492.673	7.049	29.228	6.514	0.187
6.98E-04	6.59E+04	2.00E+11	4.60E+01	409.592	6.989	33.935	6.949	0.182
3.63E-04	8.14E+04	1.95E+11	2.95E+01	259.530	7.465	42.314	3.390	0.066
3.09E-04	8.84E+04	2.14E+11	2.73E+01	323.548	7.161	39.443	1.865	0.044
2.80E-04	9.15E+04	2.15E+11	2.57E+01	306.317	7.317	39.530	0.955	0.025
2.71E-04	9.01E+04	1.99E+11	2.44E+01	274.715	7.638	43.319	1.683	0.038
2.29E-04	9.79E+04	2.15E+11	2.24E+01	307.955	7.224	39.898	1.038	0.017
1.36E-04	1.16E+05	2.11E+11	1.57E+01	310.131	7.378	40.867	0.983	0.005
6.98E-05	1.41E+05	1.94E+11	9.81E+00	313.469	8.439	46.415	0.430	0.001
6.09E-05	1.54E+05	2.22E+11	9.37E+00	314.325	7.867	43.300	0.329	0.001
8.81E-06	2.78E+05	1.90E+11	2.45E+00	408.682	10.618	55.393	0.467	0.002
2.22E-06	4.42E+05	1.92E+11	9.82E-01	465.647	13.054	76.825	0.850	0.003

Grx/Rex3	Rex	Grx	Rix	Nux	$\tau w/\rho$ Ub <sup>2</sup>	Um/Ub	u2m/Ub	t2m/DT
3.41E-03	4.60E+04	3.32E+11	1.57E+02	844.940	6.379	26.947	6.065	0.166
8.14E-04	7.53E+04	3.48E+11	6.13E+01	928.496	7.021	29.174	4.403	0.152
4.68E-04	9.15E+04	3.59E+11	4.28E+01	898.276	7.451	30.969	4.342	0.147
2.46E-04	1.11E+05	3.38E+11	2.73E+01	865.002	7.484	30.241	4.309	0.145
1.65E-04	1.28E+05	3.51E+11	2.13E+01	1001.812	8.236	35.069	7.775	0.183
1.43E-04	1.35E+05	3.53E+11	1.93E+01	908.483	8.164	36.547	7.958	0.199
1.15E-04	1.43E+05	3.36E+11	1.64E+01	534.901	8.587	48.341	7.275	0.119
1.05E-04	1.47E+05	3.30E+11	1.54E+01	360.982	8.537	50.895	5.302	0.099
9.39E-05	1.52E+05	3.30E+11	1.43E+01	379.261	8.548	51.540	4.503	0.083
3.75E-05	2.06E+05	3.28E+11	7.73E+00	315.029	9.299	55.539	0.416	0.005
3.69E-05	2.13E+05	3.58E+11	7.88E+00	370.053	8.849	57.880	0.377	0.008
1.97E-06	5.66E+05	3.56E+11	1.11E+00	497.962	13.937	82.537	0.556	0.004

## A.2 Turbulent Statistics

(a)  $Rex = 0, Grx = 3.32 \times 10^{11}$ 

yt (mm)	yu (mm)	dy (mm)	U (m/s)	T (°C)	r.m.s. $u^2$ (m/s)	r.m.s. $t^2$ (°C)	ut (°Cm/s)	su	fu	st	ft
0.55	0.51	0	0.26612	95.81	0.03723	3.3609	0.0539	--	--	--	--
0.57	0.53	0.02	0.26012	95.103	0.03837	3.374	0.04339	--	--	--	--
0.6	0.56	0.05	0.25952	94.496	0.03456	3.1441	0.01517	--	--	--	--
0.65	0.61	0.1	0.26256	93.838	0.03826	3.4026	0.01739	--	4.975	-1.6781	7.8108
0.7	0.66	0.15	0.26607	93.004	0.04213	3.6984	0.02059	--	4.7513	-1.4661	6.1352
0.75	0.71	0.2	0.2756	92.166	0.04803	4.0823	0.02269	--	5.1266	-1.4175	5.988
0.8	0.76	0.25	0.28217	91.41	0.05284	4.3288	0.02527	--	4.6234	-1.4399	6.1081
0.85	0.81	0.3	0.29068	90.651	0.05564	4.6814	0.02746	0.23584	4.9972	-1.5414	6.7774
0.9	0.86	0.35	0.30242	89.751	0.0632	5.1712	0.0228	0.29083	4.8376	-1.5347	6.5356
0.95	0.91	0.4	0.31184	89.218	0.06595	5.1767	0.02324	0.34893	4.8469	-1.3469	5.6823
1.05	1.01	0.5	0.33875	87.575	0.07664	5.9777	0.02136	0.11268	4.0895	-1.3736	5.4756
1.15	1.11	0.6	0.37182	86.298	0.08026	6.3879	-0.00187	0.14951	4.9957	-1.3503	5.5575
1.25	1.21	0.7	0.39745	84.424	0.08973	7.3929	0.00842	0.21309	4.3572	-1.2403	4.8645
1.35	1.31	0.8	0.43205	83.393	0.09922	7.7139	-0.02273	0.18744	4.6873	-1.3096	5.3172
1.45	1.41	0.9	0.46634	82.326	0.10122	7.9616	-0.04865	0.41365	4.6815	-1.2663	5.0667
1.55	1.51	1	0.4984	81.19	0.11097	8.4203	-0.05759	0.41161	4.1944	-1.1799	4.6051
1.75	1.71	1.2	0.53447	77.925	0.12025	9.8089	-0.09673	0.17676	3.93	-1.0942	4.137
1.95	1.91	1.4	0.57737	74.959	0.13471	10.854	-0.09996	0.2847	3.7472	-0.92298	3.5304
2.15	2.11	1.6	0.62998	73.914	0.13959	10.681	-0.1312	0.18962	3.4839	-0.8665	3.4234
2.35	2.31	1.8	0.66118	71.511	0.14298	11.179	-0.11456	0.23998	3.3811	-0.74206	3.064
2.55	2.51	2	0.70661	69.334	0.15319	11.781	-0.07428	0.13477	3.0215	-0.64401	2.8157
3.05	3.01	2.5	0.76375	65.337	0.16172	12.112	0.01836	-0.01157	3.1758	-0.44636	2.4905
3.55	3.51	3	0.81596	63.089	0.16799	12.269	0.00206	0.03898	3.0437	-0.35567	2.3358
4.05	4.01	3.5	0.84904	60.278	0.16977	12.086	0.17634	-0.14903	3.2684	-0.19666	2.2587
4.55	4.51	4	0.86994	58.519	0.17044	11.874	0.21162	-0.11902	3.1209	-0.11801	2.1807
5.55	5.51	5	0.88754	54.518	0.1753	11.815	0.28931	-0.09718	3.2731	0.12885	2.1586
6.55	6.51	6	0.91733	52.024	0.17334	11.049	0.35002	-0.23224	3.4934	0.26789	2.2662
7.55	7.51	7	0.91975	50.45	0.18052	10.734	0.40209	-0.13514	3.2878	0.36508	2.3337
8.55	8.51	8	0.95254	49.807	0.18429	10.152	0.44858	-0.27725	3.6884	0.39694	2.3638
9.55	9.51	9	0.95292	48.398	0.17864	9.693	0.43753	-0.17428	3.3782	0.51469	2.552
10.55	10.51	10	0.95056	47.094	0.18148	9.2803	0.42613	-0.19421	3.5689	0.60155	2.7221
13.55	13.51	13	0.95436	45.147	0.18931	8.4947	0.57332	-0.19583	3.347	0.71218	2.9653
16.55	16.51	16	0.97139	44.18	0.18704	7.8441	0.5335	-0.21779	3.5638	0.80656	3.1821
20.55	20.51	20	0.93516	42.508	0.19387	6.9896	0.57814	-0.18879	3.1521	0.90659	3.5784
25.55	25.51	25	0.94029	41.51	0.19305	6.2996	0.50172	-0.08406	3.0776	0.96216	3.8419
30.55	30.51	30	0.93421	40.491	0.19481	5.7151	0.49621	-0.11701	3.0676	0.88977	3.7997
40.55	40.51	40	0.85138	38.466	0.20204	4.6074	0.43307	-0.12983	2.8146	1.078	4.6187
50.55	50.51	50	0.83737	37.706	0.20667	4.2362	0.42712	-0.03056	2.7912	1.016	4.3767
60.55	60.51	60	0.83056	37.282	0.20841	3.9097	0.39835	-0.04949	2.8197	0.90211	4.0974
70.55	70.51	70	0.77146	36.016	0.21313	3.354	0.35186	-0.07551	2.7659	0.91609	4.0852
90.55	90.51	90	0.68532	34.609	0.214	2.8747	0.29503	0.18759	2.8297	1.0481	4.5515
100.55	100.51	100	0.65551	34.427	0.21508	2.7196	0.283	0.17277	2.8447	0.97168	4.2682
120.55	120.51	120	0.60416	33.431	0.21847	2.4151	0.28379	0.4083	2.9061	1.0468	4.48
140.55	140.51	140	0.55121	32.894	0.21863	2.0663	0.2222	0.4418	2.9325	0.87937	4.0201
160.55	160.51	160	0.49324	32.363	0.20368	1.7263	0.1419	0.50484	3.0689	1.0543	4.7157
180.55	180.51	180	0.46655	31.89	0.18939	1.5484	0.09685	0.57656	3.3254	1.124	4.5323
200.55	200.51	200	0.34962	31.571	0.16661	1.4766	-0.04058	0.75002	3.7797	0.99551	4.6652
240.55	240.51	240	0.2996	30.855	0.14506	1.126	-0.07901	0.92015	4.2703	1.2575	6.222
300.55	300.51	300	0.24739	30.579	0.12753	0.82071	-0.08379	1.357	6.4424	0.80927	4.7974

(b)  $\text{Rex} = 9.15 \times 10^4$ ,  $\text{Grx} = 3.59 \times 10^{11}$ 

yt (mm)	yu (mm)	dy (mm)	U (m/s)	T (°C)	r.m.s. $u^2$ (m/s)	r.m.s. $t^2$ (°C)	ut (°Cm/s)	su	fu	st	ft
0	0	--	--	--	--	--	--	--	--	--	--
0.55	0.52	0	0.29639	92.492	0.04592	3.6152	0.07321	--	--	--	--
0.57	0.54	0.02	0.31458	93.455	0.02665	2.7367	-0.00389	--	--	--	--
0.6	0.57	0.05	0.31445	92.902	0.0281	2.9063	-0.00284	--	--	--	--
0.65	0.62	0.1	0.31952	92.006	0.03203	3.1645	-0.00569	--	6.9341	-1.3355	6.1329
0.7	0.67	0.15	0.32574	91.176	0.03594	3.5493	-0.00797	--	6.5546	-1.3529	6.0921
0.75	0.72	0.2	0.33678	90.377	0.03766	3.8162	-0.02359	--	5.2674	-1.2703	5.6445
0.8	0.77	0.25	0.34893	89.601	0.04107	4.0219	-0.02795	--	4.9823	-1.2065	5.1539
0.85	0.82	0.3	0.36168	88.849	0.04392	4.3862	-0.03642	0.88254	5.5317	-1.3082	5.5936
0.9	0.87	0.35	0.37644	88.097	0.04874	4.6219	-0.04738	0.91233	5.5774	-1.2739	5.6897
0.95	0.92	0.4	0.39454	87.164	0.05372	5.0501	-0.06252	1.0179	6.0615	-1.2933	5.4971
1.05	1.02	0.5	0.42824	85.712	0.06073	5.451	-0.09103	0.96157	5.2342	-1.1789	5.0259
1.15	1.12	0.6	0.46718	84.185	0.07208	6.1074	-0.12739	1.1657	6.4194	-1.1819	5.0277
1.25	1.22	0.7	0.50643	82.501	0.07616	6.5884	-0.16728	1.0096	5.087	-1.1084	4.7116
1.35	1.32	0.8	0.54208	81.173	0.08538	6.9951	-0.21736	0.9903	4.7838	-1.0405	4.3976
1.45	1.42	0.9	0.5785	79.71	0.09418	7.574	-0.27919	0.99965	4.7443	-1.0972	4.6034
1.55	1.52	1	0.61424	78.7	0.10039	7.8613	-0.32683	0.84275	4.1267	-1.0127	4.1889
1.75	1.72	1.2	0.67526	75.722	0.11202	8.73	-0.40318	0.7541	3.7333	-0.93153	3.8906
1.95	1.92	1.4	0.736	73.331	0.12087	9.3746	-0.46428	0.60242	3.4104	-0.82886	3.5821
2.15	2.12	1.6	0.78392	71.146	0.12635	9.8493	-0.46409	0.45926	3.1803	-0.74201	3.3138
2.35	2.32	1.8	0.82959	68.718	0.13212	10.341	-0.47179	0.39376	3.1372	-0.64186	3.0543
2.55	2.52	2	0.8653	67.113	0.1329	10.541	-0.43368	0.3386	3.1529	-0.58234	2.9545
3.05	3.02	2.5	0.93735	63.085	0.13378	11.092	-0.36234	0.26111	3.4655	-0.40647	2.6074
3.55	3.52	3	0.98478	59.794	0.13831	11.304	-0.24019	0.34645	3.6174	-0.28335	2.4241
4.05	4.02	3.5	1.0241	57.363	0.13392	11.238	-0.15728	0.20318	3.5743	-0.17649	2.3399
4.55	4.52	4	1.0428	55.216	0.13639	11.064	-0.10685	0.29275	3.6115	-0.09208	2.3303
5.55	5.52	5	1.0818	51.7	0.14282	10.621	0.08776	0.37478	3.611	0.05476	2.3446
6.55	6.52	6	1.0991	49.565	0.14571	10.282	0.19062	0.42454	3.6194	0.15767	2.3405
7.55	7.52	7	1.1121	47.418	0.14697	9.7681	0.276	0.44593	3.6326	0.26726	2.3956
8.55	8.52	8	1.1235	46.27	0.15234	9.4908	0.35939	0.47924	3.5303	0.34124	2.484
9.55	9.52	9	1.1326	45.086	0.15477	9.1017	0.38836	0.44866	3.5362	0.4067	2.5622
10.55	10.52	10	1.1303	43.853	0.15508	8.6072	0.44762	0.43374	3.4319	0.45692	2.6538
13.55	13.52	13	1.1309	41.949	0.15681	7.8861	0.50926	0.42603	3.3483	0.51981	2.8147
16.55	16.52	16	1.1135	40.324	0.15838	7.2326	0.50264	0.3943	3.4958	0.59116	3.0323
20.55	20.52	20	1.0921	38.722	0.15878	6.7477	0.52087	0.41871	3.4183	0.6302	3.1028
25.55	25.52	25	1.0516	36.988	0.15691	6.0068	0.4563	0.39382	3.5509	0.67333	3.294
30.55	30.52	30	1.0012	35.429	0.14716	5.1209	0.36002	0.23443	3.3002	0.74334	3.5731
40.55	40.52	40	0.9009	32.774	0.1442	4.2126	0.30914	0.32491	3.2231	0.83345	3.7357
50.55	50.52	50	0.80393	30.708	0.13227	3.5037	0.23462	0.59495	3.4501	0.94502	3.9741
60.55	60.52	60	0.73046	29.358	0.12191	2.9691	0.21387	0.84134	3.8419	1.0756	4.095
70.55	70.52	70	0.65057	27.832	0.09338	2.3679	0.11234	1.4549	6.377	1.7229	6.4663
90.55	90.52	90	0.58105	26.564	0.05538	1.4346	0.03144	2.0354	13.293	3.536	18.303
100.55	100.52	100	0.56195	26.282	0.03962	1.0165	0.00971	--	--	--	--
120.55	120.52	120	0.55128	26.04	0.0247	0.49634	0.0018	--	--	--	--
140.55	140.52	140	0.54462	26.004	0.01626	0.22617	-2.41E-04	--	--	--	--
160.55	160.52	160	0.53756	25.979	0.01154	0.05171	-2.67E-05	--	--	--	--
180.55	180.52	180	0.53147	25.991	0.00925	0.03628	-1.26E-05	--	--	--	--
200.55	200.52	200	0.52436	25.988	0.00821	0.03837	1.25E-05	--	--	--	--
240.55	240.52	240	0.51819	25.979	0.00663	0.04031	1.39E-05	--	--	--	--
300.55	300.52	300	0.52211	25.996	0.00539	0.03454	-2.09E-06	--	--	--	--

(c)  $Re_x = 1.28 \times 10^5$ ,  $Gr_x = 3.51 \times 10^{11}$ 

yt (mm)	yu (mm)	dy (mm)	U (m/s)	T (°C)	r.m.s. $u^2$ (m/s)	r.m.s. $t^2$ (°C)	ut (°Cm/s)	su	fu	st	ft
0	0	--	--	--	--	--	--	--	--	--	--
0.55	0.52	0	0.31757	93.202	0.04776	3.7357	0.05736	--	--	--	--
0.57	0.54	0.02	0.29568	91.106	0.05756	4.0812	0.08681	--	--	--	--
0.6	0.57	0.05	0.31433	92.39	0.04147	3.1918	-0.0069	--	--	--	--
0.65	0.62	0.1	0.32356	91.192	0.05103	3.6716	-0.00935	--	8.403	-1.2424	5.4754
0.7	0.67	0.15	0.3306	90.462	0.05497	3.9066	-0.01411	--	9.4823	-1.2462	5.4158
0.75	0.72	0.2	0.34426	89.546	0.05772	4.2571	-0.04064	--	7.2205	-1.2191	5.4317
0.8	0.77	0.25	0.35874	88.584	0.06255	4.6134	-0.04951	--	8.4487	-1.2038	5.3802
0.85	0.82	0.3	0.37595	87.604	0.07045	5.0373	-0.06305	1.4811	8.3454	-1.2156	5.2461
0.9	0.87	0.35	0.39167	86.779	0.07298	5.2058	-0.06434	1.351	7.0666	-1.0971	4.8159
0.95	0.92	0.4	--	--	--	--	--	--	--	--	--
1.05	1.02	0.5	0.45819	84.074	0.09797	6.3668	-0.10665	1.3844	6.9254	-1.0141	4.5814
1.15	1.12	0.6	0.50004	82.438	0.10062	6.9752	-0.17866	1.2535	6.0339	-0.94133	4.1448
1.25	1.22	0.7	0.54816	81.087	0.1136	7.5884	-0.2124	1.1484	5.5265	-0.94567	4.1363
1.35	1.32	0.8	0.58985	79.099	0.12296	8.1679	-0.28835	1.0874	4.9126	-0.89944	3.8507
1.45	1.42	0.9	0.63217	78.382	0.13078	8.6208	-0.28273	0.92021	4.4221	-0.83499	3.6714
1.55	1.52	1	0.68552	77.088	0.14222	9.2624	-0.28724	0.75917	4.0849	-0.78157	3.4462
1.75	1.72	1.2	0.75689	74.572	0.15383	10.107	-0.29108	0.63407	3.7569	-0.70559	3.2663
1.95	1.92	1.4	0.81184	72.234	0.16674	10.632	-0.32084	0.62955	3.7516	-0.61515	3.0253
2.15	2.12	1.6	0.87458	70.127	0.17467	11.386	-0.17223	0.57466	3.6953	-0.59923	2.9273
2.35	2.32	1.8	0.9254	69.284	0.18269	11.717	-0.12962	0.57028	3.811	-0.5285	2.7415
2.55	2.52	2	0.95682	66.768	0.18966	11.908	-0.06281	0.68148	4.0039	-0.46423	2.6966
3.05	3.02	2.5	1.0476	63.478	0.20259	13.054	0.18926	0.5974	3.5573	-0.38545	2.4138
3.55	3.52	3	1.0999	60.545	0.21563	13.282	0.3632	0.65797	3.4343	-0.20747	2.2102
4.05	4.02	3.5	1.1499	58.581	0.23224	13.509	0.6382	0.68869	3.2605	-0.10147	2.1305
4.55	4.52	4	1.1717	56.101	0.23929	13.734	0.80301	0.72874	3.2068	0.03784	2.0683
5.55	5.52	5	1.2452	53.735	0.26523	13.923	1.2119	0.63338	2.795	0.2278	2.0875
6.55	6.52	6	1.2624	50.631	0.2756	13.511	1.4486	0.65738	2.8574	0.45655	2.2928
7.55	7.52	7	1.2785	48.382	0.28345	12.958	1.6014	0.7013	2.8721	0.61988	2.5679
8.55	8.52	8	1.2718	46.203	0.28194	12.094	1.529	0.77926	3.0929	0.81332	3.0401
9.55	9.52	9	1.2596	44.698	0.27797	11.143	1.409	0.77496	3.1223	0.94021	3.5223
10.55	10.52	10	1.2235	43.13	0.2581	10.052	1.0798	0.83787	3.4235	1.0117	4.0177
13.55	13.52	13	1.1581	40.333	0.22595	8.4384	0.77551	0.77678	3.5298	1.0039	4.4713
16.55	16.52	16	1.0919	38.35	0.1996	7.6421	0.66005	0.89109	4.2623	0.89867	4.1152
20.55	20.52	20	1.0177	35.963	0.17933	7.0404	0.59408	0.97407	4.537	0.9279	3.6395
25.55	25.52	25	0.92122	32.288	0.17047	5.6301	0.53166	1.4114	6.0038	1.4695	4.9099
30.55	30.52	30	0.85491	30.356	0.14056	4.4775	0.35375	1.5546	6.5968	2.0086	6.9197
40.55	40.52	40	0.77391	28.237	0.07863	2.1822	0.0745	2.1471	12.063	4.0232	22.418
50.55	50.52	50	0.73833	27.493	0.03572	0.74683	0.00386	--	--	--	--
60.55	60.52	60	0.73017	27.345	0.02319	0.19659	-4.16E-04	--	--	--	--
70.55	70.52	70	0.72515	27.318	0.0174	0.0369	-3.67E-05	--	--	--	--
90.55	90.52	90	0.72076	27.302	0.01297	0.03151	-9.44E-06	--	--	--	--
100.55	100.52	100	0.7149	27.27	0.0115	0.03587	2.67E-05	--	--	--	--
120.55	120.52	120	0.7154	27.27	0.00855	0.02791	3.50E-05	--	--	--	--
140.55	140.52	140	0.71135	27.248	0.00774	0.0344	2.31E-05	--	--	--	--
160.55	160.52	160	0.70694	27.227	0.00742	0.08719	9.46E-05	--	--	--	--
180.55	180.52	180	0.70147	27.207	0.00711	0.04389	9.23E-06	--	--	--	--
200.55	200.52	200	0.69594	27.173	0.00559	0.04213	4.05E-05	--	--	--	--
240.55	240.52	240	0.68892	27.144	0.00431	0.038	4.61E-05	--	--	--	--
300.55	300.52	300	0.66966	27.126	0.00508	0.02786	9.56E-06	--	--	--	--

(d)  $\text{Rex} = 1.43 \times 10^5$ ,  $\text{Grx} = 3.36 \times 10^{11}$ 

yt (mm)	yu (mm)	dy (mm)	U (m/s)	T (°C)	r.m.s. $u^2$ (m/s)	r.m.s. $t^2$ (°C)	ut (°Cm/s)	su	fu	st	ft
0	0	--	--	--	--	--	--	--	--	--	--
0.55	0.51	0	0.26972	97.086	0.03113	1.3219	-0.01477	1.7694	9.6193	-2.2778	11.702
0.57	0.53	0.02	0.27295	96.956	0.0301	1.107	-0.00559	1.3358	7.1076	-1.2438	4.8197
0.6	0.56	0.05	0.26864	96.938	0.02575	0.96958	0.00199	0.56022	4.234	-1.0721	3.7758
0.65	0.61	0.1	0.28592	96.249	0.03663	1.3597	-0.00975	1.4124	8.4837	-1.5603	6.671
0.7	0.66	0.15	0.2989	95.857	0.03885	1.5047	-0.00735	1.1116	6.2723	-2.2555	15.17
0.75	0.71	0.2	0.31231	95.597	0.04041	1.4674	-0.00565	0.88621	5.1996	-1.3714	5.819
0.8	0.76	0.25	0.33763	94.867	0.04865	1.9747	-0.02087	1.6123	8.7992	-2.0758	10.578
0.85	0.81	0.3	0.35232	94.674	0.04274	1.8385	0.00354	0.81143	5.8731	-1.9008	10.321
0.9	0.86	0.35	0.37569	94.233	0.04391	1.8256	0.00829	0.74204	6.1467	-1.0146	3.4938
0.95	0.91	0.4	0.39901	93.844	0.05339	2.3454	-0.01263	1.2827	8.0298	-2.4866	17.358
1.05	1.01	0.5	0.43805	93.564	0.04297	1.9304	0.02332	0.19717	4.4217	-1.1326	3.9715
1.15	1.11	0.6	0.48463	92.969	0.04877	2.1729	0.01169	0.5829	5.2551	-1.1375	4.005
1.25	1.21	0.7	0.54864	91.433	0.07075	2.8684	-0.04702	1.2822	7.0669	-1.4406	7.083
1.35	1.31	0.8	0.58352	91.562	0.06653	2.5095	-0.01263	0.901	6.1237	-1.0392	4.2509
1.45	1.41	0.9	0.62843	90.948	0.07547	2.8306	-0.03877	0.88367	5.5986	-1.4173	6.7881
1.55	1.51	1	0.6727	90.317	0.07294	3.0916	-0.05065	0.62857	4.355	-1.7831	10.865
1.75	1.71	1.2	0.75712	89.173	0.07897	3.0021	-0.04589	0.15928	2.6306	-1.0351	4.7844
1.95	1.91	1.4	0.83627	88.205	0.08776	3.5066	-0.09298	0.21354	3.4049	-1.8022	10.641
2.15	2.11	1.6	0.90435	87.279	0.09479	3.2377	-0.08655	-0.16138	2.4574	-0.63303	2.9522
2.35	2.31	1.8	0.97645	85.598	0.10246	3.9289	-0.13876	-0.12219	2.6397	-1.2191	6.5247
2.55	2.51	2	1.1502	81.261	0.13169	5.2991	-0.22536	0.21299	2.6664	-1.543	8.4336
3.05	3.01	2.5	1.2628	79.737	0.15046	5.1668	-0.28942	-0.097	2.0937	-1.3351	8.5161
3.55	3.51	3	1.3541	77.745	0.1612	5.6169	-0.37718	-0.27699	2.0504	-1.1335	7.8377
4.05	4.01	3.5	1.4325	75.21	0.17388	6.5419	-0.436	-0.41521	2.351	-0.89973	5.7971
4.55	4.51	4	1.5769	72.185	0.16293	6.8525	-0.63718	-0.49929	2.617	-0.01866	3.633
5.55	5.51	5	1.6673	67.259	0.16849	8.3778	-0.05733	-0.85512	4.2869	-0.4258	4.1773
6.55	6.51	6	1.7408	62.974	0.15358	8.1197	0.27196	-0.73834	4.4893	-0.10765	3.4219
7.55	7.51	7	1.7292	58.33	0.1955	8.7634	0.87805	-0.79773	4.1462	-0.10775	2.8959
8.55	8.51	8	1.6954	52.729	0.22517	7.7154	1.1844	-0.51177	3.1919	-0.17919	2.4497
9.55	9.51	9	1.5595	48.956	0.26197	7.8043	1.2188	-0.19405	2.3857	0.30643	2.9074
10.55	10.51	10	1.3902	43.245	0.17335	5.4147	0.71916	-0.13629	2.3723	0.16012	2.6158
13.55	13.51	13	1.2039	40.337	0.13956	5.4312	0.60476	0.45109	2.7058	0.15792	2.1569
16.55	16.51	16	0.84703	30.514	0.04728	1.6416	0.03846	2.3686	18.481	5.2313	37.776
20.55	20.51	20	0.79112	29.418	0.03441	0.30414	-1.56E-04	1.2143	18.222	8.8208	130.2
25.55	25.51	25	0.75659	28.963	0.02526	0.03565	-2.70E-04	0.07359	2.4109	-1.0433	12.022
30.55	30.51	30	0.74759	28.914	0.01659	0.02997	-5.43E-05	0.01166	2.4634	-1.566	16.703
40.55	40.51	40	0.74212	28.885	0.01163	0.02971	-1.69E-05	0.10032	2.8568	-1.3614	7.6788
50.55	50.51	50	0.74357	28.846	0.00838	0.04483	8.85E-06	0.36051	2.6279	-0.71757	4.8354
60.55	60.51	60	0.73667	28.813	0.00533	0.0383	7.58E-06	0.46212	4.7841	0.54042	3.5492
70.55	70.51	70	0.73112	28.798	0.00531	0.03662	5.62E-06	-0.67067	3.8635	0.18958	8.0791
90.55	90.51	90	0.72988	28.776	0.0058	0.02691	1.41E-06	-0.61496	3.1884	0.36055	8.2396
100.55	100.51	100	0.72212	28.763	0.00601	0.02541	-1.23E-08	0.23568	1.8249	-0.49194	10.074
120.55	120.51	120	0.72259	28.744	0.00538	0.02894	5.19E-06	0.129	1.6409	-1.7919	18.415
140.55	140.51	140	0.71655	28.734	0.00519	0.0303	4.41E-06	0.61156	3.5492	-1.7677	19.005
160.55	160.51	160	0.71439	28.734	0.00375	0.03019	8.17E-06	0.6446	4.8306	-1.9833	19.56
180.55	180.51	180	0.71083	28.721	0.00438	0.03257	5.28E-06	0.54931	3.6664	-2.1318	20.95
200.55	200.51	200	0.69794	28.701	0.00518	0.03651	1.33E-05	-0.4586	2.0538	-1.9165	15.44
240.55	240.51	240	0.69398	28.696	0.00554	0.03207	4.76E-06	0.23431	1.793	-1.5035	8.2543
300.55	300.51	300	0.6917	28.69	0.00532	0.03487	9.45E-06	0.67907	2.5557	-1.484	7.3455

(e)  $\text{Rex} = 1.47 \times 10^5$ ,  $\text{Grx} = 3.30 \times 10^{11}$ 

yt (mm)	yu (mm)	dy (mm)	U (m/s)	T (°C)	r.m.s. $u^2$ (m/s)	r.m.s. $t^2$ (°C)	ut (°Cm/s)	su	fu	st	ft
0	0	--	--	--	--	--	--	--	--	--	--
0.55	0.51	0	0.25724	97.543	0.02141	0.91241	-0.00407	1.1915	7.0725	-2.8433	20.402
0.57	0.53	0.02	0.26005	97.281	0.02143	0.82287	1.78E-04	0.76041	5.9057	-1.1798	4.3018
0.6	0.56	0.05	0.25991	97.131	0.02102	0.82764	0.00177	0.30526	3.2326	-1.1959	4.1633
0.65	0.61	0.1	0.26566	96.818	0.02284	0.86652	0.00282	0.21445	3.0106	-1.2445	4.4549
0.7	0.66	0.15	0.27655	96.416	0.02851	1.024	5.25E-04	0.93936	8.0495	-1.4544	5.7776
0.75	0.71	0.2	0.29198	95.959	0.03007	1.1426	0.00411	0.40733	4.0604	-1.2117	4.2782
0.8	0.76	0.25	0.30035	95.977	0.02928	1.0394	0.01174	-0.09749	2.5755	-1.4436	5.238
0.85	0.81	0.3	0.32599	95.339	0.03336	1.3139	0.0113	0.0827	2.8948	-1.2934	4.4526
0.9	0.86	0.35	0.34483	95.115	0.03659	1.311	0.01628	0.07571	3.7306	-1.2106	4.2448
0.95	0.91	0.4	0.36509	94.791	0.04004	1.5663	0.00723	0.59631	5.9631	-2.0127	10.636
1.05	1.01	0.5	0.4092	94.42	0.036	1.4014	0.02014	-0.22993	2.523	-1.3781	4.9644
1.15	1.11	0.6	0.46222	93.511	0.04687	1.7758	0.0144	0.96717	9.0361	-1.2443	4.3421
1.25	1.21	0.7	0.50553	93.144	0.04564	1.7671	0.01603	-0.02914	2.567	-1.267	4.5916
1.35	1.31	0.8	0.55407	92.161	0.05474	2.137	0.01611	0.04643	2.7167	-1.025	3.5818
1.45	1.41	0.9	0.60284	91.516	0.06105	2.4955	-0.0127	0.36336	3.6947	-1.8141	10.81
1.55	1.51	1	0.64731	91.221	0.0613	2.2468	-0.00707	0.16058	2.8544	-1.0884	3.9738
1.75	1.71	1.2	0.73491	89.785	0.07081	2.7013	-0.02704	0.00441	2.5577	-0.94721	3.3292
1.95	1.91	1.4	0.81161	88.838	0.08427	2.8273	-0.05565	-0.25407	2.3192	-0.82003	3.213
2.15	2.11	1.6	0.88494	87.755	0.09124	3.0013	-0.06945	-0.37922	2.4374	-0.70784	3.0966
2.35	2.31	1.8	0.95215	86.786	0.09708	3.1498	-0.09153	-0.51609	2.5669	-0.66596	3.0133
2.55	2.51	2	1.0071	85.795	0.09643	3.1981	-0.11132	-0.69086	2.6995	-0.45869	2.8431
3.05	3.01	2.5	1.127	83.082	0.12528	3.6789	-0.19186	-0.34311	2.5771	-0.09406	2.6405
3.55	3.51	3	1.2502	80.87	0.1406	3.9271	-0.24632	-0.31027	2.1414	-0.0797	3.3696
4.05	4.01	3.5	1.3574	78.943	0.15297	4.1208	-0.36285	-0.47769	2.2441	0.21022	2.5956
4.55	4.51	4	1.4447	76.795	0.16817	4.6749	-0.53982	-0.54286	2.2529	0.48557	2.3224
5.55	5.51	5	1.5682	73.365	0.18911	5.4614	-0.75082	-0.77557	2.6976	0.61152	2.3366
6.55	6.51	6	1.664	69.138	0.16889	6.8445	-0.70015	-0.619	3.0009	0.42791	3.0332
7.55	7.51	7	1.7829	65.217	0.12709	5.7337	-0.33378	-0.45941	3.4262	0.75358	3.8618
8.55	8.51	8	1.8153	59.64	0.11414	6.0954	0.19446	0.13975	3.1202	-0.17447	3.3323
9.55	9.51	9	1.7901	55.931	0.14283	7.1091	0.45153	-0.01734	3.3584	-0.19674	2.5646
10.55	10.51	10	1.7317	51.467	0.16423	6.7302	0.64476	-0.159	3.6097	-0.2448	1.9528
13.55	13.51	13	1.4378	43.736	0.16116	5.3014	0.66677	-0.34143	2.5088	0.14398	2.1803
16.55	16.51	16	1.2376	40.158	0.13405	5.0918	0.59449	0.42042	2.4485	0.21208	1.8219
20.55	20.51	20	1.0156	34.474	0.05263	3.6488	0.15028	0.62007	4.57	1.5362	4.7598
25.55	25.51	25	0.87396	30.587	0.02551	0.62282	-0.00547	-0.34856	5.2664	3.405	38.073
30.55	30.51	30	0.81095	29.528	0.03054	0.13344	-0.00251	-0.2318	2.2604	2.3736	36.892
40.55	40.51	40	0.77557	29.05	0.02507	0.04689	-3.35E-04	-0.03167	2.2818	0.01104	3.22
50.55	50.51	50	0.76575	28.953	0.0173	0.02501	-3.61E-05	0.00515	2.2175	-0.77082	8.3985
60.55	60.51	60	0.76198	28.926	0.01089	0.02525	-1.51E-06	-0.01029	3.1444	-0.57573	7.1879
70.55	70.51	70	0.7564	28.903	0.00734	0.0318	1.00E-06	-0.41266	3.0332	-1.8641	17.86
90.55	90.51	90	0.75564	28.868	0.00494	0.04036	1.25E-05	-0.71079	4.1142	-1.6252	9.5976
100.55	100.51	100	0.75082	28.864	0.00661	0.03645	-2.84E-06	-0.48311	2.2582	-1.0432	3.6823
120.55	120.51	120	0.7488	28.832	0.00611	0.04195	1.06E-05	-0.12753	1.7752	0.04147	2.0658
140.55	140.51	140	0.74394	28.815	0.00571	0.03855	1.74E-06	0.47005	2.329	0.5803	2.9448
160.55	160.51	160	0.73592	28.8	0.00352	0.03391	9.26E-06	0.28427	4.0239	0.84934	4.912
180.55	180.51	180	0.73632	28.787	0.00345	0.0314	7.34E-06	0.24818	3.8094	0.36957	7.6997
200.55	200.51	200	0.73218	28.786	0.00427	0.03398	8.01E-06	-0.79896	5.0577	-0.15849	11.059
240.55	240.51	240	0.72519	28.765	0.00618	0.02935	-4.38E-06	-0.35678	1.956	-0.86596	14.627
300.55	300.51	300	0.71751	28.754	0.00445	0.02719	2.85E-06	0.83439	4.0371	-0.86909	11.283

(f)  $\text{Rex} = 2.13 \times 10^5$ ,  $\text{Grx} = 3.58 \times 10^{11}$ 

yt (mm)	yu (mm)	dy (mm)	U (m/s)	T (°C)	r.m.s. $u^2$ (m/s)	r.m.s. $t^2$ (°C)	ut (°Cm/s)	su	fu	st	ft
0	0	--	--	--	--	--	--	--	--	--	--
0.55	0.51	0	0.28238	98.396	0.00559	0.03329	8.16E-06	0.57933	3.3898	-1.3347	9.4968
0.57	0.53	0.02	0.28315	98.178	0.00658	0.03367	-2.12E-06	0.35059	2.2322	-1.4642	11.383
0.6	0.56	0.05	0.28771	97.948	0.00672	0.04217	6.31E-06	-0.47827	2.7995	-1.2509	6.2431
0.65	0.61	0.1	0.29841	97.595	0.00743	0.03515	4.30E-06	-0.05862	2.1062	-0.92737	9.2557
0.7	0.66	0.15	0.31232	97.245	0.00726	0.04696	-1.06E-05	0.28499	2.7773	0.19817	4.0321
0.75	0.71	0.2	0.33109	96.933	0.00821	0.03864	-2.62E-05	-0.16551	2.5339	-1.1446	7.0589
0.8	0.76	0.25	0.3512	96.595	0.00872	0.0389	-3.02E-05	0.00822	2.4632	-0.205	7.6954
0.85	0.81	0.3	0.37561	96.292	0.0081	0.04314	-1.94E-05	-0.40787	3.251	-1.076	6.9953
0.9	0.86	0.35	0.4013	95.971	0.00928	0.04332	-4.29E-05	-0.16055	2.6021	0.26037	5.7796
0.95	0.91	0.4	0.42688	95.695	0.00885	0.04675	-2.85E-05	-0.32902	2.8584	-0.92357	5.6535
1.05	1.01	0.5	0.48442	95.085	0.00905	0.04256	-4.44E-05	-0.26798	3.021	-0.63666	6.6497
1.15	1.11	0.6	0.54215	94.503	0.00959	0.05043	-5.58E-05	-0.37646	2.7353	0.14221	5.1593
1.25	1.21	0.7	0.59752	93.929	0.00971	0.05311	-6.89E-05	0.26999	3.0285	0.40215	3.4671
1.35	1.31	0.8	0.65675	93.374	0.01006	0.05827	-7.94E-05	-0.31845	2.7662	-0.58309	2.9865
1.45	1.41	0.9	0.7128	92.806	0.00993	0.04968	-6.46E-05	0.1459	3.6068	-0.30866	5.2553
1.55	1.51	1	0.76504	92.254	0.01053	0.06603	-8.98E-05	0.04303	3.3631	0.04819	3.1755
1.75	1.71	1.2	0.87085	91.09	0.00957	0.06764	-1.20E-04	-0.06666	4.0287	-0.40661	2.9695
1.95	1.91	1.4	0.96525	89.918	0.01025	0.06504	-1.42E-04	0.0936	2.6619	-0.41879	8.6474
2.15	2.11	1.6	1.0486	88.778	0.01002	0.08557	-1.45E-04	0.31671	2.3918	-0.17472	2.6392
2.35	2.31	1.8	1.0933	87.634	0.01172	0.08618	-1.97E-04	0.59774	2.7355	-0.0411	3.7908
2.55	2.51	2	1.1847	86.474	0.01045	0.08589	-1.71E-04	-0.6897	4.1104	0.19828	2.8501
3.05	3.01	2.5	1.3818	83.645	0.01279	0.10427	-2.83E-04	0.44141	2.4303	0.00361	3.0127
3.55	3.51	3	1.5468	80.837	0.00991	0.10753	-6.40E-05	-0.64326	5.1558	-0.04761	3.0305
4.05	4.01	3.5	1.6848	78.05	0.00996	0.12076	-4.11E-05	0.30816	4.4539	-0.01582	2.7336
4.55	4.51	4	1.8041	75.318	0.01301	0.12769	-2.71E-04	-0.73738	3.1319	-0.02936	3.1339
5.55	5.51	5	1.9698	70.023	0.01028	0.13542	3.92E-05	-0.63531	4.6376	0.15691	3.4706
6.55	6.51	6	2.0696	64.94	0.01262	0.16151	-1.63E-04	-0.70634	3.5291	-0.06112	2.9517
7.55	7.51	7	2.1093	60.094	0.01288	0.16781	-1.67E-04	-0.60384	3.1256	-0.05093	3.0018
8.55	8.51	8	2.1069	55.599	0.01013	0.19319	2.94E-04	-0.38976	3.9689	-0.16141	2.8623
9.55	9.51	9	2.0599	51.503	0.01027	0.26323	8.41E-04	0.03929	3.2696	0.02392	2.8602
10.55	10.51	10	1.9956	47.742	0.01374	0.27751	2.87E-04	0.00169	2.5523	-0.03819	2.9991
13.55	13.51	13	1.7307	38.846	0.01268	0.33112	0.00199	0.25043	2.9901	0.09006	3.0944
16.55	16.51	16	1.4907	33.116	0.01299	0.20493	8.50E-04	-0.58154	3.5468	0.11881	3.3818
20.55	20.51	20	1.2782	28.963	0.00847	0.06858	1.82E-04	-0.3599	4.4084	0.13193	4.2271
25.55	25.51	25	1.1674	26.825	0.0074	0.04349	6.69E-05	-0.55253	4.5974	-0.89237	4.3476
30.55	30.51	30	1.1233	26.072	0.01074	0.02852	5.59E-06	0.15779	1.9878	0.3068	7.437
40.55	40.51	40	1.1086	25.762	0.00852	0.0339	2.87E-05	0.716	3.534	-1.1887	4.6702
50.55	50.51	50	1.0997	25.706	0.0068	0.04152	3.38E-05	0.05763	4.3774	0.21233	3.5056
60.55	60.51	60	1.0978	25.69	0.00875	0.03855	2.14E-05	7.67E-04	4.0676	0.2646	5.8098
70.55	70.51	70	1.0967	25.687	0.0062	0.03268	3.01E-05	0.16963	3.7395	1.0205	4.4165
90.55	90.51	90	1.0916	25.673	0.0082	0.03134	9.78E-07	0.16236	3.7031	0.41491	7.8467
100.55	100.51	100	1.091	25.651	0.00848	0.02403	-1.52E-05	0.79569	3.6608	-0.08258	6.8667
120.55	120.51	120	1.0942	25.634	0.01128	0.02703	-1.56E-05	0.37151	1.6439	-0.88417	9.7379
140.55	140.51	140	1.0931	25.628	0.01052	0.02538	-1.84E-08	0.63072	1.9103	-0.50861	6.7207
160.55	160.51	160	1.09	25.625	0.00868	0.02867	1.51E-05	1.3367	3.761	-1.2225	13.067
180.55	180.51	180	1.0948	25.632	0.01199	0.02503	-2.11E-05	0.27386	1.3958	-0.736	7.6353
200.55	200.51	200	1.1013	25.653	0.01132	0.02794	-1.34E-04	-1.835	5.3255	-0.51504	11.913
240.55	240.51	240	1.0999	25.667	0.01047	0.02651	-8.72E-05	-2.0173	6.0916	0.79176	6.2993
300.55	300.51	300	1.0891	25.649	0.00478	0.024	1.89E-05	-0.74908	5.0182	-0.22534	6.6627



# APPENDIX B

## HOT WIRE DATA PROCESSING

## PROGRAM

```

C*****
C
C      t720. f
C          cal. of N.C exp data
C          voltage of the output H.W -> velocity and temperature
C
C
C
C
C          Programmed by Y. Hattori
C          Date      '99.02.22
C*****
C
C      implicit real*8 (a-h, o-z)
C      parameter (n =150000)
C      parameter (ns=1000)
C      parameter (nl=1000)
C      parameter (n2=120000 +ns+nl)
C      parameter (n2= 58000 +ns+nl)
C      real*8 eu (n), et (n), u (n), t (n), a (n)
C      real*8 bu (n), bt (n)
C      character namel*14
C      character name2*14
C
C 1. set initial condition and read data.
C   1.1 condition
C      flag
C      data itco, itay/1, 1/
C      output
C      data iwav, itou/0, 1/
C      s. f.
C      data sf/ 500. d0/
C      data sf/2000. d0/
C      dt=1. d0/sf
C      H. W.
C      data hdl, hd/2. d-3, 3. 1d-6/

```

```

data rh, cp, rb/1. 935d4, 1. 340d2, 3. 887d-3/
data ro, to/19. 70825d0, 1. 53d0/
data rs/3. 8d1/
c   tw=to+(rs/ro-1. d0)/rb
    tw=240. 124368d0
data c / 2. 879206d4 /
data al0/ 0. 0000d0 /
data al1/ 1. 0642d0 /
data al2/ 1. 3775d0 /
data al3/-1. 7038d1 /
data al4/ 4. 3920d1 /
data al5/-4. 0478d1 /
data al6/ 1. 2653d1 /
c   data a0 /-5. 6113d-1/
c   data a1 / 1. 5333d1 /
c   data a2 /-5. 8994d0 /
c   data a3 / 2. 2676d0 /
c   data a4 /-2. 9015d-1/
c   data ah0/ 1. 7079d0 /
c   data ah1/ 9. 0513d0 /
c   data ah2/-0. 0546d0 /
c   data ah3/ 0. 0586d0 /
c   data ah4/ 0. 0000d0 /
c   Property of air (at T=273K)
    data pr, ra, an/0. 720d0, 24. 087d-3, 13. 331d-6/
c   eo
c   eo*eo/(tw-t(i))=eoa*t(i)+eob
    data eoa, eob/1. 52386d-5, 1. 19382d-2/
c
c   SOR
    data ru, rt/1. 0d0, 1. 0d0/
    data eru, ert/1. d-5, 1. d-5/
c
c   1.2 read input data (voltage of the O.P HW)
    write(*,*) 'input file name(for input)'
    read(*,1110) name1
1110  format(al4)
    open(1, file=name1, status='old')
    do 110 i=1, n2
    read(1,*) et(i), a(i), eu(i)
110  continue
    close(1)
c
c   1.3 voltage
    do 120 i=1, n2
    et(i)=1. 25d0*et(i)
    eu(i)=1. 25d0*eu(i)
    a(i) =1. 25d0*a(i)
120  continue
c
c   1.4 from et to t
    do 130 i=1, n2
    t(i)=30. d0*et(i)
130  continue
c
c   1.5 from eu to u
    do 140 i=1, n2
    eo2=(eob+eoa*t(i))*(tw-t(i))
    eo =dsqrt(eo2)
    if (eu(i). lt. eo) then

```

```

        write (9, *) 'cation cation cation'
    end if
    u(i) = c*((eu(i)*eu(i)-eo*eo)/(tw-t(i)))**2
    u(i) = dsqrt(u(i))
    if (u(i).lt.10.d-1) then
        u(i) = al0+al1*u(i)+al2/2.d0*u(i)**2+al3/3.d0*u(i)**3
&        +al4/4.d0*u(i)**4+al5/5.d0*u(i)**5+al6/6.d0*u(i)**6
    else
        u(i)=u(i)*u(i)
    endif
140 continue
c
    itotal=0
c
    5 continue
c
    itotal=itotal+1
c
    do 170 i=1,n2
        bt(i)=t(i)
        bu(i)=u(i)
170 continue
c
c 2. flozen turbulence
c 2.1 cal. Um
    au=0.d0
    do 210 i=ns,n2-n1
        au=au+u(i)
210 continue
    au=au/dbl(n2-n1+1)
c
c 2.2 time delay
    if (itay.eq.0) then
        it=0
    else if (itay.eq.1) then
        tt=hdl/au
        it=tt/dt
    endif
c
c 3. cariblation e
c 3.1 cal. e at U=0
    do 310 i=ns,n2
        eo2=(eob+eo*a*(i-it))*(tw-t(i-it))
        eo=dsqrt(eo2)
c
c 3.2 cal. u
    u(i) = c*((eu(i)*eu(i)-eo*eo)/(tw-t(i-it)))**2
    u(i) = dsqrt(u(i))
    if (u(i).lt.10.d-1) then
        u(i) = al0+al1*u(i)+al2/2.d0*u(i)**2+al3/3.d0*u(i)**3
&        +al4/4.d0*u(i)**4+al5/5.d0*u(i)**5+al6/6.d0*u(i)**6
    else
        u(i)=u(i)*u(i)
    endif
310 continue
c
c 4. cariblation T
    t(1)=30.d0*et(1)
    do 410 i=2,n2-n1
        if (itco.eq.0) then

```

```

        tm=0. d0
        else if (itco.eq.1) then
            tf =0. 5d0*(tw+t(i))+273. 15d0
            prf=pr*(tf/273. 15d0)**(-. 04d0)
            raf=ra*(tf/273. 15d0)**0. 8d0
            anf=an*(tf/273. 15d0)**1. 76d0
            thn= 0. 42d0*prf**0. 2*raf/hd
            thf= 0. 57d0*prf**0. 33*raf*dsqrt(u(i+it))/dsqrt(hd*anf)
            tm=0. 25d0*rh*cp*hd/(thn+thf)
        end if
        t(i)= 30. d0*et(i)
        &      +30. d0*(1. 0d0*tm*(et(i)-et(i-1))/dt)
c      t(i)=30. d0*et(i)+30. d0*(0. 5d0*tm*(et(i+1)-et(i-1))/dt)
c      write(8,1012) thf, tm
410 continue
1012 format(1h, 2e13. 3)
c
c 5. check
        do 510 i=ns, n2-n1
            u(i)=bu(i)+ru*(u(i)-bu(i))
            t(i)=bt(i)+rt*(t(i)-bt(i))
510 continue
        erum=0. d0
        ertm=0. d0
        do 520 i=ns, n2-n1
            erru=(u(i)/bu(i)-1. d0)
            errt=(t(i)/bt(i)-1. d0)
            erum=max(erru, erum)
            ertm=max(errt, ertm)
520 continue
c      write(20,1020) ium, itm, erum, ertm
        if(erum.gt.eru) go to 5
        if(ertm.gt.ert) go to 5
1020 format(1h, 2i7, 2e14. 3)
c
c 6. output
c 6.1 toukei
        au=0. d0
        at=0. d0
        nt=n2-n1-ns-it+1
        ne=n2-n1-it
        do 610 i=ns, ne
            au=au+u(i+it)
            at=at+t(i)
610 continue
c
        au=au/dbl(n2)
        at=at/dbl(n2)
c
        u2=0. d0
        ut=0. d0
        t2=0. d0
        t3=0. d0
        t4=0. d0
        u2=0. d0
        u3=0. d0
        u4=0. d0
        do 620 i=ns, ne
            u2 =u2 +(u(i+it)-au)*(u(i+it)-au)
            ut =ut +(u(i+it)-au)*(t(i)-at)

```

```

    t2 =t2 + (t (i) -at) * (t (i) -at)
    u3 =u3 + (u (i+it) -au) * (u (i+it) -au) * (u (i+it) -au)
    u4 =u4 + (u (i+it) -au) * (u (i+it) -au) * (u (i+it) -au) * (u (i+it) -au)
    t3 =t3 + (t (i) -at) * (t (i) -at) * (t (i) -at)
    t4 =t4 + (t (i) -at) * (t (i) -at) * (t (i) -at) * (t (i) -at)
620  continue
c
    u2 =dsqrt (u2 /db1e (nt))
    ut =      (ut /db1e (nt))
    t2 =dsqrt (t2 /db1e (nt))
    su =u3/db1e (nt) /u2/u2/u2
    fu =u4/db1e (nt) /u2/u2/u2/u2
    st =t3/db1e (nt) /t2/t2/t2
    ft =t4/db1e (nt) /t2/t2/t2/t2
c
    if (itou. eq. 1) then
        write (*, *) ' input file name (for output-toukei) '
        read (*, 1610) name2
1610    format (a14)
        open (2, file=name2, status=' unknown' )
        write (2, 1620) au, at, u2, t2, ut, su, fu, st, ft
        close (2)
1620    format (1h , 9e15. 5)
    end if
c 6. 2 wave
    if (iwav. eq. 1) then
        write (*, *) ' input file name (for output wave) '
        read (*, 1630) name2
        open (2, file=name2, status=' unknown' )
        do 630 i=ns, ne
            time=time+dt
            ut= (u (i+it) -au) * (t (i) -at)
            u2= (u (i+it) -au) + (u (i+it) -au)
            t2= (t (i) -at) + (t (i) -at)
            write (2, 1640) time, u (i+it), t (i), u2, t2, ut
630    continue
        close (2)
1630    format (a14)
1640    format (1h , 6e15. 5)
        endif
c
    stop
    end

```



# APPENDIX C

## PROGRAM FOR LINEAR STABILITY ANALYSIS

### C.1 Calculation of Base flow

```

c#####
c#
c# <Scheme>
c# Parabolic Solution Scheme Applied to Boundary Layer Equation
c# (PASSABLE)
c#
c# <Configuration>
c# Mixed Convection along a Vertical Plate
c#
c# <Point>
c# To calculate the initial condition for OS eq
c#
c# Original :Dr. M. A. Leschziner
c# Programmed:Yasuo Hattori
c#
c# Date: Oct. 19, 1999
c#
c#####
c mclami2. f
c#####
c block data
c#####
c***purpose:input of indices and set initial data
c
c implicit real*8 (a-h, o-z)
c parameter (in= 5001)
c
c*** variable
c real*8 u (in), v (in), t (in), dudx (in), dvdx (in), dtdx (in)
c*** file name
c character*15 fni, fnm (9)
c
c*** variable
c common var (in, 3), varu (in, 3), varu2 (in, 3)
c equivalence (var (1, 1), u (1)), (var (1, 2), v (1)), (var (1, 3), t (1))
c*** file name

```

```

      common/iout/fni, fnm
c*** variable
      common/ivari/nvar, inu, inv, int, ivar
c*** physical properties
      common/ppro/rl, pr, dn
c*** grid
      common/igrid/y(in), ydif(in), ys(in), yp(in), yd(in)
      &          , deltayl, yk, ny, nym1
      common/icopde/dyl(in), ddyl(in), dy2(in), ddy2(in)
      common/istep/dx, xd, xlast, xstart, xnheat
c*** coefficient of discretize equation
      common/icoef/adn(in), ads(in), adp(in), aup(in), bp(in), sp(in)
c*** development of boundary layer
      common/ibdev/grx, rex, rix
c*** flag
      common/index/incont, iprsta, itest
c*** boundary condition
      common/bc/uinf, tinf, ubc, tbc
c*** relaxation
      common/irelx/insolv(3)
      common/irelx2/urf(3)
c*** error
      common/ierr/erru, errv, errt
      common/ieps/epsu, epsv, epst
c*** iteration
      common/iiter/iter1, iter2
      common/icp/xstop(9), ixiter
c
c****physical properties and related data
      data rl/5.304d-4/
      data pr/0.710d0/
      data dn/1.920d-5/
c*** boundary condition (m/s, theta)
c      data uinf/1.00d-5/
      data uinf/0.10d0/
c      data uinf/0.20d0/
c      data uinf/0.30d0/
c      data uinf/0.50d0/
c      data uinf/1.00d0/
c      data uinf/3.00d0/
      data tinf/0.00d0/
c****distance related data
c      data ny, deltayl, yk/ 201, 2.768718d-5, 1.03d0/
      data ny, deltayl, yk/ 5001, 3.000000d-6, 1.001d0/
      data xnheat/0.d0/
      data xlast /1.3301d0/
c      data dx/1.d-5/
      data dx/3.d-6/
      data xstop/2.44d-2, 3.83d-2, 6.16d-2, 7.85d-2, 1.06d-1
      &          , 1.55d-1, 2.66d-1, 5.26d-1, 1.33d0/
c****general data
      data urf/2*0.7d0, 0.7d0/
      data epsu, epsv, epst/2*1.d-5, 1.d-5/
c****control indices (1:Yes, 2:No)
      data nvar, inu, inv, int
      &          /3, 1, 2, 3/
c * cal of equation*
      data insolv/1, 1, 1/
      data incont/1/
c * term of print*

```



```

      data iprsta/200/
c * test cal *
      data itest/0/
c
c****I/O data file-name(included wild card within 12-characters)
c
c      1***5****1**
      data fni    /' iter. dat' /
      data fnm    /' x1. dat', ' x2. dat', ' x3. dat', ' x4. dat', ' x5. dat'
&               , ' x6. dat', ' x7. dat', ' x8. dat', ' x9. dat' /
c
      end
c
c=====
      program mclami2
c=====
c
c*****
c      main program routine
c*****
c
c****purpose: contorol of operation
c
      implicit real*8 (a-h,o-z)
      parameter (in= 5001)
      real*8 u(in), v(in), t(in)
      character*15 fni, fnm(9)
      common var(in,3), varu(in,3), varu2(in,3)
      equivalence (var(1,1), u(1)), (var(1,2), v(1)), (var(1,3), t(1))
      common/iout/fni, fnm
      common/ivari/nvar, inu, inv, int, ivar
      common/ppro/rl, pr, dn
      common/igrd/y(in), ydif(in), ys(in), yp(in), yd(in)
&               , deltayl, yk, ny, nym1
      common/icopde/dyl(in), ddyl(in), dy2(in), ddy2(in)
      common/istep/dx, xd, xlast, xstart, xnheat
      common/icoef/adn(in), ads(in), adp(in), aup(in), bp(in), sp(in)
      common/ibdev/grx, rex, rix
      common/index/incont, iprsta, itest
      common/bc/uinf, tinf, ubc, tbc
      common/irelx/insolv(3)
      common/irelx2/urf(3)
      common/ierr/erru, errv, errt
      common/ieps/epsu, epsv, epst
      common/iiter/iter1, iter2
      common/icp/xstop(9), ixiter
c
c****:grid related calculations
c
      xstart=-xnheat
      nym1=ny-1
      call grid
c
c****:set initial conditions and Calculation reference quantities
c
      call init
      xd=xstart
      iter1=0
      ixiter=1
c

```

```

c*****
c                      marching roop
c*****
c
c=====store upstream quantities
c
1000 continue
    xu=xd
    xd=xu+dx
    grx=(xd/rl)**3
    rex=ubc*xd
    if (rex.eq. 0. d0) then
        rix=1e30
    else
        rix=grx/rex/rex
    end if
    if (xd.ge. 0. d0) t(1)=1. d0
c
    do 10 ivar=1, nvar
    do 10 j=1, ny
        varu2(j, ivar)=varu(j, ivar)
        varu(j, ivar) =var(j, ivar)
    10 continue
c
c=====solution of equations
c=====velocity filed
    iter2=0
    2000 continue
c-----calculate u-momentum equation
    if (insolv(inu).eq. 1) call calcu
c-----calculate v-velocity from continuity
    if (incont.eq. 1) call cont
c=====termal filed
    if (insolv(int).eq. 1) call calct
c
999  iter2=iter2+1
    if (iter2.gt. 10000) then
c      if (iter2.gt. 3000) then
        write(6, *) '>>> divergence <<<'
        stop
    endif
    if (itest.eq. 1) write(6, 505) iter2, erru, errt
505  format (1h, i6, 6(2x, e10. 3))
    if (erru.gt. epsu) go to 2000
    if (errv.gt. epsv) go to 2000
    if (errt.gt. epst) go to 2000
c
c=====termination of forward step
c
    call outpi
    iter1=iter1+1
    if (xd.ge. xstop(ixiter). and. ixiter.le. 9) then
        call outpm
        ixiter=ixiter+1
    endif
    if (xd.lt. xlast) go to 1000
c
    stop
end
c

```

```

c=====
      subroutine grid
c=====
c
c****purpose:set initial grid for non-expanding geometry
c
      implicit real*8 (a-h, o-z)
      parameter (in= 5001)
c
      common/igrid/y (in), ydif (in), ys (in), yp (in), yd (in)
&      , deltayl, yk, ny, nym1
      common/icopde/dyl (in), ddyl (in), dy2 (in), ddy2 (in)
c
      do 10 j=1, ny
          sj=dbl (j)
10  y (j)=deltayl* (yk** (sj-1. d0)-1. d0) / (yk-1. d0)
c
      do 20 j=2, ny
20  ydif (j)=y (j)-y (j-1)
c
      yd (1)=y (2)*0. 5d0
      ys (1)=yd (1)
c
      do 30 j=2, ny
          yd (j)=ydif (j)-yd (j-1)
30  ys (j)=yd (j)+yd (j)
c
      ys (ny)=ys (ny)*0. 5d0
c
      do 50 j=2, ny-1
          di1=ydif (j+1)* (ydif (j)+ydif (j+1))
          dyl (j)=ydif (j)/di1
          ddyl (j)=2. d0/di1
          di2=ydif (j)* (ydif (j)+ydif (j+1))
          dy2 (j)=ydif (j+1)/di2
50  ddy2 (j)=2. d0/di2
c
      return
      end
c
c=====
      subroutine init
c=====
c
c****purpose:set initial condition and data
c
      implicit real*8 (a-h, o-z)
      parameter (in= 5001)
      real*8 u (in), v (in), t (in), dudx (in), dvdx (in), dtdx (in)
c
      common var (in, 3), varu (in, 3), varu2 (in, 3)
      equivalence (var (1, 1), u (1)), (var (1, 2), v (1)), (var (1, 3), t (1))
      common/ppro/rl, pr, dn
      common/igrid/y (in), ydif (in), ys (in), yp (in), yd (in)
&      , deltayl, yk, ny, nym1
      common/bc/uinf, tinf, ubc, tbc
c
      u (1)=0. d0
      t (1)=0. d0
      ubc =uinf/dn

```

```

      tbc =tinf
c
      do 10 i=2, ny
        u (i) =ubc
        t (i) =tbc
      10 continue
c
      return
      end
c
c=====
      subroutine calc
c=====
c
c*****purpose:Calculation of physical quantities
c
      implicit real*8 (a-h, o-z)
      parameter (in= 5001)
      real*8 u (in), v (in), t (in)
      real*8 bu (in), bt (in)
c
      common var (in, 3), varu (in, 3), varu2 (in, 3)
      equivalence (var (1, 1), u (1)), (var (1, 2), v (1)), (var (1, 3), t (1))
      common/ivari/nvar, inu, inv, int, ivar
      common/ppro/rl, pr, dn
      common/igrd/y (in), ydif (in), ys (in), yp (in), yd (in)
      &      , deltay1, yk, ny, nym1
      common/icopde/dyl (in), ddyl (in), dy2 (in), ddy2 (in)
      common/istep/dx, xd, xlast, xstart, xnheat
      common/icoef/adn (in), ads (in), adp (in), aup (in), bp (in), sp (in)
      common/ibdev/grx, rex, rix
      common/irelx/insolv (3)
      common/irelx2/urf (3)
      common/ierr/erru, errv, errt
      common/ieps/epsu, epsv, epst
c
c-----
      entry calcu
c*****purpose:Calculation of u-velocity from momentum equation
c
      ivar=inu
c
      do 5 j=1, ny
5      bu (j) =u (j)
c
      bp (1) =0. d0
      def=1. d0
      gam=def*dx/ydif (2)
      cov=v (2) *dx
c
      do 10 j=2, nym1
        ps=cov/gam
        ap=1. d0-0. 1d0*dabs (ps)
        if (ap. le. 0. d0) ap=0. d0
        ads (j) =gam*dmax1 (0. d0, ap**5. d0) +dmax1 (cov, 0. d0)
        def=1. d0
        gam=def*dx/ydif (j+1)
        cov=v (j+1) *dx
        pn=cov/gam
        ap=1. d0-0. 1d0*dabs (pn)

```

```

      if (ap. le. 0. d0) ap=0. d0
      adn(j)=gam*dmax1(0. d0, ap**5. d0)+dmax1(-cov, 0. d0)
      prod= rl**(-3)*t(j)
      if (u(j). le. 0. d0) then
        sp(j)=0. d0
      else
        sp(j)=dmax1(-prod, 0. d0)/u(j)*dx*ys(j)
      end if
      aup(j)=varu(j, inu)*ys(j)
      adp(j)=adn(j)+ads(j)+aup(j)+sp(j)
      aup(j)=aup(j)*varu(j, ivar)
      bp(j)=dmax1(prod, 0. d0)*dx*ys(j)+aup(j)
10 continue
c
c-----solve equation
      call solve
c
c-----error of f. d. e
      erru=0. d0
c
      do 20 j=2, nym1
        if (bu(j). le. 0. d0) go to 20
        err1=dabs(u(j)/bu(j)-1. d0)
20 erru=dmax1(err1, erru)
c
      return
c
c-----
      entry cont
c****purpose:Calculation of v-velocity from continuety equation
c
      v(1)=0. d0
c
      do 50 j=1, nym1
        v(j+1)= (varu(j, inu)-u(j))/dx*ys(j)+v(j)
50 continue
c
      if (cbca. gt. 1. d0) goto 52
      v(ny) = (-1. d0)/(y(ny)-y(ny-1))
c
      do 52 j=2, nym1
        if (dabs(v(j)). lt. dabs(v(ny))) goto 52
      v(j)=v(ny)
c 52 continue
      return
c
c-----
      entry calct
c****purpose:Calculation of Temperatuere from Energy equation
c
      ivar=int
c
      do 205 j=1, ny
205 bt(j)=t(j)
      bp(1)=0. d0
      if (xd. ge. 0. d0) bp(1)=1. d0
      def=1. d0/pr
      gam=def*dx/ydif(2)
      cov=v(2)*dx
c
      do 210 j=2, nym1

```

```

      ps=cov/gam
      ap=1. d0-0. 1d0*dabs (ps)
      if (ap. le. 0. d0) ap=0. d0
      ads (j)=gam*dmax1 (0. d0, ap**5. d0)+dmax1 (cov, 0. d0)
      def=1. d0/pr
      gam=def*dx/ydif (j+1)
      cov=v (j+1) *dx
      pn=cov/gam
      ap=1. d0-0. 1d0*dabs (pn)
      if (ap. le. 0. d0) ap=0. d0
      adn (j)=gam*dmax1 (0. d0, ap**5. d0)+dmax1 (-cov, 0. d0)
      prod=0. d0
      if (t (j). le. 0. d0) then
        sp (j)=0. d0
      else
        sp (j)=dmax1 (-prod, 0. d0) /t (j) *dx*ys (j)
      endif
      sp (j)=0. d0
      aup (j)=varu (j, inu) *ys (j)
      adp (j)=adn (j) +ads (j) +aup (j) +sp (j)
      aup (j)=aup (j) *varu (j, ivar)
210 bp (j)=dmax1 (prod, 0. d0) *dx*ys (j) +aup (j)
c
c-----solve equation
      call solve
c
c-----error of f. d. e
      errt=0. d0
c
      do 220 j=2, nym1
        if (bt (j). le. 0. d0) go to 220
        err1=dabs (t (j) /bt (j) -1. d0)
220 errt=dmax1 (err1, errt)
c
      return
      end
c
c=====
      subroutine solve
c=====
c
c*****purpose:Calculation of tri-diagonal-matrix-algorithm
c
      implicit real*8 (a-h, o-z)
      parameter (in= 5001)
      real*8 u (in), v (in), t (in)
      real*8 a (in), b (in), c (in), d (in)
c
      common var (in, 3), varu (in, 3), varu2 (in, 3)
      equivalence (var (1, 1), u (1)), (var (1, 2), v (1)), (var (1, 3), t (1))
      common/ivari/nvar, inu, inv, int, ivar
      common/igrid/y (in), ydif (in), ys (in), yp (in), yd (in)
      & , deltay1, yk, ny, nym1
      common/icoef/adn (in), ads (in), adp (in), aup (in), bp (in), sp (in)
      common/irelx2/urf (3)
c
      a (1)=0. d0
      b (1)=0. d0
      c (1)=bp (1)
      d (1)=0. d0

```

```

      jl=nym1
c
      do 10 j=2, jl
        a(j)=adn(j)
        b(j)=ads(j)
        c(j)=bp(j)+(1.d0-urf(ivar))*adp(j)/urf(ivar)*var(j,ivar)
        d(j)=adp(j)/urf(ivar)
      10 continue
c
      do 20 j=2, jl
        dm=1.d0/(d(j)-b(j)*a(j-1))
        a(j)=a(j)*dm
        c(j)=(c(j)+b(j)*c(j-1))*dm
      20 continue
c
      do 30 j=nym1, 1, -1
        var(j,ivar)=a(j)*var(j+1,ivar)+c(j)
      30 continue
c
      return
      end
c
c=====
      subroutine output
c=====
c
      implicit real*8 (a-h, o-z)
      parameter(in= 5001)
      common var(in, 3), varu(in, 3), varu2(in, 3)
      equivalence (var(1, 1), u(1)), (var(1, 2), v(1)), (var(1, 3), t(1))
c
      real*8 u(in), v(in), t(in), dudx(in), dvdx(in), dtdx(in)
      character*15 fni, fnm(9)
c
      common/ppro/rl, pr, dn
      common/iout/fni, fnm
      common/ivari/nvar, inu, inv, int, ivar
      common/igrd/y(in), ydif(in), ys(in), yp(in), yd(in)
      &          , deltayl, yk, ny, nym1
      common/icopde/dyl(in), ddy1(in), dy2(in), ddy2(in)
      common/istep/dx, xd, xlast, xstart, xnheat
      common/ibdev/grx, rex, rix
      common/index/incont, iprsta, itest
      common/iiter/iter1, iter2
      common/icp/xstop(9), ixiter
c
c-----
      entry outpi
c****purpose:output initial data & marching roop data
c
      open(3, file=fni, status='unknown')
      if (iter1.eq.1) then
        write(3, 601)
      end if
601 format(1h , 5x, 'grx', 9x, 'rex', 9x, 'rix', 9x, 'nux'
      &      , 9x, 'tau', 9x, 'umax', 9x, 'x', 7x' iter2')
      if (mod(iter1, iprsta).ne.1) then
        go to 598
      else
        umax=0.d0

```

```

c
do 599 j=2, nym1
  if (u(j).gt.umax) then
    umax=u(j)
  else
    end if
599 continue
c
dtdyw= (t (2)-t (1)) / (y (2)-y (1))
dudyw= (u (2)-u (1)) / (y (2)-y (1))
dnux=-dtdyw*xd
tau = dudyw*rl*rl
umax=umax*dn
write (3, 611) grx, rex, rix, dnux, tau, umax, xd, iter2
endif
611 format (1h , 7e12. 4, 2x, i4)
598 continue
return
c
c-----
entry outpm
c*****purpose:output of calculation data in progress
c
open (2, file=fnm(ixiter), status='unknown')
c
do 40 j=1, ny
  dvdx (j) = (varu (j, inv) -v (j)) /dx
  dudx (j) = (varu (j, inu) -u (j)) /dx
  dtdx (j) = (varu (j, int) -t (j)) /dx
40 continue
c
a1= (y (2)-y (1))
a2= (y (3)-y (2))
c
ya=0. d0
ua=0. d0
va=0. d0
ta=1. d0
dvdxdy= (dvdx (2)-dvdx (1)) / (y (2)-y (1))
dvdxdx= (v (1)-2. d0*varu (1, inv)+varu2 (1, inv)) /dx/dx
dudxdy= (dudx (2)-dudx (1)) / (y (2)-y (1))
dudydy=-2. d0/a1/a2* (u (2)-u (1))+2. d0/ ((a1+a2) *a2) * (u (3)-u (1))
dtdxa=dtdx (1)
dtdy= (t (2)-t (1)) / (y (2)-y (1))
dvdxax=dvdx (1)
write (2, 441) ya, ua, va, ta,
& dvdxdy, dudydy, dvdxdx, dudxdy, dtdxa, dtdy, dvdxax
c
do 41 j=2, ny-1
  dudydy= (u (j+1)-u (j)) *ddy1 (j) - (u (j)-u (j-1)) *ddy2 (j)
  dvdxdy= (dvdx (j+1)-dvdx (j)) *dy1 (j) + (dvdx (j)-dvdx (j-1)) *dy2 (j)
  dvdxdx= (v (j)-2. d0*varu (j, inv)+varu2 (j, inv)) /dx/dx
  dudxdy= (dudx (j+1)-dudx (j)) *dy1 (j) + (dudx (j)-dudx (j-1)) *dy2 (j)
  dtdxa = dtdx (j)
  dtdy = (t (j+1)-t (j)) *dy1 (j) + (t (j)-t (j-1)) *dy2 (j)
  ya=y (j)
  ua=u (j)
  va=v (j)
  ta=t (j)
  dvdxax=dvdx (j)

```



```
41 write (2, 441) ya, ua, va, ta,  
    &          dvdxdy, dudydy, dvdxdx, dudxdy, dtdxa, dtdy, dvdx  
c          close (2, status='keep')  
441 format (1h , 11e20. 12)  
    return  
c  
    end
```

## C.2 Calculation of Eigenvalue Problem

```

c f90 -o mcstab1 mcstab1.f $LINK_FNL -lapack
c
c mcstab2.f
c
c config. combined convection along a vertical plate
c
c                                     Date: Oct. 12, 1999 - Aug. 13, 1999
c
c -----
c
c n: number of collocation points
c tf1: trial function for momentum eq.
c tf2: trial function for energy eq.
c ocl: matrix of eigen value problem
c oc2: matrix of eigen value problem
c
c --- main ---
c
c   parameter (n=128, ip1=2*(n+1), ip2=n+1)
c   parameter (lwork=8*ip1)
c   parameter (ny= 201)
c
c   implicit real*8 (a-h, p-z), complex*16 (o)
c
c   dimension tf1(0:4, 0:ip2, ip2), tf2(0:4, 0:ip2, ip2)
c   dimension ocl(ip1, ip1), oc2(ip1, ip1)
c
c   complex*16 lambdal(ip1), lambdar(ip1)
c   complex*16 zero
c   complex*16 vl(ip1, ip1), evec(ip1, ip1)
c   complex*16 work(lwork), rwork(lwork)
c   real*8      dgp1cg, pi,
c   &           eval_r(ip1), eval_i(ip1), evec_r(ip1, ip1),
c   &           evec_i(ip1, ip1)
c   integer     l(ip1)
c   character   fni*14, fno*14
c
c   inp= 0
c   pr = 0. 71d0
c   oi = (0. d0, 1. d0)
c   zero= (0. d0, 0. d0)
c
c   write(*,*) 'input alc, ax'
c   read(*,*) alc, ax
c
c   al=alc*ax
c   al=alc*51. 18d0
c   al=alc*40. 62d0
c   al=alc*35. 48d0
c   al=alc*28. 16d0
c   al=alc*18. 85d0
c
c   gr=6. 701d9
c
c   write(*,*) 'input file name (fni)'

```

```

      read(*,1110) fni
      write(*,*) 'output file name (fno)'
      read(*,1110) fno
1110 format(a14)
c
      call trialf(tf1,tf2)
      call matrix(pr,al,gr,tf1,tf2,oc1,oc2,fnf,inp,ny,ym)
      call ZGEGV('N','V',ip1,oc1,ip1,oc2,ip1,lambdal,
&              lambdar,vl,ip1,evec,ip1,work,lwork,
&              rwork,info)
      write(*,*) 'info=',info
c
      do i=1,ip1
c
        write(11,*) i,lambdar(i)
        if(lambdar(i).ne.zero) then
          eval_r(i) = real(lambdal(i)/lambdar(i))
          eval_i(i) = imag(lambdal(i)/lambdar(i))
          do j=1, ip1
            evec_r(j,i) = real(evec(j,i))
            evec_i(j,i) = imag(evec(j,i))
          enddo
        endif
      enddo
      do i=1, ip1
        l(i)=i
      enddo
111 continue
      key = 0
      do i=1, ip1
        do j=1, ip1
          if(eval_i(j).le.eval_i(i)) then
            key = 1
            ctmp = eval_i(i)
            eval_i(i) = eval_i(j)
            eval_i(j) = ctmp
            ctmp = eval_r(i)
            eval_r(i) = eval_r(j)
            eval_r(j) = ctmp
            ntmp = l(i)
            l(i) = l(j)
            l(j) = ntmp
          endif
        enddo
      enddo
      if(key.ne.0) goto 222
      goto 111
222 continue

      open(1,file=fno,status='unknown')
      open(2,file='evec_r.dat',status='unknown')
      open(3,file='evec_i.dat',status='unknown')
      open(4,file='info.dat',status='unknown')
      ii=0
      do i=1, ip1
        if(eval_r(i).ne.0.d0 .and. eval_i(i).ne.0.d0) then
          ii=ii+1
          write(1,*) ii, eval_r(i), eval_i(i)
          write(2,*) ii, (evec_r(j,l(i)), j=1, n/2+1)
          write(3,*) ii, (evec_i(j,l(i)), j=1, n/2+1)
        endif
      enddo

```

```

        enddo
        write (4, 555) inp, fni, gr, alc, ax, ym, ny, n, i i
        close (4)
        close (3)
        close (2)
        close (1)
c
555 format (1h , i2, 2x, a8, 4e12. 5, 2x, i4, 2x, i4, 2x, i4)
        stop
        end
c
c --- evaluation of trial function at collocation point ---
c
        subroutine trialf (tf1, tf2)
        parameter (n=128, ip1=2* (n+1), ip2=n+1)
        implicit real*8 (a-h, p-z), complex*16 (o)
        dimension tf1 (0:4, 0:ip2, ip2), tf2 (0:4, 0:ip2, ip2)
        dimension dtf1 (0:4, 0:ip2), dtf2 (0:4, 0:ip2)
c
        pi = 2. d0*dasin (1. d0)/dble (n+2)
c
        do 1 i=1, ip2
            x = dcos (dble (i) *pi)
c
            call diff1tf (1, x, dtf1)
            call diff1tf (2, x, dtf2)
c
            do 1 k=0, 4
                do 1 j=0, n
                    tf1 (k, j, i) = dtf1 (k, j)
                    tf2 (k, j, i) = dtf2 (k, j)
1 continue
c
        return
        end
c
c --- differentiation of trial function ---
c
        subroutine diff1tf (ic, x, dtf)
        parameter (n=128, ip1=2* (n+1), ip2=n+1)
        implicit real*8 (a-h, p-z), complex*16 (o)
        dimension dch (0:4, 0:ip2), dtf (0:4, 0:ip2)
c
        if (ic. eq. 1) then
            f0 = (1. d0-x**2) **2
            f1 = -4. d0*x+ 4. d0*x**3
            f2 = -4. d0 +12. d0*x**2
            f3 = +24. d0*x
            f4 = 24. d0
        else
            f0 = 1. d0 -x**2
            f1 = -2. d0*x
            f2 = -2. d0
            f3 = 0. d0
            f4 = 0. d0
        endif
c
        call diffch (x, dch)
c
        do 1 i=0, n

```

```

      dtf(0, i) = f0*dch(0, i)
      dtf(1, i) = f1*dch(0, i) +      f0*dch(1, i)
      dtf(2, i) = f2*dch(0, i) + 2. d0*f1*dch(1, i) +      f0*dch(2, i)
      dtf(3, i) = f3*dch(0, i) + 3. d0*f2*dch(1, i) + 3. d0*f1*dch(2, i)
&      +      f0*dch(3, i)
      dtf(4, i) = f4*dch(0, i) + 4. d0*f3*dch(1, i) + 6. d0*f2*dch(2, i)
&      + 4. d0*f1*dch(3, i) +      f0*dch(4, i)
1 continue
  return
end

c
c --- differentiation of chebyshev series---
c
  subroutine diffch(x, dch)
  parameter (n=128, ip1=2*(n+1), ip2=n+1)
  implicit real*8 (a-h, p-z), complex*16 (o)
  dimension dch(0:4, 0:ip2)

c
  do 1 i=0, 4
    do 1 j=0, 1
      dch(i, j) = 0. d0
1 continue

c
  dch(0, 0) = 1. d0
  dch(0, 1) = x
  dch(1, 1) = 1. d0

c
  do 2 j=2, n
    dch(0, j) = 2. d0*x*dch(0, j-1) - dch(0, j-2)
    dch(1, j) = 2. d0*x*dch(1, j-1) - dch(1, j-2) + 2. d0*dch(0, j-1)
    dch(2, j) = 2. d0*x*dch(2, j-1) - dch(2, j-2) + 4. d0*dch(1, j-1)
    dch(3, j) = 2. d0*x*dch(3, j-1) - dch(3, j-2) + 6. d0*dch(2, j-1)
    dch(4, j) = 2. d0*x*dch(4, j-1) - dch(4, j-2) + 8. d0*dch(3, j-1)
2 continue

c
  return
end

c
c --- matrix ---
c
  subroutine matrix(pr, al, gr, tf1, tf2, oc1, oc2, fni, inp, ny, ym)
  parameter (n=128, ip1=2*(n+1), ip2=n+1)
c
  parameter (ny= 201)
  implicit real*8 (a-h, p-z), complex*16 (o)
  complex*16 zero
  character*15 fn
  dimension oc1(ip1, ip1), oc2(ip1, ip1)
  dimension tf1(0:4, 0:ip2, ip2), tf2(0:4, 0:ip2, ip2)
  real*8 y(ny), u(ny), v(ny), t(ny),
&      dvdxdy(ny), dudydy(ny), dvdxdx(ny), dudxdy(ny),
&      dtdx(ny), dtdy(ny), dvdx(ny)
  real*8 sv(ny), sdvxdy(ny), sdvdxdx(ny), sdvdx(ny)
  real*8 yc(ip2), uc(ip2), vc(ip2), tc(ip2),
&      dvdxdc(ip2), dudydc(ip2), dvdxdc(ip2), dudxdyc(ip2),
&      dtdxc(ip2), dtdyc(ip2)
  real*8 xl(ip2), d(ip2)
  character fni*14, fno*14

c
  oi= (0. d0, 1. d0)
  zero= (0. d0, 0. d0)

```

```

c      open (1, file=fni, status='unknown')
c
c      do 41 j=1, ny-1
c          read (1, 441) ya, ua, va, ta,
&          dvdxdy, dudydy, dvdxdx, dudxdy, dtdxa, dtdya, dvdx
c
c          y(j)=ya
c          u(j)=ua
c          sv(j)=va
c          t(j)=ta
c
c          sdvxdy(j)=dvdxdy
c          dudydy(j)=dudydy
c          sdvdx(x)=dvdxdx
c          dudxdy(j)=dudxdy
c
c          dtdx(j)=dtdxa
c          dtdy(j)=dtdya
c          sdvdx(j)=dvdx
41 continue
441 format (1h , 11e20. 12)
close (1)
c
c      do 42 j=2, ny-2
c          v(j)=0. 5d0*(sv(j)+sv(j+1))
c          dvxdy(j)=0. 5d0*(sdvxdy(j)+sdvxdy(j+1))
c          dvdx(j)=0. 5d0*(sdvdx(j)+sdvdx(j+1))
c          dvdx(j)=0. 5d0*(sdvdx(j)+sdvdx(j+1))
42 continue
c
c          v(1)=0. d0
c          dvxdy(1)=(dvdx(2))/(y(2)-y(1))
c          dvdx(1)=0. d0
c
c      do 1 i=1, ip1
c          do 1 j=1, ip1
c              oc1(i, j) = zero
c              oc2(i, j) = zero
1 continue
c
c      pi = 2. d0*dasin (1. d0)/dble (n+2)
c
c      do 51 j=1, ny-2
c          if (t(ny-j).lt. 1. d-3) then
c              ym=3. d0*y(ny-j)
c          end if
51 continue
c
c      do 100 k=1, ip2
c          x = dcos (dble (k)*pi)
c          x1(k)=0. 5d0*ym*(1. d0-x)
c          d(k) = -2. d0/ym
c
c      do 100 l=1, ny
c          if (y(l).le. x1(k) .and. y(l+1) .gt. x1(k)) then
c              uc(k)= u(l)+(x1(k)-y(l))*(u(l+1)-u(l))/(y(l+1)-y(l))
c              vc(k)= v(l)+(x1(k)-y(l))*(v(l+1)-v(l))/(y(l+1)-y(l))
c              tc(k)= t(l)+(x1(k)-y(l))*(t(l+1)-t(l))/(y(l+1)-y(l))
c

```

```

      dvdxdy(k) = dvxdy(l)
&      + (x1(k)-y(l)) * (dvxdy(l+1)-dvxdy(l)) / (y(l+1)-y(l))
      dudydy(k) = dudydy(l)
&      + (x1(k)-y(l)) * (dudydy(l+1)-dudydy(l)) / (y(l+1)-y(l))
      dvdxdc(k) = dvdxdc(l)
&      + (x1(k)-y(l)) * (dvdxdc(l+1)-dvdxdc(l)) / (y(l+1)-y(l))
      dudxdc(k) = dudxdc(l)
&      + (x1(k)-y(l)) * (dudxdc(l+1)-dudxdc(l)) / (y(l+1)-y(l))
c
      dtdxc(k) = dtdxc(l)
&      + (x1(k)-y(l)) * (dtdxc(l+1)-dtdxc(l)) / (y(l+1)-y(l))
      dtdyc(k) = dtdyc(l)
&      + (x1(k)-y(l)) * (dtdyc(l+1)-dtdyc(l)) / (y(l+1)-y(l))
c
      end if
100 continue
c
      do 2 i=1, ip2
        write(9,441) x1(i), uc(i), vc(i), tc(i)
&      , dvdxdy(i), dudydy(i), dvdxdc(i), dudxdc(i), dtdxc(i), dtdyc(i)
        do 2 j=1, ip2
c ddx. ne. 0.
          if (inp. eq. 1) then
            ocl(i,j) = -( tfl(4,j-1,i)*d(i)**4
&                        -2. d0*al*al*tfl(2,j-1,i)*d(i)**2
&                        + al**4*tfl(0,j-1,i))
&
&      +vc(i)*(tfl(3,j-1,i)*d(i)**3
&      -al*al*tfl(1,j-1,i)*d(i))
&
&      -(dvdxdc(i)-dudxdc(i))*tfl(1,j-1,i)*d(i)
&
&      +oi*( al*uc(i)*(tfl(2,j-1,i)*d(i)**2
&      -al*al*tfl(0,j-1,i))
&
&      +al*(dvdxdy(i)-dudydy(i))*tfl(0,j-1,i))
            ocl(i,ip2+j)
&      = -gr*tf2(1,j-1,i)*d(i)
            oc2(i,j) = oi*(tfl(2,j-1,i)*d(i)**2-al*al*tfl(0,j-1,i))
            oc2(i,ip2+j)
&      = zero
            ocl(ip2+i,j)
&      = dtdxc(i)*tfl(1,j-1,i)*d(i)
&
&      -oi*al*dtdyc(i)*tfl(0,j-1,i)
            ocl(ip2+i,ip2+j)
&      = -1. d0/pr*(tf2(2,j-1,i)*d(i)*d(i)-al*al*tf2(0,j-1,i))
&
&      +vc(i)*tf2(1,j-1,i)*d(i)
&
&      +oi*al*uc(i)*tf2(0,j-1,i)
            oc2(ip2+i,j)
&      = zero
            oc2(ip2+i,ip2+j)
&      = oi*tf2(0,j-1,i)
c
c ddx. eq. 0. d0
          else if (inp. eq. 0) then
            ocl(i,j) = -( tfl(4,j-1,i)*d(i)**4
&                        -2. d0*al*al*tfl(2,j-1,i)*d(i)**2
&                        + al**4*tfl(0,j-1,i))
&
&      +oi*( al*uc(i)*(tfl(2,j-1,i)*d(i)**2
&                        -al*al*tfl(0,j-1,i))
&
&      +al*(-dudydy(i))*tfl(0,j-1,i))
            ocl(i,ip2+j)
&      = -gr*tf2(1,j-1,i)*d(i)
            oc2(i,j) = oi*(tfl(2,j-1,i)*d(i)**2-al*al*tfl(0,j-1,i))

```

```

        oc2 (i, ip2+j)
&          = zero
        oc1 (ip2+i, j)
&          =
&          -oi*al*dtdyc (i) *tf1 (0, j-1, i)
        oc1 (ip2+i, ip2+j)
&          = -1. d0/pr* (tf2 (2, j-1, i) *d (i) *d (i) -al*al*tf2 (0, j-1, i))
&          +oi*al*uc (i) *tf2 (0, j-1, i)
        oc2 (ip2+i, j)
&          = zero
        oc2 (ip2+i, ip2+j)
&          = oi*tf2 (0, j-1, i)
        endif
c
        aolar= imag (oc1 (i, j))
        aolbr= imag (oc1 (i, ip2+j))
        aolcr= imag (oc1 (ip2+i, j))
        aoldr= imag (oc1 (ip2+i, ip2+j))
        ao2ar= imag (oc2 (i, j))
        ao2br= imag (oc2 (i, ip2+j))
        ao2cr= imag (oc2 (ip2+i, j))
        ao2dr= imag (oc2 (ip2+i, ip2+j))
c        write (11, 777) i, j, aolar, aolbr, aolcr, aoldr
c        write (12, 777) i, j, ao2ar, ao2br, ao2cr, ao2dr
2      continue
777    format (1h , 2i5, 4e13. 5)
        return
        end

```